

A NEW APPROACH TO DESIGN MICROSTRIP LOW PASS FILTER

by

G. M. Rafiquzzaman

A thesis submitted in partial fulfillment of the requirement for the degree of Master of Science in
Electrical and Electronic Engineering



Khulna University of Engineering & Technology

Khulna 920300, Bangladesh.

July 2015

Declaration

This is to certify that the thesis work entitled “*A New Approach To Design Microstrip Low Pass Filter*” has been carried out by *G. M. Rafiquzzaman* in the *Department of Electrical and Electronic Engineering*, Khulna University of Engineering and Technology, Khulna Bangladesh. The above thesis work or any part of this work has not been submitted anywhere for the award of any degree or diploma.

Signature of Supervisor

Signature of Candidate

Acknowledgement

Alhamdulillah, praise be to Allah, the Cherisher and Sustainer of the world, most Gracious, most Merciful Lord. Praise is to Allah for enabling me to complete this analysis and research for the new approach to design microstrip low pass filter thesis.

First and foremost, I would like to present my deepest appreciation and gratitude to my supervisor **Dr. Mohammad Nurunnabi Mollah**, Professor, Department of Electrical and Electronic Engineering, Khulna University of Engineering & Technology (KUET) for his scholastic guidance, constructive suggestion, valuable advices and all the possibilities and opportunities he has provided me with throughout my graduate life. I am more than glad to have found the chance to work with him. Completing this thesis could not be possible without his help.

I am also grateful to **Dr. Md. Abdur Rafiq**, Professor, Department of Electrical and Electronic Engineering and **Dr. Md. Shahjahan**, Professor, Department of Electrical and Electronic Engineering, KUET, for various suggestions about my thesis work.

Finally I would like to thank members of my family, my friends (special thanks to **Abu Talha Sadi**) and staff members for their exceptional support, encouragement, help, and unparalleled patience with me during this study and my entire life.

(G. M. Rafiqzaman)

Abstract

With the emergence of novel wireless technologies, the demands for larger bandwidth, high efficiency and high capacity RF and microwave devices have been growing tremendously. The recent implementations in solid state and semiconductor materials give us hope for future applications. It should be remarked that although many of the ideas could have been proposed much earlier, it is only recently that they were identified or demonstrated due to various technological advances. The electromagnetic bandgap (EBG) is introduced to improve the performances of existing RF active and passive devices. Electromagnetic Band Gap (EBG) structures produced a wide variety of design alternatives for researchers working in the area of microwave and photonics. The focus is now towards on finding real applications combined with detailed modeling. Due to the incredible potential of EBGs, there are huge applications in which they can be used. New companies have also started to exploit the commercial potential of this technology.

This thesis describes the planar EBG structures in the forms of conventional circular and rectangular photonic bandgaps (PBGs) and dumbbell shaped defected ground structures (DGSs). Novel PBGs in the form of non-uniform Binomial and *Chebyshev* distributions of unit PBG cells have been proposed. This novel PBGSs contains fewer ripples with lesser height or ripple free passband and wide stopband properties, which are very useful to suppress higher order harmonics in the lowpass filters (LPF). The dumbbell shaped DGSs study has been described with the gap width and length and the size of dumbbell slots. Some novel designs have been proposed such as; non-uniform dumbbell shaped DGSs with Binomial and *Chebyshev* distribution, hybrid dumbbell shaped DGS and PBGS and modified hybrid dumbbell shaped DGS and PBGS configurations. The novel designs perform better than the conventional DGSs reported in the literature. The DGSs yield perfect LPF responses with negligible passband ripples and extremely wide stopband.

In this thesis, we have investigated on uniform circular, rectangular and dumbbell shaped DGS structures with different filling factor (FF). Therefore, FF is not a single valued parameter. In our study, we have defined the FF as the ratio of central dumbbell shaped DGS element and inter-element spacing. And then for the better performance, we have focused on different Binomially and *Chebyshev* distributed dumbbell shaped DGSs. This research conveys the performance of low pass filter using those distributions at about 4 GHz cutoff frequency. These distributions remove the unwanted insertion loss in the band rejection region. Sufficient explanations have been provided to validate the total research works in the thesis. Finally, comparing the insertion loss (IL) and return loss (RL) performances of the LPFs with binomially and *Chebyshev* distributed dumbbell shaped DGSs and hybrid DGSs. Binomially distributed DGSs and hybrid DGSs provide improved performance than conventional PBGSs and *Chebyshev* distributed dumbbell shaped DGSs in terms of suppression of the ripple in the passband and return and insertion-loss bandwidths.

Contents

| Contents | Pages |
|---|--------------|
| Declaration | ii |
| Board of Examiners | iii |
| Acknowledgements | iv |
| Abstract | v |
| List of figures | |
| List of tables | |
| Acronyms and abbreviations | |
| Chapter 1: Introduction | |
| 1.1 Electromagnetic Bandgap Structures (EBGS) | 1 |
| 1.2 Objective of the Thesis | 3 |
| 1.3 Thesis Outline | 4 |
| Chapter 2: Literature Survey | |
| 2.1 Introduction | 5 |
| 2.2 Applications of EBGS | 5 |
| 2.2.1 Resonators and Filters using EBG Structures | 5 |
| 2.2.2 EBG Tuned Microwave Devices | 7 |
| 2.2.3 Miniaturization | 8 |
| Chapter 3: Filter Terminologies and Conventional Filter Design | |
| 3.1 Introduction | 9 |
| 3.2 Network Variables | 9 |
| 3.3 Scattering Parameters | 10 |
| 3.4 Symmetrical Network Analysis | 12 |
| 3.5 ABCD Parameters | 13 |
| 3.6 Filter | 14 |
| 3.6.1 Advantages of Filters | 14 |
| 3.6.2 Microwave | 15 |
| 3.6.3 Microwave filter | 15 |
| 3.6.4 General Use of Filter Principles in Terms of Microwave Components | 16 |
| 3.6.5 Definition of terms used for microwave filter design | 16 |
| 3.6.6 Periodic Structures | 17 |
| 3.6.7 Capacitively loaded transmission-line-circuit analysis | 18 |
| 3.6.8 Circuit Analysis of a Periodic Structure | 19 |
| 3.6.9 Analysis of Infinite Periodic Structures | 20 |
| 3.7 Electromagnetic Bandgap Structures (EBGS) | 21 |
| 3.7.1 Types of Electromagnetic Bandgap Structures | 21 |
| 3.7.2 PBG Structures | 23 |
| 3.8 Dumbbell Shaped Defected Ground Structures | 26 |
| 3.9 Microstrip Lines | 26 |
| 3.10 Different Circuit Theories Based on the Frequency of Operation | 29 |

| | | |
|------|--|----|
| 3.11 | Conventional Filter Design | 30 |
| | 3.11.1 Filter Design by the Image Parameter Method | 30 |
| | 3.11.2 Filter Design by the Insertion Loss Method | 37 |
| | 3.11.3 Filter Implementation | 39 |
| 3.12 | Low-Pass Filter Design Procedure Using Stubs | 42 |
| 3.13 | Stepped-Impedance Low-Pass Filters | 49 |
| 3.14 | Conclusions | 51 |

Chapter 4: EBGs assisted T-line for LPF

| | | |
|-----|--|----|
| 4.1 | Microstrip Lines | 52 |
| | 4.1.1 Microstrip Structure | 52 |
| | 4.1.2 Waves in Microstrip | 52 |
| 4.2 | Definition of Electromagnetic Bandgap Structure (EBGS) | 52 |
| 4.3 | Analysis methods for EBG structures | 53 |
| 4.4 | Analysis methods for Dumbbell Shaped DGS structures | 54 |
| 4.5 | Uniform PBG (UPBG) Configurations Applied To Microstrip Lines | 55 |
| | 4.5.1 Design of Microstrip Transmission Line over Uniform PBGS (uniform circular PBGS) | 55 |
| | 4.5.2 Results | 59 |
| 4.6 | Compactness | 64 |
| 4.7 | Conclusions | 65 |

Chapter 5: Non-uniform EBGs for LPF

| | | |
|-----|---|----|
| 5.1 | Introduction | 66 |
| 5.2 | Theory of Non-uniform 1-D Microstrip PBGSs | 66 |
| | 5.2.1 Binomial Distribution | 66 |
| | 5.2.2 Chebyshev Distribution | 67 |
| 5.3 | Design of LPF Using 1-D Microstrip PBGSs | 68 |
| | 5.3.1 Design Principles | 68 |
| | 5.3.2 Non-Uniform PBG Structures | 69 |
| | 5.3.3 Results of Non-Uniform PBG Structures | 71 |
| | 5.3.4 Non-Uniform Dumbbell Shaped Defected Ground Structures | 72 |
| | 5.3.5 Results of Non-Uniform Dumbbell Shaped Defected Ground Structures | 83 |
| 5.4 | Conclusions | 96 |

Chapter 6: Conclusions and Future Works

| | | |
|-----|-----------------------------------|----|
| 6.1 | Conclusions | 97 |
| 6.2 | Fulfilling the Goal of the Thesis | 98 |
| 6.3 | Recommendation for Future Work | 98 |

List of Figures

| Figure No. | Description | Page No. |
|-------------|--|----------|
| Figure 1.1 | Geometry of a 3 rows (2-D) of uniform square EBGs beneath the transmission line. | 1 |
| Figure 2.1 | UC-PBG structure | 6 |
| Figure 2.2 | Schematic diagram of a BPF over UC-PBG | 7 |
| Figure 3.1 | Two-port network showing network variables. | 10 |
| Figure 3.2 | Symmetrical two-port networks with (a) even-mode excitation, and (b) odd-mode excitation. | 13 |
| Figure 3.3 | Graphical representation of different types of filter. | 14 |
| Figure 3.4 | Communication Frequency spectrum | 15 |
| Figure 3.5 | Examples of periodic structures. (a) Periodic stubs on a microstrip line. (b) Periodic diaphragms in a waveguide. | 18 |
| Figure 3.6 | Equivalent circuit of a periodically loaded transmission line. | 18 |
| Figure 3.7 | (a) Equivalent circuit model of a unit cell, (b) a transmission line cascaded by unit cells. | 19 |
| Figure 3.8 | Three dimensional EBG structure | 22 |
| Figure 3.9 | Two dimensional EBG structure | 22 |
| Figure 3.10 | One dimensional EBG structure | 23 |
| Figure 3.11 | Different PBG structures | 23 |
| Figure 3.12 | Bumpy metal sheet: (a) electric field extends across the bumps at the lower edge and (b) electric field wraps around the bumps at the upper edge | 23 |
| Figure 3.13 | Corrugated metal surface | 24 |
| Figure 3.14 | Periodic metal connected to ground with via holes to yield high-impedance surface. | 25 |
| Figure 3.15 | Microstrip with etched periodic pattern in the ground plane (circular pattern) | 25 |
| Figure 3.16 | Geometry of a unit cell of a dumbbell shape DGS. | 26 |
| Figure 3.17 | A microstrip transmission line | 26 |
| Figure 3.18 | Characteristic impedance and effective permittivity of microstrip line. | 28 |
| Figure 3.19 | Different circuit-theories based on the frequency of operation. | 29 |
| Figure 3.20 | Microstrip transmission line: (a) 3D view; (b) 2D side view. | 30 |
| Figure 3.21 | Stripline cross-section. | 30 |
| Figure 3.22 | A two-port network terminated in its image impedances. | 31 |
| Figure 3.23 | A two-port network terminated in its image impedances and driven with a voltage generator. | 32 |
| Figure 3.24 | Low-pass constant- k filter sections in T and π forms. (a) T-section. (b) π -section. | 33 |

| | | |
|-------------|--|----|
| Figure 3.25 | Typical passband and stopband characteristics of the low-pass constant- k sections | 34 |
| Figure 3.26 | High-pass constant- k filter sections in T and π forms. (a) T-section. (b) π -section. | 34 |
| Figure 3.27 | Development of an m -derived filter section from a constant- k section. | 35 |
| Figure 3.28 | m -Derived filter sections. (a) Low-pass T-section. (b) High-pass T-section. | 35 |
| Figure 3.29 | Typical attenuation responses for constant- k , m -derived, and composite filters. | 36 |
| Figure 3.30 | A bisected π -section used to match $Z_{i\pi}$ to Z_{iT} | 36 |
| Figure 3.31 | The final four-stage composite filter. | 36 |
| Figure 3.32 | Maximally flat and equal-ripple low-pass filter responses ($N = 3$). | 38 |
| Figure 3.33 | Elliptic function low-pass filter response. | 38 |
| Figure 3.34 | The process of filter design by the insertion loss method. | 39 |
| Figure 3.35 | Richards' transformation. (a) For an inductor to a short-circuited stub. (b) For a capacitor to an open-circuited stub. | 41 |
| Figure 3.36 | The Four Kuroda Identities | 42 |
| Figure 3.37 | Ladder circuits for low-pass filter prototypes and their element definitions. (a) Prototype beginning with a shunt element. (b) Prototype beginning with a series element. | 43 |
| Figure 3.38 | Attenuation versus normalized frequency for maximally flat filter prototypes. | 44 |
| Figure 3.39 | Attenuation versus normalized frequency for equal-ripple filter prototypes. (a) 0.5 dB ripple level. (b) 3.0 dB ripple level. | 45 |
| Figure 3.40 | Filter design procedure. Lumped-element low-pass filter prototype. | 46 |
| Figure 3.41 | Using Richards' transformations to convert inductors and capacitors to series and shunt stubs. | 47 |
| Figure 3.42 | Adding unit elements at the ends of the filter. | 47 |
| Figure 3.43 | Applying the second Kuroda identity. | 47 |
| Figure 3.44 | After impedance and frequency scaling of the design. | 48 |
| Figure 3.45 | Microstrip fabrication of the final filter. | 48 |
| Figure 3.46 | Amplitude responses of lumped-element and distributed-element low-pass filter. | 48 |
| Figure 3.47 | 6 element (a) Low-pass filter prototype circuit. (b) Stepped-impedance implementation. (c) Microstrip layout of final filter. | 50 |
| Figure 3.48 | Amplitude response of the stepped-impedance low-pass filter, with (dotted line) and without (solid line) losses. | 51 |
| Figure 4.1 | General microstrip structure. | 52 |
| Figure 4.2 | Lumped LC model for EBG analysis. | 53 |
| Figure 4.3 | Periodic transmission line method for EBG analysis | 53 |

| | | |
|-------------|---|----|
| Figure 4.4 | Geometry of a unit cell of a dumbbell shape DGS | 54 |
| Figure 4.5 | The equivalent circuit of dumbbell shaped DGS unit | 55 |
| Figure 4.6 | (a)Geometry of a 50-ohm microstrip transmission line where 2-D (three lines) uniform circular PBGSs are etched in the ground plane. (b) The filling factor (FF) explanation ($FF = r/a$). | 57 |
| Figure 4.7 | Geometry of a standard 50-ohm transmission line with 1-D uniform circular PBGSs etched in the ground plane. | 57 |
| Figure 4.8 | 2-D (three lines) of square patterned PBGSs under standard 50 ohm transmission line. | 58 |
| Figure 4.9 | 1-D square patterned periodic structures under standard 50-ohm transmission line. | 58 |
| Figure 4.10 | 1-D Dumbbell shaped DGSs patterned periodic structures under standard 50-ohm transmission line. | 58 |
| Figure 4.11 | IE3D simulated S-parameters versus frequency of an ideal 50-ohm transmission line. | 59 |
| Figure 4.12 | Simulated S-parameter performances of a standard 50- ohm transmission line perturbed by 2-D (three lines) uniform circular PBGSs in the ground plane. | 60 |
| Figure 4.13 | Simulated S-parameter performances of a standard 50 ohm transmission line perturbed by 1-D (one line) uniform circular PBGSs in the ground plane. | 61 |
| Figure 4.14 | S-parameters performances of three lines uniform square-patterned PBG structures | 61 |
| Figure 4.15 | Simulated S-parameter performances of a standard 50 ohm transmission line perturbed by 1-D (one line) uniform rectangular PBGSs in the ground plane. | 62 |
| Figure 4.16 | S-parameters performances of three lines uniform Dumbbell shaped DGS structures. | 63 |
| Figure 4.17 | 1-D square patterned periodic structures under standard 50-ohm transmission line. The substrate is Taconic having dielectric constant of 2.45 and height of 31 mils. The inter-element spacing, $a = 20.86$ mm, element width and length, $b = 5.215$ mm. | 63 |
| Figure 4.18 | Simulated insertion loss performances of a standard 50 ohm transmission line perturbed by 1-D (one line) uniform rectangular PBGSs vs. Dumbbell shaped DGS in the ground plane. | 64 |
| Figure 5.1 | Pascal's Triangle | 66 |
| Figure 5.2 | Geometry of circular uniform PBGS. The PBG elements are having radius of r_0 etched in the ground plane. | 67 |
| Figure 5.3 | Geometry of circular non-uniform PBGSs etched in the ground plane. The central two elements have largest value and the remaining PBGS follow Chebyshev distribution. | 68 |

| | | |
|-------------|--|----|
| Figure 5.4 | Geometry of a binomially distributed circular patterned PBGS designed by varying the radius of PBGSs etched in the ground plane. | 68 |
| Figure 5.5 | Geometry of a binomially distributed rectangular patterned PBGS designed by varying the arm lengths of PBGSs etched in the ground plane. | 69 |
| Figure 5.6 | Geometry of a Chebyshev distributed circular patterned PBGS designed by varying the radius of PBGSs etched in the ground plane. | 69 |
| Figure 5.7 | Geometry of a binomially distributed rectangular patterned PBGS designed by varying the arm lengths of PBGSs etched in the ground plane. | 70 |
| Figure 5.8 | S-parameters performance of a transmission line over binomially distributed circular patterned PBGS according to design 1 | 70 |
| Figure 5.9 | S-parameters performance of a transmission line over binomially distributed rectangular patterned PBGS according to design 2 | 71 |
| Figure 5.10 | S-parameters performance of a transmission line over Chebyshev distributed circular patterned PBGS according to design 3 | 71 |
| Figure 5.11 | S-parameters performance of a transmission line over Chebyshev distributed rectangular patterned PBGS according to design 4 | 72 |
| Figure 5.12 | Insertion loss performance of a unit cell of dumbbell shaped DGS with variable larger slots of 240, 220, 200 and 180 mils respectively | 73 |
| Figure 5.13 | Insertion loss performance of a unit cell of dumbbell shaped DGS with variable gap distances of 20, 30, 40 and 50 mils respectively. | 74 |
| Figure 5.14 | Insertion loss performance of a unit cell of dumbbell shaped DGS with variable width of narrow slots of 240, 220, 200 and 180 mils respectively. | 74 |
| Figure 5.15 | Geometry of a Binomially distributed LPF designed by varying narrow slot width (w) and length (b) of PBGS of dumbbell shaped DGS etched in the ground plane. | 75 |
| Figure 5.16 | Geometry of a Binomially distributed LPF designed by varying length (b) of PBGS of the dumbbell shaped DGS etched in the ground plane. | 76 |
| Figure 5.17 | Geometry of a Binomial distributed LPF designed by varying narrow slot width (w) of the DGS etched in the ground plane. | 76 |
| Figure 5.18 | Geometry of a Binomially distributed LPF designed by varying both length (b) of PBGS and width (w) of the narrow slot of the dumbbell shaped DGS and interleaved square PGBS etched in the ground plane. | 77 |
| Figure 5.19 | Geometry of a Binomially distributed LPF designed by varying both width (a) of PBGS and width (w) of the narrow slot of the | 77 |

| | | |
|-------------|---|----|
| | dumbbell shaped DGS and lengths of the interleaved PGBS etched in the ground plane. | |
| Figure 5.20 | Geometry of a <i>Chebyshev</i> distributed LPF designed by varying narrow slot widths (w) and lengths (b) of larger slots of dumbbell shaped DGS etched in the ground plane. | 78 |
| Figure 5.21 | Geometry of a <i>Chebyshev</i> distributed LPF designed by varying both length (b) of PBGS and width (w) of the narrow slot of the dumbbell shaped DGS and interleaved square PGBS etched in the ground plane. | 78 |
| Figure 5.22 | Geometry of a <i>Chebyshev</i> distributed LPF designed by varying both length (b) of PBGS and width (w) of the narrow slot of the dumbbell shaped DGS and varying length of interleaved square PGBS etched in the ground plane. | 79 |
| Figure 5.23 | Geometry of a <i>Chebyshev</i> distributed LPF designed by varying both length (b) of PBGS and width (w) of the narrow slot of the dumbbell shaped DGS and varying width of interleaved square PGBS etched in the ground plane. | 80 |
| Figure 5.24 | Geometry of a <i>Chebyshev</i> distributed LPF designed by varying both width (b) of larger slots and width (w) of the narrow slot of the dumbbell shaped DGS and varying width of interleaved square PGBS etched in the ground plane. | 81 |
| Figure 5.25 | Geometry of a <i>Chebyshev</i> distributed LPF designed by varying both width (b) of larger slots and width (w) of the narrow slot of the dumbbell shaped DGS and varying lengths of interleaved square PGBSs etched in the ground plane. | 81 |
| Figure 5.26 | Geometry of a <i>Chebyshev</i> distributed LPF designed by varying widths (w) narrow slots and widths (b) of larger slots of dumbbell shaped DGS etched in the ground plane. | 82 |
| Figure 5.27 | Geometry of a Binomial and <i>Chebyshev</i> distributed LPF designed by varying widths (w) narrow slots by <i>Chebyshev</i> distribution and widths (b) of larger slots of dumbbell shaped DGS by binomial distribution etched in the ground plane. | 83 |
| Figure 5.28 | S-parameters performance of a transmission line over dumbbell shaped DGSs according to design 1 | 84 |
| Figure 5.29 | S-parameters performance of a transmission line over dumbbell shaped DGSs according to design 2 | 84 |
| Figure 5.30 | S-parameters performance of a transmission line over DGSs according to design 3. | 85 |
| Figure 5.31 | S-parameters performance of a transmission line over hybrid dumbbell shaped DGSs according to design 4 | 86 |
| Figure 5.32 | S-parameters performance of a transmission line over hybrid dumbbell shaped DGSs according to design 5 | 87 |

| | | |
|-------------|--|----|
| Figure 5.33 | S-parameters performance of a transmission line over dumbbell shaped DGSs according to design 6 | 88 |
| Figure 5.34 | S-parameters performance of a transmission line over hybrid DGSs according to design 7. | 89 |
| Figure 5.35 | S-parameters performance of a transmission line over hybrid DGSs according to design 8 | 90 |
| Figure 5.36 | S-parameters performance of a transmission line over hybrid DGSs according to design 9 | 91 |
| Figure 5.37 | S-parameters performance of a transmission line over hybrid DGSs according to design 10. | 92 |
| Figure 5.38 | S-parameters performance of a transmission line over hybrid DGSs according to design 11 | 93 |
| Figure 5.39 | S-parameters performance of a transmission line over dumbbell shaped DGSs according to design 12 | 94 |
| Figure 5.40 | S-parameters performance of a transmission line over dumbbell shaped DGSs according to design 13 | 95 |

List of Tables

| Table No. | Description | Page No. |
|------------------|---|-----------------|
| Table 3.1 | Element values for maximally flat, low-pass filter prototypes | 44 |
| Table 3.2 | Element Values for Equal-Ripple Low-Pass Filter Prototypes | 46 |
| Table 3.3 | 6 Elements Stepped Impedance LPF Design | 50 |
| Table 5.1 | Comparison of some structures with their S-Parameter performances | 95 |

List of Abbreviations

| | | |
|----------------------|----------|--|
| EBGS | : | Electromagnetic bandgap structure |
| PBGS | : | Photonic bandgap structure |
| UPBGS | : | Uniform PBGS |
| UWB | : | Ultra Wideband |
| SAR | : | Specific Absorption Rate |
| FF | : | Filling factor |
| BPF | : | Bandpass filter |
| DGS | : | Defected ground structure |
| MEMS | : | Micro electro mechanical systems |
| CPW | : | Coplanar waveguide |
| AMC | : | artificial magnetic conducting |
| UC-PBG | : | Uniplanar compact-photonic bandgap |
| EM | : | Electromagnetic |
| PC | : | Photonic crystal |
| 1-D, 2-D, 3-D | : | One dimensional, two dimensional, three dimensional |
| RF | : | Radio frequency |
| IL | : | Insertion Loss |
| RL | : | Return Loss |
| SWS | : | Slow wave structures |
| TEM | : | Transverse Electric and Magnetic |
| FDTD | : | Finite Difference Time-Domain |
| FEM | : | Finite Element Method |
| MOM | : | Method of moments |
| dB | : | Decibel |
| BW | : | Bandwidth |
| LPF | : | Lowpass filter |
| FSS | : | Frequency selective surfaces |
| VNA | : | Vector network analyzer |

List of Major Symbols

| | | |
|-------------------------|---|---------------------------------|
| ϵ_r | : | Dielectric constant |
| ϵ_{eff} | : | Effective relative permittivity |
| C_0 | : | Speed of light in free space |
| γ | : | Propagation constant |
| β | : | Phase Constant |
| π | : | Pi = 3.1415927 |
| ω | : | Angular frequency |
| k | : | Wave number (/m) |
| α | : | Attenuation constant |
| λ_g | : | Guided wavelength |
| λ_0 | : | Wavelength in air |
| Z_0 | : | Characteristic impedance |
| f_0 | : | Center frequency |
| S | : | Scattering parameters |

Chapter-1

Introduction

1.1 Electromagnetic Bandgap Structures (EBGS)

Electromagnetic bandgap materials are one of the most rapidly advancing materials in the electromagnetic arena. They have ability to induce the propagation of electromagnetic waves to a level that was not possible earlier [1]. Electromagnetic Band Gap (EBG) structures produced a wide variety of design alternatives for researchers working in the area of microwave and photonics. The focus is now towards on finding real applications combined with detailed modeling. Due to the incredible potential of EBGs, they find potential application in filter, antennas, waveguides, phased arrays and many other microwave devices and components [1]. New companies have also started to exploit the commercial potential of this technology [2].

Due to their unique properties, EBG materials are very popular for the researchers. Generally, EBG structures are the artificial periodic structures that assist the propagation of electromagnetic waves in a specified band of frequencies for all incident angles and all polarization states [3]. EBG structures are always used as a part of microwave devices in order to improve the performance of devices, especially to improve the gain patterns and to decrease the losses in transmissions. EBG structures are also known as high impedance surface due to their ability to suppress the surface wave at certain operational frequencies. In recent years, there has been a rapid increase in utilization of Electromagnetic bandgap (EBG) structures in electromagnetic and antenna community [4-5]. The sample design of EBG structure (square patterned 2-D structure beneath the transmission line) is shown in figure 1.1.

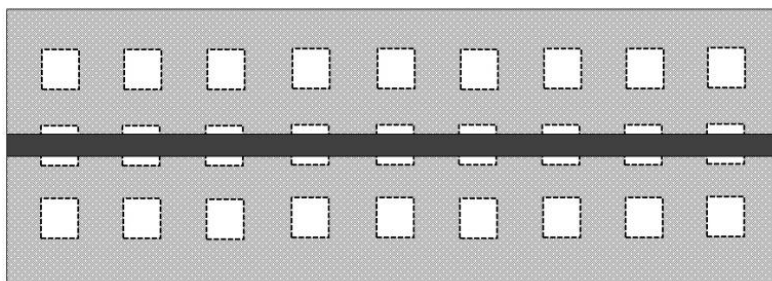


Figure 1.1: Geometry of a 3 rows (2-D) of uniform square EBGs beneath the transmission line.

The EBG structure is originated from the two papers published by Eli Yablonovitch and Sajeev John in 1987 [6-7] and breaks the traditional microwave circuit confined design to surface components and distributions of the medium circuit plane. In the 1980's Yoblonovitch stated that this PBG, produced by periodic variation in the refractive index of the structure, can be very useful as it could be used to eliminate the spontaneous emission of photons at certain frequency bands. Eli Yablonovitch introduced band gap which can control

radiation of light arbitrarily induced, and Sajeev John presented band gap which can ponder light waves into focus. They used the idea of capitalizing on the Bragg condition to construct materials that block all incoming light of a particular wavelength. The Bragg's condition is met when the planes of a crystal are situated such that each plane reflects a little of the incoming light [6].

In 1987, Yablonovitch published the first physical review letter discussing how to establish three dimensional periodic variation using PBG crystals. He fabricated the crystal structure by mechanically drilling holes of diameter in millimeter into a high dielectric constant material. That patterned material is known as "Yablonovitch" prohibited incident microwave signals from propagating in any direction. It manifested 3-D Band Gap.

Since 1987, other scientists have cited the potential of materials that completely reflect certain electromagnetic frequencies; these new findings have been valuable resources throughout the scientific community. In 1990, K. M. Ho, C. T. Chan and C. M. Soukoulis introduced computational demonstration of PBG band structure. From 1990, there had been several works on quantum electrodynamics in a PBG. In 1991, 2D system of PBG had experimented by S. Shultz and 3D system of PBG had experimented by A. Z. Genack & N, Garcia. In 1995, large scale 2D PBG macroporous silicon had introduced by U. Gruning and V. Lehman and woodpile structures had been introduced by E. Ozbay, S. Noda and S. Lin. That photonic bandgap structure obtained by stacking Alumina rods and the gap is between 12 and 14 GHz [8].

EBG structures received great attention due to their interesting properties, and their applications are spreading as fast as the advancement of the wireless communication systems and the fabrication technology. A multitude of basic EBG applications exists, especially within the microwave and low millimeter-wave region, for example, in electronically scanned phased arrays, high-precision GPS, Bluetooth, mobile telephony, waveguides, antennas, low loss-coplanar lines, and compact integrated filters [9–14]. In the microwave domain, many developments concern the direct control of the electromagnetic energy and its transmission: mirrors, electromagnetic windows, and radiation pattern control. Other applications include duplexers and controllable EBG materials.

EBG structures are used to prevent some undesired operating modes and control harmonics especially for ultra wideband (UWB) applications where several other applications coexist. More attention is being paid to the shielding property of the EBG to reduce specific absorption rate (SAR) into mobile phone operator's hand and head [15–17]. Also, it can shield the antennas from unwanted multipath signals which is important in multipoint communications [9]. In microwave filtering, the broad stopband can be exploited to suppress spurious passbands [18]. In addition to these, a standard waveguide can be modified by placing of electromagnetic crystal on the two sidewalls of a waveguide [19], potentially creating a very efficient wave guiding structure.

EBG structures have different forms such as bumpy surface, corrugated surface, metal pad or high-impedance surface and planar EBG structures. Normally the ground plane is etched by EBGs with different shape and different lattice structures. The shape may be uniform and

non-uniform and named as square, rectangular, triangular and honeycomb etc. Different shapes and sizes of EBGs provide different S-parameter performances. The EBG structures are also called the photonic bandgap structures (PBGs). The location of the EBG elements under the microstrip transmission line greatly influences the performance of the transmission line. However, one of their main significances is their ability to generate stopband performance. This concept is highly preferred for harmonic suppression of the filter.

Another significance of EBGs is their ability to provide slow-wave properties. For the compact design this property is used. Practically EBGs can be used in amplifiers, mixers, filters, waveguides, antennas and many other devices to improve their performances.

1.2 Objective of the Thesis

The main objectives of this thesis are to design novel low pass filter by EBG/PBG assisted microstrip transmission lines. PBG assisted transmission lines are investigated to see the improved performance in terms of ripple free smoother passband and wider stopband of the low pass filter (LPF). The goal of this research is to design a wider, deeper and steeper LPF using the ground plane of an ideal transmission line. PBG assisted low pass filter suppresses the stopband harmonics.

The motive of choosing the proper PBG structure is to achieve better performance from all the conventional designs. Firstly, the goal is to make the proper selection of PBG units, which will generate distinct passband and stopband characteristics of the designed frequency. The thesis will be limited mainly to circular, square and dumbbell shape patterned PBG structures. Uniform PBG structures have same filling factor (FF). FF is defined to be the volumetric ratio of one unit cell to the single PBG element. FF controls the width and depth of the stopband [20].

The general concept of increasing the stopband is the enhancement of FF. But beyond some value of FF the passband transmission suffers from the worst performances. This research will be carried out on non-uniform PBG structures with Binomial [21] and Chebyshev distributions [22]. The amplitudes of the PBG elements are calculated as per the coefficients of the distributions.

Next Dumbbell shaped DGSs will be investigated. In the open literature, researchers used Dumbbell shaped DGS structures having Binomial and Chebyshev distributions to improve the performance of the LPF design [23]. Such configurations need careful attention for both top and bottom layers of planar substrates. Attention will be focused to develop LPF performance by the perturbed ground plane only. The objectives of this thesis are:

- Design of novel EBG/PBG elements will provide distinct passband and stopband properties. The PBG elements with Binomial and *Chebyshev* distributions will be focused.
- Designing a low pass filter (LPF) over a 50 Ω transmission line assist with EBGs in the ground plane of the transmission line.
- Implementation of 1-D PBGs (Conventional PBGS and DGS) instead of 2-D PBGs in case of LPF design.

- The use of co-efficient of non-uniform distribution, namely Binomial and *Chebyshev* distributions to calculate the amplitude of the PBG elements that are used to replace the conventional PBG structures.
- Reducing the ripple from the passband of the low pass filter.
- Design of keeping the stopband level below -20 dB.
- Investigation into non-uniform Dumbbell shaped DGSs.
- Implementation of uniform and non-uniform PBG and dumbbell shaped DGS elements to improve the performance of the low pass filter.
- Investigating the hybrid designs of DGS-PBGS those will also achieve better performance.
- Realization of whole EBG/PBG assisted LPF structures with their designs.

1.3 Thesis Outline

The followings are the outline of the thesis:

- In **chapter 1**, the introduction of the thesis is reported. This chapter explains about the electromagnetic bandgap structures with its historical background. There also explains about the defected ground structures and their significance. The goals and propositions of low-pass filter have also been explained.
- In **chapter 2**, a comprehensive literature survey of PBG structures is reported. The investigations of the previous researchers are reported in this chapter.
- In **chapter 3**, transmission lines, microwave filters and their network analysis have been reported that results in the motivation, reasoning and the proposition of novel structures against the available structures in the literature. Also, the conventional low-pass filter structures are presented. The design equations are presented. The complexity of the conventional low-pass filter and the motivation of selecting the EBGs are reported in the literature.
- In **chapter 4**, uniform PBGSs and dumbbell shaped DGSs have been reported to see their performance. The 2-D and 1-D structures have been reported and described the reasoning about choosing the 1-D structure instead of 2-D structures.
- In **chapter 5**, non-uniform PBGSs, dumbbell shaped DGSs and hybrid DGSs have been reported to see their improved performance over conventional regular PBGSs. A nonuniformity in amplitudes will be realized by implementing Binomial and *Chebyshev* distribution in the designs.
- In **chapter 6**, conclusions and recommendation for future work have been presented.

Chapter-2

Literature Survey

2.1 Introduction

Various works on the recent development of Electromagnetic bandgap structures (EBGSs) has been reported in this chapter. EBG structures are found to play vital roles in enhancing the performance of the microwave components and devices. The stopband characteristic causes the significant improvement in the performance by suppressing surface waves, leakage and spurious transmission. Filling factor (FF) is one of the important controlling factors to yield wider and distinct stopband that should be optimized to maintain a smoother transmission in the passband. In the literature for uniform circular and rectangular patterned PBGSs the optimum filling factors are considered. These types of designs are considered as the conventional PBG structure design. Besides, the researchers have worked out on dumbbell shaped EBGS.

2.2 Application of EBGS

The modern microwave communication system requires high performance, compact size and low cost devices. To fulfil the requirement and to enhance performance some new structures like Photonic Bandgap Structure (PBGS), Defected Ground Structure (DGS), Substrate integrates waveguide (SIW) etc. are existing on the communication system. Recently, many researchers paid more attention to photonic bandgap structures (PBGSs) due to their unique properties. A summary of their works in this section are briefly discussed in this section.

2.2.1 Resonators and Filters using EBG Structures

- **Resonators**

Resonators based on EBG technology have been recently proposed as an alternative to current technologies [24-27]. Resonator structures can be fabricated on different laminates by using inexpensive standard printed circuit board (PCB) processing techniques and can be used in commercial products. Tim Eular and John Papapolymeror proposed a micro-machined resonator at 45 GHz based on defect induced EBG laminate with high quality factor and low losses [24].

- **Filters**

Some other researchers also designed high quality factor filters [24, 25], with high isolation [26] and low insertion losses [26, 27] with wide bandwidth. The concept of EBGs has been utilized to develop the devices of high isolation with high quality factor that can integrate monolithically with other components. According to the demands, Chappel and his co-workers designed 2, 3, and 6 pole filters using mettalo-dielectric EBG lattice. Chappel also designed a wide bandgap structure using the high-k ceramics, which was embedded into a polymer to create an EBG substrate. J.C Vardaxoglu et. al. also proposed a tunable wide bandgap using mettalo-dielectric EBGs [28]. Hell and his team proposed a reconfigurable

EBG cavity resonator with low insertion losses [29]. The use of EBG circuits for filter applications [19, 30-33] in microwave technology has been proposed in different ways. Vesna Radistic designed the EBG by etching a 2-D structure of holes in the ground plane of the microstrip circuit [30].

○ **Low Pass Filter (LPF)**

To produce compact designs using the "Uniplanar Compact EBG Structures" where, the slow wave effect is produced by a distributed LC two-dimensional structure, which allows a considerable size reduction in the circuit. A spurious-free band pass filter and high-performance, low pass filter using a coupled microstrip, was proposed by Fei-Ran Yang and his group [30].

In this case, the UC-PBG structure shown in figure 2.1 is used in the ground plane to improve the performance of conventional LPF [30]. A small portion of the 50-ohm feed line is placed on the perforated ground plane (UC-PBG plane), the remaining being on the solid ground plane. Duroid substrate is used with $\epsilon_r = 10.2$ and the thickness of the substrate is 25 mils. The width of the 50-ohm microstrip is 24 mils. The simulation result shows the wider stopband above 6 GHz and S_{21} is found to be under -30 dB for a wide frequency range. Within the stopband range, the return loss is found to be about 0 dB, indicating very little radiation loss which also verifies the PBG property. A stepped-impedance LPF with seven reactive elements has been chosen by [34].

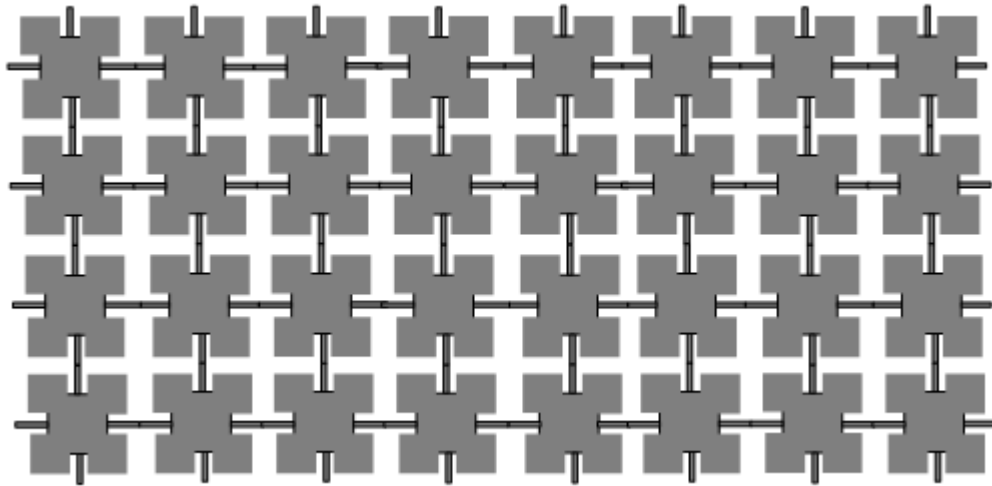


Figure 2.1: UC-PBG structure

From the comparison of PBG assisted and conventional filter, important findings are:

1. Maximum attenuation is increased from 20 dB to 58 dB due to the PBG application.
2. Spurious passband is completely suppressed.
3. The passband loss is comparable to the conventional LPF.
4. Application of PBG structure maintains matching conditions.
5. It does not increase the conductor loss.

○ Bandpass Filters (BPF)

Conventional parallel-coupled band pass filters (BPF) need extra filters to suppress the spurious transmission that results the increase of insertion loss. It is reported [35] that the use of extra filters can be avoided by just applying PBG to obtain a compact microstrip BPF with intrinsic spurious rejection. The well-matched microstrip on the UC-PBG ground plane is suited as a low-loss transmission line. The generated spurious passbands at higher harmonics can be suppressed with the aid of PBGS as it provides a wide and deep stopband. The physical length of the filter circuit is reduced as well due to the slow-wave effect of the UC-PBG structure. Fig. 2.2 shows the schematic of a microstrip BPF on the UC-PBG ground.

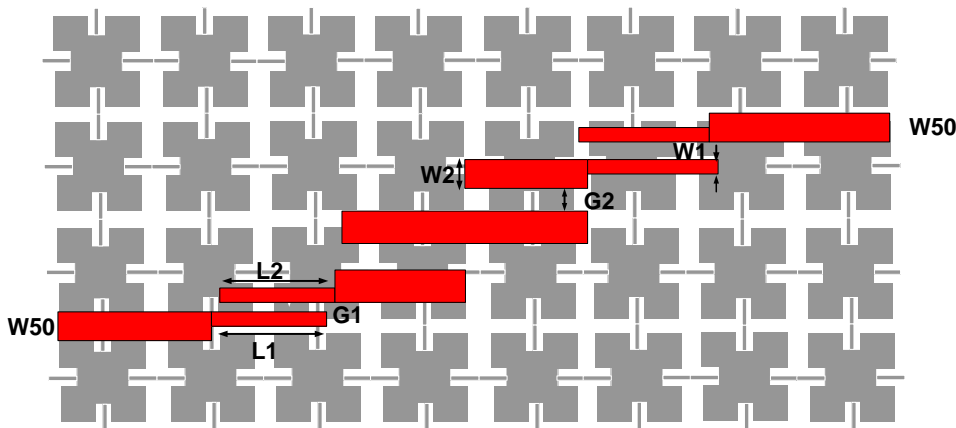


Fig. 2.2: Schematic diagram of a BPF over UC-PBG

The reference [34] narrates the standard design procedures of the parallel-coupled BPF. The requirements are [35]:

At the frequency of 12 GHz and 17 GHz, transmission co-efficient of a conventional BPF are seen to be -10 dB and -5 dB respectively. On the other hand the UC-PBG assisted filter provides the spurious suppression of 30-40 dB. Though the length of the microstrip resonator has been scaled accordingly to the slow-wave factor, but the coupling gap remains same, which results the increased fractional bandwidth (21.6 %) at 6 GHz center frequency. Like conventional BPF the coupling co-efficiency can be optimized to improve the bandpass characteristics of the PBG assisted BPF. Including the effect of two SMA connectors, the minimum insertion loss of the PBG assisted filter is found to be 1.9 dB at 6.39 GHz.

Loptegi and his researchers also designed different band pass filters using defect ground structures [19]. Ducaín Nescic proposed a PBG microstrip slow wave structure. This proposed structure exhibits slow wave and low pass characteristics. It was fabricated by using modified microstrip line, without etching the ground plane [31-33].

2.2.2 EBG Tuned Microwave Devices

In micro electro mechanical systems (MEMS) fabrication technologies, the position of the switches and membrane was modified electrically and local properties of the EBG components were modulated. In the fourth alternative, they use different dielectric substrates

are used in which the EBG structures were designed. By changing the permittivity and the permeability of the substrate, by using external electric or magnetic field, they achieve tuning in the EBG components is achieved.

A tunable filter using fractural electromagnetic bandgap structure was designed, simulated and fabricated, and its tuning was achieved using micro-machined capacitive bridge [36]. Another ultra wide bandstop filter was designed and tuned using MEMS switches based on EBG co-planar waveguides [37]. Tunable electromagnetic bandgap structures are based on ferroelectric or ferromagnetic thin films were also reported in the literature [38]. To achieve tunable EBG performance ferroelectric capacitors are also considered [36] [39]. In addition, to achieve tunable electromagnetic bandgap EBG performance, ferroelectric varactors are considered in LC circuits, for periodically loading coplanar waveguides (CPWs). Asymmetric or symmetric tuning of the bandgap width was achieved by changing the capacitance of the varactors in LC circuits [38]. Yongje Sung presented a novel approach to obtain the electromagnetic bandgap structure with a wide tunable stopband filter using dumbbell shaped defected ground structure (DGS) [40]. Miguel and researcher also proposed a multiple frequency tuned photonic bandgap microstrip structure [41].

2.2.3 Miniaturization

Miniaturization of microwave devices and antennas has become increasingly important in recent years. Modern wireless communication systems require small microwave elements that are relevant to high-level integrated into compact lightweight systems.

Miniaturization can be achieved by several techniques. Roger et al designed a magnetic conductor to reduce its size and cost. In order to do that, they integrated some capacitance of the FSS without resorting to a second layer of overlapping patches [42]. By increasing the capacitor and inductor in Sivenpiper High Impedance Surface, the size of the EBG cell was reduced [43]. Feresidis et al [44] introduced the concept of closely coupled metallo dielectric electromagnetic band-gap structure, and designed 2-D double layer dipole arrays. These arrays are closely packed.

It is well known that at certain frequencies outside the band gap, periodic structures support waves, commonly termed as slow waves, with reduced phase velocity and guided wavelength with respect to the wave propagating in a comparable homogeneous medium. This property can be exploited for the miniaturization of microwave elements, such as the triple array elements [45]. An approach to this is to examine the elements with periodic loading. Multiple-order periodic loading of basic elements possesses a good degree of flexibility in the design [45, 46]. Fractal-type structures are subsequently produced using a second order loading. This can also be used for multiband artificial magnetic conducting (AMC) designs [46]. Another way of increasing the length of the loading stubs without increasing the unit cell and at the same time to increasing the capacitive coupling between successive elements is the inter-digital topology. The loadings of successive dipoles are shifted so that they can extend to the full length allowed by the array geometry.

Chapter-3

Filter Terminologies and Conventional Filter Design

3.1 Introduction:

Filter networks are essential building elements in many areas of RF/microwave engineering. Such networks are used to select/reject or separate/combine signals at different frequencies in a host of RF/microwave systems and equipment. Although the physical realization of filters at RF/microwave frequencies may vary, the circuit network topology is common to all.

At microwave frequencies, voltmeters and ammeters for the direct measurement of voltages and currents do not exist. For this reason, voltage and current, as a measure of the level of electrical excitation of a network, do not play a primary role at microwave frequencies. On the other hand, it is useful to be able to describe the operation of a microwave network such as a filter in terms of voltages, currents, and impedances in order to make optimum use of low-frequency network concepts.

It is the purpose of this chapter to describe two port network concepts, network parameters and periodic structures and provide equations that are useful for the analysis of filter networks.

3.2 Network Variables:

Most RF/microwave filters and filter components can be represented by a two-port network, as shown in Figure 3.1, where V_1 , V_2 and I_1 , I_2 are the voltage and current variables at the ports 1 and 2, respectively, Z_{01} and Z_{02} are the terminal impedances, and E_s is the source or generator voltage. Note that the voltage and current variables are complex amplitudes when we consider sinusoidal quantities. For example, a sinusoidal voltage at port 1 is given by

$$v_1(t) = |V_1| \cos(\omega t + \phi) \quad (3.1)$$

We can then make the following transformations:

$$v_1(t) = |V_1| \cos(\omega t + \phi) = \text{Re}|V_1|e^{j(\omega t + \phi)} = \text{Re}V_1e^{j\omega t} \quad (3.2)$$

Where, Re denotes “the real part of” the expression that follows it. Therefore, one can identify the complex amplitude V_1 defined by

$$V_1 = |V_1| e^{j\phi} \quad (3.3)$$

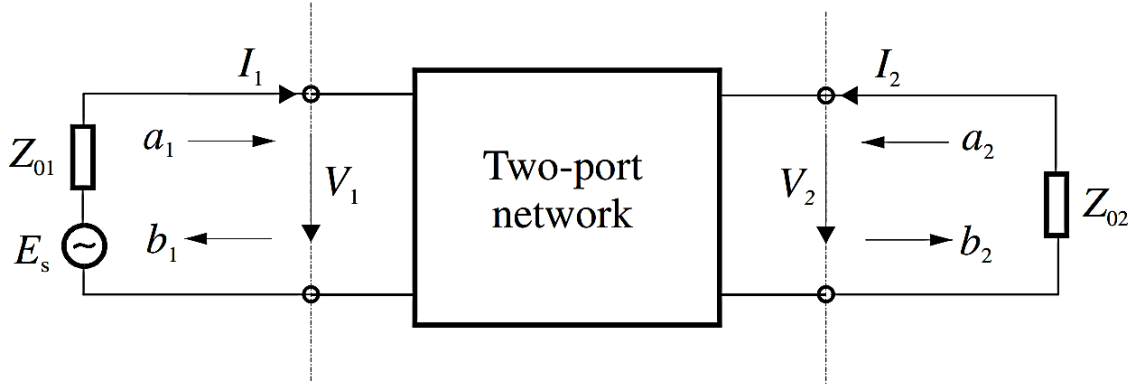


Figure 3.1: Two-port network showing network variables.

It is difficult to measure the voltage and current at microwave frequencies, the wave variables a_1 , b_1 and a_2 , b_2 are introduced, with 'a' indicating the incident waves and 'b' the reflected waves. The relationships between the wave variables and the voltage and current variables are defined as

$$V_n = \sqrt{Z_{0n}}(a_n + b_n) \quad (3.4a)$$

$$I_n = \frac{1}{\sqrt{Z_{0n}}}(a_n - b_n)$$

For $n=1$ and 2

$$a_n = \frac{1}{2} \left(\frac{V_n}{\sqrt{Z_{0n}}} + \sqrt{Z_{0n}} I_n \right) \quad (3.4b)$$

$$b_n = \frac{1}{2} \left(\frac{V_n}{\sqrt{Z_{0n}}} - \sqrt{Z_{0n}} I_n \right)$$

The above definitions guarantee that the power at port n is

$$P_n = \frac{1}{2} \text{Re}(V_n \cdot I_n^*) = \frac{1}{2} (a_n a_n^* - b_n b_n^*) \quad (3.5)$$

Where, the asterisk denotes a conjugate quantity. It can be recognized that $a_n a_n^*/2$ is the incident wave power and $b_n b_n^*/2$ is the reflected wave power at port n .

3.3 Scattering Parameters:

The scattering or S parameters of a two-port network are defined in terms of the wave variables as

$$S_{11} = \left. \frac{b_1}{a_1} \right|_{a_2=0} \quad S_{12} = \left. \frac{b_1}{a_2} \right|_{a_1=0} \quad (3.6)$$

$$S_{21} = \left. \frac{b_2}{a_1} \right|_{a_2=0} \quad S_{22} = \left. \frac{b_2}{a_2} \right|_{a_1=0}$$

Where $a_n = 0$ implies a perfect impedance match (no reflection from terminal impedance) at port n . These definitions may be written as

$$\begin{bmatrix} b_1 \\ b_2 \end{bmatrix} = \begin{bmatrix} S_{11} & S_{12} \\ S_{21} & S_{22} \end{bmatrix} \begin{bmatrix} a_1 \\ a_2 \end{bmatrix} \quad (3.7)$$

Where, the matrix containing the S parameters is referred to as the scattering matrix or S matrix, which may simply be denoted by [S].

The parameters S_{11} and S_{22} are also called the reflection coefficients, whereas S_{12} and S_{21} the transmission coefficients. These are the parameters directly measurable at microwave frequencies. The S parameters are in general complex, and it is convenient to express them in terms of amplitudes and phases, i.e., $S_{mn} = |S_{mn}| e^{j\phi_{mn}}$ for $m, n = 1, 2$. Often their amplitudes are given in decibels (dB), which are defined as

$$20 \log |S_{mn}| \text{ dB} \quad m, n = 1, 2 \quad (3.8)$$

Where, the logarithm operation is base 10. For filter characterization, we may define two parameters:

$$\begin{aligned} L_A &= -20 \log |S_{mn}| \text{ dB} \quad m, n = 1, 2 \quad (m \neq n) \\ L_R &= -20 \log |S_{nn}| \text{ dB} \quad n = 1, 2 \end{aligned} \quad (3.9)$$

Where, L_A denotes the insertion loss between ports n and m and L_R represents the re-turn loss at port n . Instead of using the return loss, the voltage standing wave ratio *VSWR* may be used. The definition of *VSWR* is

$$VSWR = \frac{1 + |S_{nn}|}{1 - |S_{nn}|} \quad (3.10)$$

Whenever a signal is transmitted through a frequency-selective network such as a filter, some delay is introduced into the output signal in relation to the input signal. There are other two parameters that play role in characterizing filter performance related to this delay. The first one is the phase delay, defined by

$$\tau_p = \frac{\phi_{21}}{\omega} \text{ seconds} \quad (3.11)$$

Where, ϕ_{21} is in radians and ω is in radians per second. Port 1 is the input port and port 2 is the output port. The phase delay is actually the time delay for a steady sinusoidal signal and is not necessarily the true signal delay because a steady sinusoidal signal does not carry information; sometimes, it is also referred to as the carrier delay [47]. The most important parameter is the group delay, defined by

$$\tau_d = \frac{d\phi_{21}}{d\omega} \text{ seconds} \quad (3.12)$$

This represents the true signal (baseband signal) delay, and is also referred to as the envelope delay.

In network analysis or synthesis, it may be desirable to express the reflection parameter S_{11} in terms of the terminal impedance Z_{01} and the so-called input impedance $Z_{in 1} = V_1/I_1$, which is

the impedance looking into port 1 of the network. Such an expression can be deduced by evaluating S_{11} in (3.6) in terms of the voltage and current variables using the relationships defined in (3.4b). This gives

$$S_{11} = \left. \frac{b_1}{a_1} \right|_{a_2=0} = \frac{V_1/\sqrt{Z_{01}} - \sqrt{Z_{01}}I_1}{V_1/\sqrt{Z_{01}} + \sqrt{Z_{01}}I_1} \quad (3.13)$$

Replacing V_1 by $Z_{in 1} I_1$ results in the desired expression

$$S_{11} = \frac{Z_{in 1} - Z_{01}}{Z_{in 1} + Z_{01}} \quad (3.14)$$

Similarly, we can have

$$S_{22} = \frac{Z_{in 2} - Z_{02}}{Z_{in 2} + Z_{02}} \quad (3.15)$$

Where, $Z_{in2} = V_2/I_2$ is the input impedance looking into port 2 of the network. Equations (3.14) and (3.15) indicate the impedance matching of the network with respect to its terminal impedances. The S parameters have several properties that are useful for network analysis. For a reciprocal network $S_{12} = S_{21}$. If the network is symmetrical, an additional property, $S_{11} = S_{22}$, holds. Hence, the symmetrical network is also reciprocal. For a lossless passive network the transmitting power and the reflected power must equal to the total incident power. The mathematical statements of this power conservation condition are

$$S_{21}S_{21}^* + S_{11}S_{11}^* = 1 \text{ or } |S_{21}|^2 + |S_{11}|^2 = 1 \quad (3.16)$$

$$S_{12}S_{12}^* + S_{22}S_{22}^* = 1 \text{ or } |S_{12}|^2 + |S_{22}|^2 = 1$$

3.4 Symmetrical Network Analysis:

If a network is symmetrical, it is convenient for network analysis to bisect the symmetrical network into two identical halves with respect to its symmetrical interface. When an even excitation is applied to the network, as indicated in Figure 3.2(a), the symmetrical interface is open-circuited, and the two network halves become the two identical one-port, even-mode networks, with the other port open-circuited. In a similar fashion, under an odd excitation, as shown in Figure 3.2 (b), the symmetrical interface is short-circuited and the two network halves become the two identical one-port, odd-mode networks, with the other port short-circuited. Since any excitation to a symmetrical two-port network can be obtained by a linear combination of the even and odd excitations, the network analysis will be simplified by first analyzing the one-port, even- and odd-mode networks separately, and then determining the two-port network parameters from the even- and odd-mode network parameters.

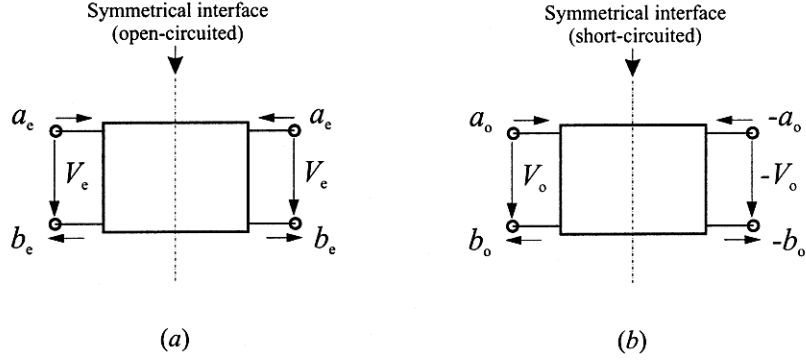


Figure 3.2: Symmetrical two-port networks with (a) even-mode excitation, and (b) odd-mode excitation.

For example, the one-port, even- and odd-mode S parameters are

$$S_{11e} = \frac{b_e}{a_e} \quad S_{11o} = \frac{b_o}{a_o} \quad (3.17)$$

Where, the subscripts e and o refer to the even mode and odd mode, respectively. For the symmetrical network, the following relationships of wave variables hold

$$\begin{aligned} a_1 &= a_e + a_o & a_2 &= a_e - a_o \\ b_1 &= b_e + b_o & b_2 &= b_e - b_o \end{aligned} \quad (3.18)$$

Letting $a_2=0$, we have from (3.17) and (3.18) that

$$\begin{aligned} a_1 &= 2a_e = 2a_o \\ b_1 &= S_{11e}a_e + S_{11o}a_o \\ b_2 &= S_{11e}a_e - S_{11o}a_o \end{aligned} \quad (3.19)$$

Substituting these results into the definitions of two-port S-parameters gives

$$\begin{aligned} S_{11} &= \left. \frac{b_1}{a_1} \right|_{a_2=0} = \frac{1}{2}(S_{11e} + S_{11o}), & S_{21} &= \left. \frac{b_2}{a_1} \right|_{a_2=0} = \frac{1}{2}(S_{11e} - S_{11o}) \\ S_{22} &= S_{11} \text{ and } S_{21} = S_{12} \end{aligned} \quad (3.20)$$

Let, Z_{ine} and Z_{ino} represent the input impedances of the one-port, even- and odd-mode networks. According to (3.14), the reflection coefficients in (3.17) can be given by

$$S_{11e} = \frac{Z_{ine} - Z_{01}}{Z_{ine} + Z_{01}} \quad \text{and} \quad S_{11o} = \frac{Z_{ino} - Z_{01}}{Z_{ino} + Z_{01}} \quad (3.21)$$

3.5 ABCD Parameters:

The ABCD parameters of a two-port network are given by

$$A = \left. \frac{V_1}{V_2} \right|_{I_2=0} \quad B = \left. \frac{V_1}{-I_2} \right|_{V_2=0} \quad (3.22)$$

$$C = \left. \frac{I_1}{V_2} \right|_{I_2=0} \quad D = \left. \frac{I_1}{-I_2} \right|_{V_2=0}$$

These parameters are actually defined in a set of linear equations in matrix notation

$$\begin{bmatrix} V_1 \\ I_1 \end{bmatrix} = \begin{bmatrix} A & B \\ C & D \end{bmatrix} \begin{bmatrix} V_2 \\ -I_2 \end{bmatrix} \quad (3.23)$$

Where, the matrix comprised of the ABCD parameters is called the ABCD matrix. Sometimes, it may also be referred to as the transfer or chain matrix. The ABCD parameters have the following properties:

$$AD - BC = 1 \quad \text{For a reciprocal network} \quad (3.24)$$

$$A = D \quad \text{For a symmetrical network} \quad (3.25)$$

If the network is lossless, then A and D will be purely real and B and C will be purely imaginary.

3.6 Filter:

A filter is a two-port network used to control the frequency response at a certain point in an RF or microwave system by providing transmission at frequencies within the passband of the filter and attenuation in the stopband of the filter [48]. Typical frequency responses include low-pass, highpass, bandpass, and band-reject characteristics. The frequency response can be classified into a number of different band-forms describing which frequency bands the filter passes (the passband) and which it rejects (the stopband):

- Low-pass filter** – low frequencies are passed, high frequencies are attenuated.
- High-pass filter** – high frequencies are passed, low frequencies are attenuated.
- Band-pass filter** – only frequencies in a frequency band are passed.
- Band-stop filter or band-reject filter** – only frequencies in a frequency band are attenuated.

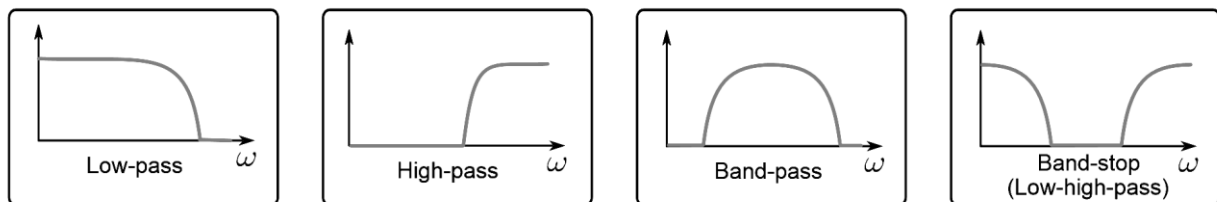


Figure 3.3: Graphical representation of different types of filter [49].

Applications can be found in virtually any type of RF or microwave communication, radar, or test and measurement system.

3.6.1 Advantages of Filters:

Filters are at the heart of many design problems. They are used to separate or combine signals of different frequencies, such as in multichannel communications systems, or in components such as frequency converters. The electromagnetic spectrum is limited and has to be shared; filters are used to confine the radiation from high-power transmitters within assigned spectral

limits; conversely, other filters are used to protect receivers from interference outside their operating bands. Filter like networks occur in impedance matching, as between two transmission lines of different characteristic impedances; or between a resistive generator and a reactive load. Sometimes it is necessary to obtain certain phase characteristics, for example, to compensate for the phase distortion produced by another filter or dispersive structure components whose design benefits from filter theory range from directional couplers to circular polarizers.

3.6.2 Microwave:

Electromagnetic waves at the frequency range of about 2 to 40 GHz are referred to as microwave. Microwave radio operates in unlicensed bands are 2.4 GHz and 5.7 GHz and are licensed band it could operate like 6 GHz, 7 GHz, 8 GHz, 9 GHz, 10 GHz, 11 GHz, 13 GHz, 15 GHz, 18 GHz, 23 GHz and 38 GHz frequency bands. At these frequencies, highly directional beams are possible and microwave is quite suitable for point-to-point transmission. Concentrating all the energy into a small beam using a parabolic antenna gives a much higher signal to noise ratio, but the transmitting and receiving antennas must be accurately aligned with each other. It's an unbounded transmission medium. Microwave is mainly used for satellite communications.

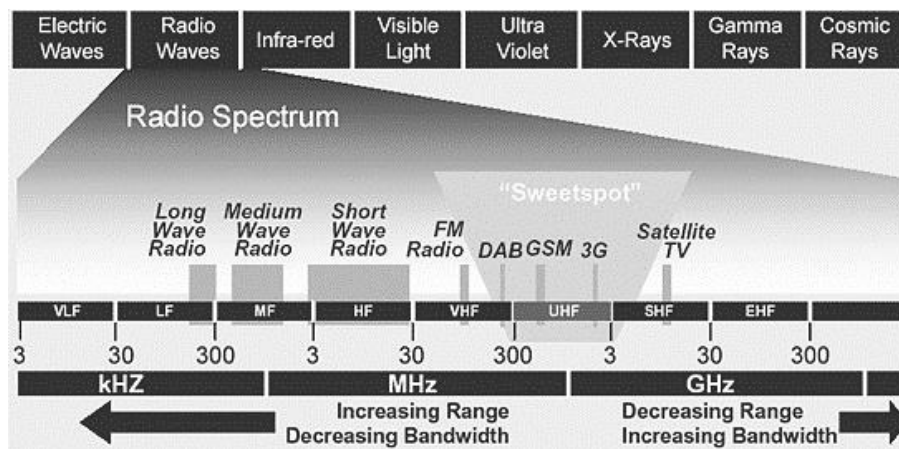


Figure 3.4: Communication Frequency spectrum

A microwave includes an antenna, radio, multiplexes, waveguide and feed cables. Based on capacity and radio equipment, antenna size, tower heights and terrain evaluation will play a major role in how it will be planned and construct the system. These four factors also will dedicate system reliability, multi-path fading, fade margins calculations, freshnel zone clearance, interference analysis, system diversity and long distance specifications.

3.6.3 Microwave Filter:

Microwave components are the most important components in receivers. The main functions of the filters are: (1) to reject undesirable signals outside the filter pass band and (2) to separate or to combine signals according to their frequency. A microwave filter is defined as the two port network, which is used to control the frequency response at a certain point in a microwave system by providing transmission at frequencies within the passband of the filter and attenuation in the stopband of the filter.

In microwave frequencies lumped elements never used and thus transmission line selections are used which behave as inductors and capacitors. The important thing is this filter minimizes the losses of the passband. The great advantage is it is not only reduces the overall losses for a transistor, but also improves the noise figure when used with a receiver.

3.6.4 General Use of Filter Principles in Terms of Microwave

Components:

As can be readily seen by extrapolating from discussions in preceding sections, microwave filter design techniques when used in their most general way are fundamental to the efficient design of a wide variety of microwave components. Generally, these techniques are basic to the designs when selecting, rejecting or channeling of energy of different frequencies is important. It is also important to achieve energy transfer with low reflection over a wide band and to achieve a controlled time delay. The possible specific practical situations where such considerations arise are too numerous and varied to permit any attempt to treat them individually herein.

3.6.5 Definition of terms used for microwave filter design:

- **Insertion loss (IL):**

Insertion loss is equal to the difference in dB power measured at the filter input and at the filter output. The power measured at the filter input is equal to the measured Power when the filter is replaced by a properly matched power meter or network analyzer. The input impedance of the measuring instrument should be equal to the characteristic impedance of the filter or system. Unless otherwise specified, Mini-Circuits filters are designed for 50 ohm systems. Similarly, the power measured at the filter output is equal to the measured power when the filter is terminated by the same measuring instrument as discussed. The insertion loss will be equal to the sum of three loss factors. One is the loss due to the impedance mismatch at the filter input, the second is due to the mismatch at the filter output, and the third is due to the dissipative loss associated with each reactive element within the filter.

Mathematically, insertion loss means 10 times of the logarithmic values of the ratio of transmitting power to the incident power.

$$\text{insertion loss} = 10 \log_{10} \left(\frac{p_t}{p_i} \right) \quad (3.26)$$

- **Return Loss (RL):**

Return loss is the loss of power in the signal returned/reflected by a discontinuity in a transmission line. This discontinuity can be a mismatch with the terminating load or with a device inserted in the line. It is usually expressed as a ratio in decibels (dB). Return loss is related to both standing wave ratio (SWR) and reflection coefficient (Γ). Increasing return loss corresponds to lower SWR. Return loss is a measure of how well devices or lines are matched. A match is good if the return loss is high. A high return loss is desirable and results in a lower insertion loss.

Mathematically, insertion loss means 10 times of the logarithmic values of the ratio of reflecting power to the incident power.

$$\text{return loss} = 10 \log_{10} \left(\frac{p_r}{p_i} \right) \quad (3.27)$$

- **Pass Band:**

Pass band is equal to the frequency range for which the filter insertion loss is less than a specified value. For example, most of the Mini-Circuits' low-pass filter (LPF) models are specified to have a maximum insertion loss value of 1 dB within the pass band.

- **Stop Band:**

Stop band is equal to the frequency range at which the filter insertion loss is greater than a specified value. For example, most of the Mini-Circuits' low-loss filter (LPF) models are characterized by the frequency range where the insertion loss is greater than 20 dB and 40 dB in the stop band. These two values are arbitrary; they could easily have been chosen for some other values. The purpose of selecting 20 dB and 44 dB is twofold. One is to provide the design engineer with a simple means to calculate the frequency selectivity of the filter. The second is to allow a quick calculation of the suitability of the filter in a particular situation. Since 20 dB or 40 dB represent sufficient loss requirements in many systems, these values were chosen. The data in this handbook provide actual loss values as a function of frequency. For many Mini-Circuit filters the stop band losses can exceed 60dB.

- **Cutoff Frequency:**

Cut-off frequency, f_{co} is the frequency at which the filter insertion loss is equal to 3dB. It is a very convenient point of expressing the pass band and stop band boundary points. In addition, it allows a convenient means to normalize the frequency response of a filter. For example, if the frequency of a low-pass filter (LPF) response were divided by f_{co} then the resulting response would be "normalized" to f_{co} . The normalized response allows the design engineer to quickly specify the filter needed to meet his system requirements.

- **Slow Wave:**

Electromagnetic waves having the velocity lower than the velocity of light in free space are called slow waves. Periodic perturbation in the ground plane provides periodic discontinuity. Slow wave structures (SWS) are promising candidates for compact designs.

3.6.6 Periodic Structures:

An infinite transmission line or waveguide periodically loaded with reactive elements is an example of a periodic structure. As shown in Figure 3.5, periodic structures can take various forms, depending on the transmission line media being used. Often the loading elements are formed as discontinuities in the line itself, but in any case they can be modeled as lumped reactance in shunt (or series) on a transmission line, as shown in Figure 3.6. Periodic structures support slow-wave propagation (slower than the phase velocity of the unloaded line), and have passband and stopband characteristics similar to those of filters; they find application in traveling-wave tubes, masers, phase shifters, and antennas.

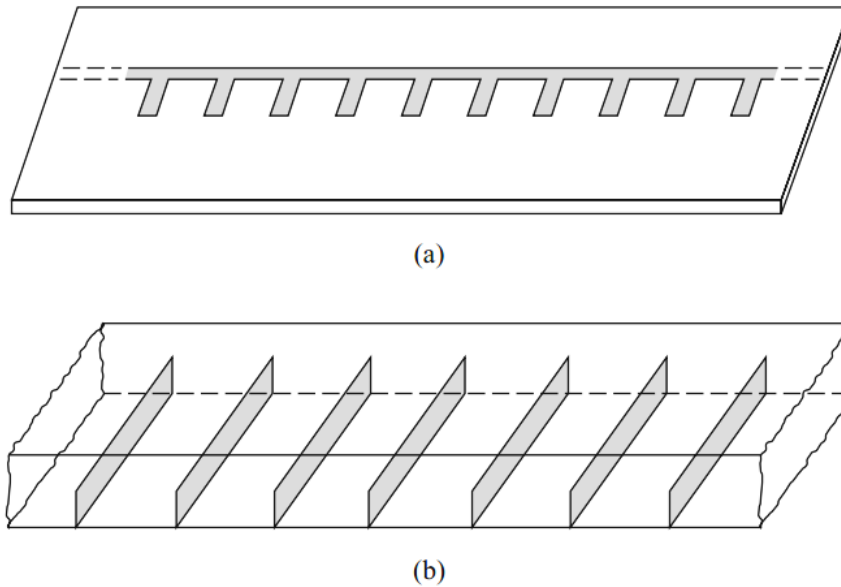


Figure 3.5.: Examples of periodic structures. (a) Periodic stubs on a microstrip line. (b) Periodic diaphragms in a waveguide.

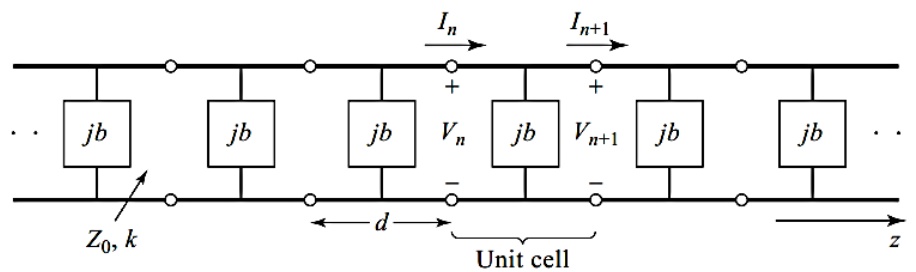


Figure 3.6.: Equivalent circuit of a periodically loaded transmission line. The unloaded line has characteristic impedance Z_0 and propagation constant k .

3.6.7 Capacitively loaded transmission-line-circuit analysis:

A simple capacitively loaded transmission line can be analyzed to conceive the idea of periodic structures. The velocity of EM wave in a physically smooth transmission line can be written as

$$V_p = \frac{1}{\sqrt{LC}} = \frac{1}{\sqrt{\mu_0 \epsilon_0 \epsilon_r}} \quad (3.28)$$

Where,

V_p is the phase velocity of EM wave.

L is the series inductance per unit length.

C is the shunt capacitance per unit length.

ϵ_r is the dielectric constant of the medium surrounding the conductor.

ϵ_0 and μ_0 are free-space values of the permittivity and permeability respectively.

From equation (3.28) it is seen that with the value of the dielectric constant (ϵ_r), the phase velocity of EM waves reduces. One problem arises in this simplest way of reducing the phase velocity. If the value of dielectric constant is increased then the higher-order mode of wave propagates. To avoid this propagation, the cross sectional dimensions of the line must be reduced accordingly. This is the limitation of increasing the value of dielectric constant to get the reduced value of the phase velocity of EM waves.

We know $LC = \mu_0\epsilon$ for dielectric media. So any attempt of increasing the value of C to reduce the phase velocity is restricted here. Because if the value of C is increased the value of L will be automatically reduced to maintain the relation, $LC = \mu_0\epsilon$ in a physically smooth transmission line. Under this circumstance, the restriction of a physically smooth transmission line can be relaxed instead of an electrical smooth line. An effective increase in the shunt capacitance per unit length (C) can be achieved without disturbing the value of inductance per unit length (L) by loading lumped shunt capacitance at periodic intervals where the spacing between the loaded shunt capacitance are small compared with the wavelength. At this stage, though the line is not physically smooth, but it will be an electrically smooth line. Under this condition the capacitance will be increased which can be observed from the following equation of the phase velocity.

$$V_p = \frac{1}{\sqrt{(C + C_0/d)L}} = \frac{\omega}{\beta} \quad (3.29)$$

Where C_0/d is the loaded lumped capacitance per unit length and C_0 is the capacitance loaded per interval d .

There are many ways of obtaining periodic structures. One of the simplest ways is to load a thin diaphragm at regular intervals in a coaxial transmission line. The diaphragm may be machined as the integral part of the center conductor. The fringing electric field in the vicinity of the diaphragm increases the local storage of the electric energy and hence giving more extra shunt capacitance.

3.6.8 Circuit Analysis of a Periodic Structure

A transmission line can be considered as the combination of finite unit cells of the structure. Figure 3.7(a) is the equivalent circuit of a basic unit cell of a capacitively loaded coaxial line and Figure 3.7(b) is the complete transmission line composed of the basic unit cell.

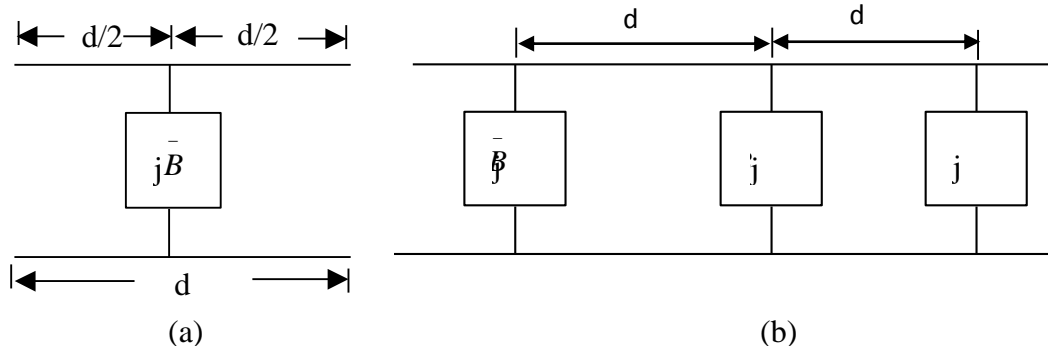


Figure 3.7: (a) Equivalent circuit model of a unit cell, (b) a transmission line cascaded by unit cells. The unit cell may be divided into three parts as a transmission line of length $d/2$ on either side of normalized susceptance B .

3.6.9 Analysis of Infinite Periodic Structures:

We first consider the propagation characteristics of the infinite loaded line shown in Figure 3.6. Each unit cell of this line consists of a length, d , of transmission line with a shunt susceptance across the midpoint of the line; the susceptance, b , is normalized to the characteristic impedance, Z_0 . If we consider the infinite line as being composed of a cascade of identical two-port networks, we can relate the voltages and currents on either side of the n^{th} unit cell using the ABCD matrix:

$$\begin{bmatrix} V_n \\ I_n \end{bmatrix} = \begin{bmatrix} A & B \\ C & D \end{bmatrix} \begin{bmatrix} V_{n+1} \\ I_{n+1} \end{bmatrix} \quad (3.30)$$

Where A , B , C and D are the matrix parameters for a cascade of a transmission line section of length $d/2$, a shunt susceptance b , and another transmission line section of length $d/2$. The reader can verify that $AD - BC = 1$, as required for reciprocal networks.

For a wave propagating in the $+z$ direction, we must have

$$V(z) = V(0)e^{-\gamma z} \quad (3.31)$$

$$I(z) = I(0)e^{-\gamma z}$$

for a phase reference at $z = 0$. Since the structure is infinitely long, the voltage and current at the n^{th} terminals can differ from the voltage and current at the $n + 1$ terminals only by the propagation factor, $e^{-\gamma d}$. Thus,

$$V_{n+1} = V_n e^{-\gamma d} \quad (3.32)$$

$$I_{n+1} = I_n e^{-\gamma d}$$

Using this result in (3.28) gives the following:

$$\begin{bmatrix} V_n \\ I_n \end{bmatrix} = \begin{bmatrix} A & B \\ C & D \end{bmatrix} \begin{bmatrix} V_{n+1} \\ I_{n+1} \end{bmatrix} = \begin{bmatrix} V_{n+1} e^{\gamma d} \\ I_{n+1} e^{\gamma d} \end{bmatrix} \quad (3.33)$$

For a nontrivial solution, the determinant of the above matrix must vanish:

$$AD + e^{2\gamma d} - (A + D)e^{\gamma d} - BC = 0 \quad (3.34)$$

or, since $AD - BC = 1$,

$$1 + e^{2\gamma d} - (A + D)e^{\gamma d} = 0$$

$$e^{-\gamma d} + e^{\gamma d} = A + D$$

$$\cosh \gamma d = \frac{A+D}{2} = \cos \theta - \frac{b}{2} \sin \theta \quad (3.35)$$

Now, if $\gamma = \alpha + j\beta$, we have that

$$\cosh \gamma d = \cosh \alpha d \cosh \beta d + j \sinh \alpha d \sinh \beta d = \cos \theta - \frac{b}{2} \sin \theta \quad (3.36)$$

Since the right-hand side of (3.36) is purely real, we must have either $\alpha = 0$ or $\beta = 0$.

- **Explanation**

Case 1: $\alpha = 0, \beta \neq 0$. This case corresponds to a nonattenuated propagating wave on the periodic structure, and defines the passband of the structure. Equation (3.36) reduces to

$$\cosh \beta d = \cos \theta - \frac{b}{2} \sin \theta \quad (3.37a)$$

which can be solved for β if the magnitude of the right-hand side is less than or equal to unity. Note that there are an infinite number of values of β that can satisfy (3.37a).

Case 2: $\alpha \neq 0, \beta = 0, \pi$. In this case the wave does not propagate, but is attenuated along the line; this defines the stopband of the structure. Because the line is lossless, power is not dissipated, but is reflected back to the input of the line. The magnitude of (3.36) reduces to

$$\cosh \alpha d = \left| \cos \theta - \frac{b}{2} \sin \theta \right| \geq 1 \quad (3.37b)$$

which has only one solution ($\alpha > 0$) for positively traveling waves; $\alpha < 0$ applies for negatively traveling waves. If $\cos \theta - (b/2) \sin \theta \leq -1$, (2.37b) is obtained from (3.36) by letting $\beta = \pi$; then all the lumped loads on the line are $\lambda/2$ apart, yielding an input impedance the same as if $\beta = 0$.

Thus, depending on the frequency and normalized susceptance values, the periodically loaded line will exhibit either passbands or stopbands, and so can be considered as a type of filter. It is important to note that the voltage and current waves defined in (3.31) and (3.33) are meaningful only when measured at the terminals of the unit cells, and do not apply to voltages and currents that may exist at points within a unit cell. These waves are similar to the elastic waves (Bloch waves) that propagate through periodic crystal lattices.

3.7 Electromagnetic Bandgap Structures (EBGS)

3.7.1 Types of Electromagnetic Bandgap Structures (EBGS)

EBG structures are periodic in nature, which may be realized by drilling, cuffing, and etching on the metal or dielectric substrates. They may be formed in the ground plane or over the substrate. On the basis of dimensions EBG structures are categorized as one dimensional (1-D), two dimensional (2-D), and three dimensional (3-D) periodic structures that satisfies Bragg's conditions, i.e., inter-cell separation (period) is close to half guided wavelength ($\lambda_g/2$). They are capable of forbidding electromagnetic propagation in either all or selected directions [62] [51].

1. 3-D EBG Crystals

In the beginning a 3D EBG was designed only. A successful attempt to obtain a 3D periodic dielectric structure was made in Iowa State University (ISU) [4]. It was called the woodpile structure as shown in the figure 2.8. Three dimensional EBG crystals have periodicity along all the three dimensions and the remarkable feature is that these systems can have complete band gaps, therefore, that propagation states are not allowed in any direction [52]. Although, a perfect 3-D EBG structure is required to block all waves in all directions, but then these structures are difficult to fabricate and integrate. From the literature, we learned that 2-D EBG could be even more valuable. 2-D EBG structures are easy to fabricate and are capable of maintaining a similar control on the wave propagation in the structure as the 3-D structure.

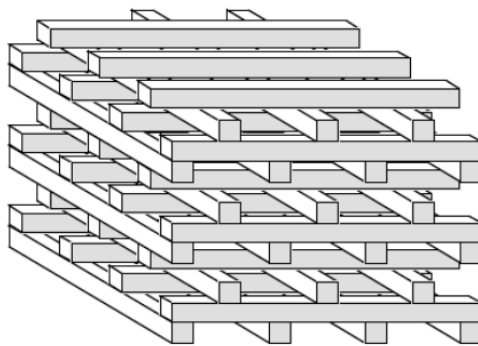


Figure 3.8: Three dimensional EBG structure [51]

2. 2-D EBG Crystals

These crystals have periodicity in two dimensions and are homogeneous along the third direction, or we can say that, all variations happen in the two dimensions, whereas everything is constant along the third dimension, thereby propagation is allowed along one axis of the crystal [51]. These 2-D EBG structures have substantial advantages in terms of compactness, stability, and fabrication, which make them more attractive for microwave devices [52]. One of the greatest advances in the development of these 2-D EBG structures in microwave range has been their implementation in microstrip technology.

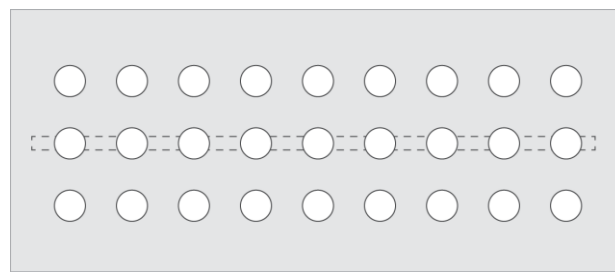


Figure 3.9: Two dimensional EBG structure[53] [54].

3. 1-D EBG Crystals

One dimensional EBG structures can also be implemented in microstrip technology. 1-D EBG structures have periodicity of two different media along one direction only. These basic crystals exhibit three important phenomena: photonic band gaps, localized modes, and

surface states. However, as the index contrast is only along one direction, the band gaps and bound states are limited to that direction. Nevertheless, these simple structures show most of the features of 2-D and 3-D EBG crystals [55].

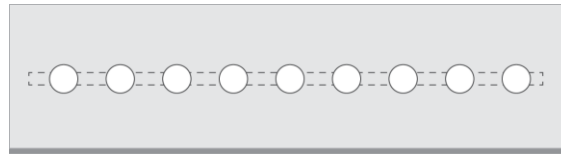


Figure 3.10 One dimensional EBG structure [56].

3.7.2 PBG Structures

PBG structures are periodic in nature, which may be realized by drilling, cutting and etching on the metal or substrates. They may be formed in the ground plane or over the substrate. The transmission line can also be modified to form PBG characteristics without having any perturbation in the ground plane [57], [58], [59]. This new idea can be extended to filter, antenna and other microwave component and devices where the complexity of packaging is minimized. The PBG configuration is categorized as shown in Fig. 2.11. On the basis of dimension, PBG structures may be divided into 1-D, 2-D and 3-D PBGSs. Planar PBG structures and their applications to antennas has been reported in [60]. Following are the descriptions of different PBG structures.

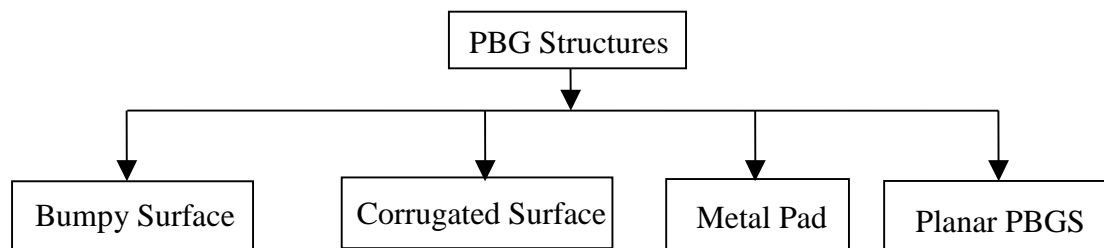


Figure 3.11: Different PBG structures

- **Bumpy Surface**

Several configurations have been reported in the literature. The first structure is made by drilling a periodic pattern of holes in the substrate or etching a periodic pattern of circles in the ground plane. A bumpy metal sheet [61]-[63] has a narrow surface wave band-gap. Electric field wraps around the bumps at the upper edge of the band gap and the electric field also extends across the bumps at the lower edge of the band-gap, hence a slow wave structure is formed. Bumpy surface is shown in Fig. 3.12.

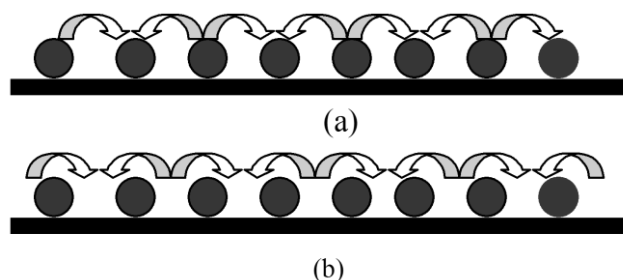


Figure 3.12: Bumpy metal sheet: (a) electric field extends across the bumps at the lower edge and (b) electric field wraps around the bumps at the upper edge

- **Corrugated Surface**

A corrugated surface [36][64] is a metal slab into which a series of vertical slots are cut. The slots are narrow so that many of them fit within one wavelength across the slab. Each slot can be regarded as a parallel plate transmission line, running down into the slab, and shorted at the bottom. If the slots are one quarter-wavelength deep, then the short circuit at the bottom is transformed by the length of the slots into an open circuit at the top end. Thus the impedance at the top end is very high. In this situation the surface impedance is capacitive and transverse magnetic (TM) surface waves are forbidden. Furthermore, a plane wave polarized with the electric field perpendicular to the ridges will appear to be reflected with no phase reversal. Corrugated surface is shown in Fig. 3.13.

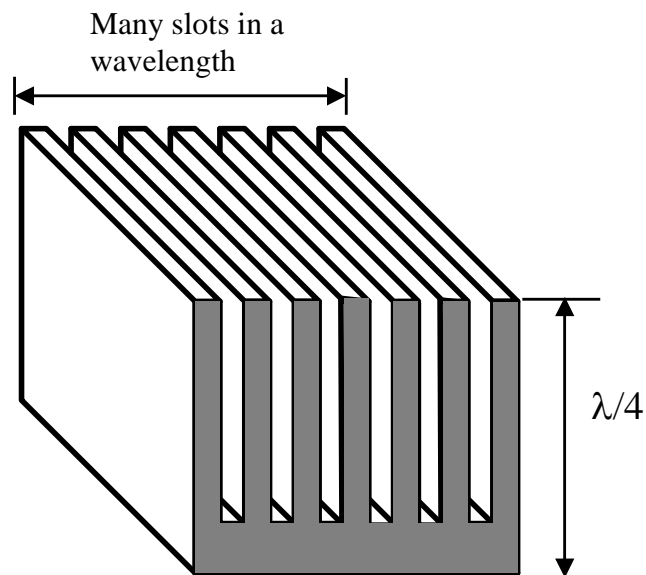


Figure 3.13: Corrugated metal surface

- **Metal Pad or High-Impedance Surface**

A more effective and compact approach, compared to the corrugated surfaces, which makes use of a triangular or square lattice of metal pads connected to ground with vias, has been recently proposed and applied in [65] to enhance the gain of planar antennas. These structures are the first realization of planar compact electromagnetic crystals with a complete stop-band in the microwave range. This type of structure with a triangular lattice of hexagonal metal plates and square vias to ground is shown in Figure 3.14.

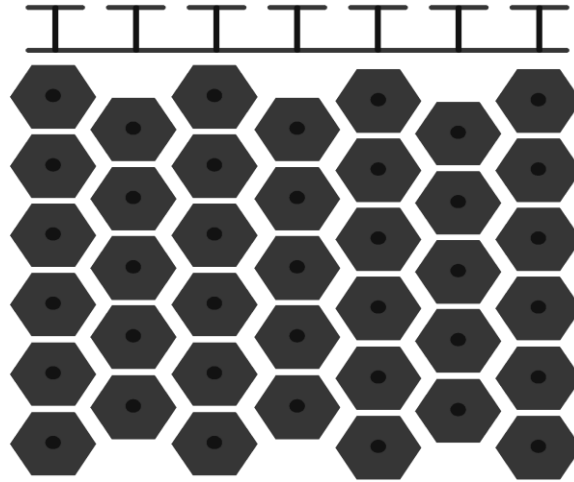


Figure 3.14: Periodic metal connected to ground with via holes to yield high-impedance surface.

• Planar EBG Structures

EBG technology represents a major breakthrough with respect to the current planar approaches, mainly due to their ability to guide and efficiently control electromagnetic waves. As the frequency increases, a planar structure that integrates the antenna, mixers, local oscillator, and all peripheral circuitry onto one single substrate becomes an attractive option.

Planar EBG's are of particular interest at microwave frequencies due to ease of fabrication. These EBG's are usually periodic in one and two dimensions. Planar EBG structures consist of uniformly distributed periodic metallic patterns on one side of a dielectric slab. They exhibit some interesting features such as distinctive passband and stopband, slow wave effects, low attenuation in the passband and suppression of surface waves when serving as the ground of the planar microstrip circuit. Several Planar EBG configurations have been reported in the literature like uni-planar designs without vertical vias, one and two dimensional EBG transmission line design, etc. in which they used EBG basis points with different geometries, and shapes like circular shape, square, hexagonal, fork shape, plus sign and many more. In some planar devices, they create defects by creating a discontinuity in a periodic pattern. For example, in a planar circular defect induced EBG structure with triangular lattice, they remove some circles or change their size for creating some discontinuity.

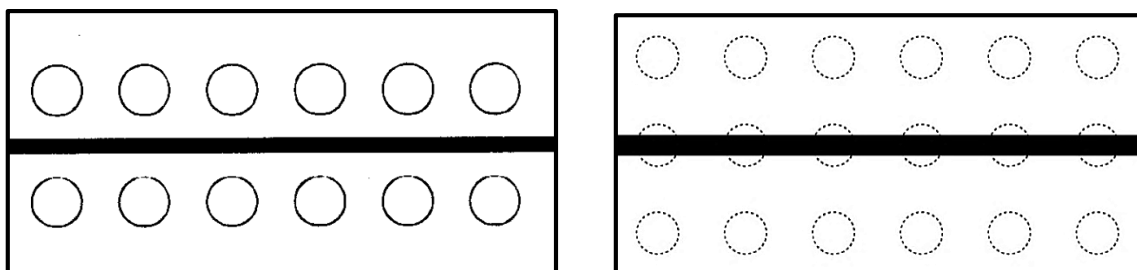


Figure 3.15: Microstrip with etched periodic pattern in the ground plane (circular pattern)[50]

3.8 Dumbbell Shaped Defected Ground Structures

Dumbbell Shaped Defected ground structures (DGS) are an area of increasing interest. It produces band rejection in certain frequency bands, and hence, is also known as electromagnetic bandgap (EBG) structures. Dumbbell Shaped DGS has been used to realize various passive and active device compact structures and to suppress the harmonics.

Any defect etched in the ground plane of the microstrip line disturbs its current distribution and can give rise to increasing effective capacitance and inductance. A broader area attached to simple slot heads etched in the ground plane of a microstrip line increases its effective length. A variety of attached area shapes such as triangular, square, circular, etc. have different effects. In this literature, new compact dumbbell shaped slot geometry is presented to serve as a Dumbbell Shaped DGS unit element for the microstrip lines (Figure 3.16).

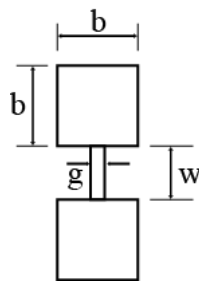


Figure 3.16: Geometry of a unit cell of a dumbbell shape DGS. The arm length of a larger square patterned slot is 'b'. The vertical slot is a rectangular patterned slot with $w \times g$ dimension; w is known as width and g is known as gap.

3.9 Microstrip Lines

The microstrip belongs to the group of parallel plate transmission line consist of a single ground plane and an open strip conductor separated by a dielectric substrate. Figure 3.17 shows the most commonly used microstrip transmission line for microwave integrated circuits. This line is the major component for making a filter. The electromagnetic field in the microstrip line is not confined only to the dielectric because of the fringing; the effective relative permittivity ϵ_{eff} is less than the relative permittivity ϵ_r of the substrate. The electromagnetic waves in microstrip propagate in TEM (transverse electric magnetic) mode, which is characterized by electric and magnetic field that exists only in the plane perpendicular to the axis of the propagation. Practical microstrip lines, shown in Figure 3.17, have width-to-height ratios w/h that are not necessarily much greater than unity, and can vary over the interval $0.1 < w/h < 10$. Typical heights h are of the order of millimeters.

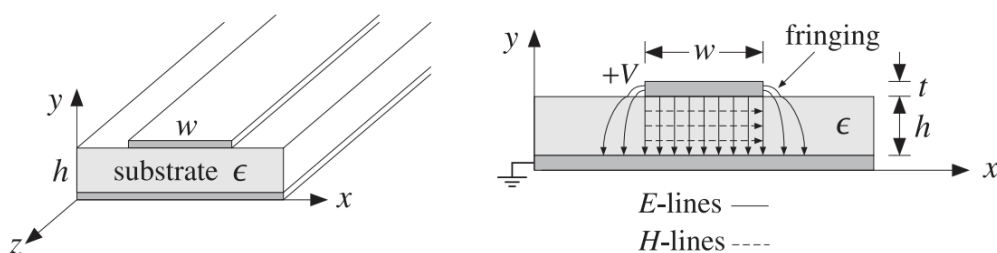


Figure 3.17: A microstrip transmission line.

Fringing effects cannot be ignored completely and the simple assumptions about the fields of the parallel plate line are not valid. For example, assuming a propagating wave in the z -direction with z, t dependence of $e^{j\omega t - j\beta z}$ with a common β in the dielectric and air, the longitudinal-transverse decomposition gives:

$$\nabla_T \times E_Z \times \hat{z} - j\beta \hat{z} \times E_T = -j\omega \mu H_T$$

In particular, we have for the x -component:

$$\partial_y E_Z + j\beta E_y = -j\omega \mu H_x$$

The boundary conditions require that the components H_x and $D_y = \epsilon E_y$ continuous across the dielectric-air interface (at $y = h$). This gives the interface conditions:

$$\partial_y E_Z^{air} + j\beta E_y^{air} = \partial_y E_Z^{diel} + j\beta E_y^{diel}$$

$$\epsilon_0 E_y^{air} = \epsilon E_y^{diel}$$

Combining the two conditions, we obtain:

$$\partial_y (E_Z^{diel} - E_Z^{air}) = j\beta \frac{\epsilon - \epsilon_0}{\epsilon} E_y^{air} = j\beta \frac{\epsilon - \epsilon_0}{\epsilon} E_y^{diel} \quad (3.38)$$

Because E_y is non-zero on either side of the interface, it follows that the left-hand side of Eq. (2.38) cannot be zero and the wave cannot be assumed to be strictly TEM. However, E_y is small in both the air and the dielectric in the fringing regions (to the left and right of the upper conductor). This gives rise to the so-called *quasi-TEM approximation* in which the fields are assumed to be approximately TEM and the effect of the deviation from TEM is taken into account by empirical formulas for the line impedance and velocity factor.

In particular, the air-dielectric interface is replaced by an effective dielectric, filling uniformly the entire space, and in which there would be a TEM propagating mode. If we denote by ϵ_{eff} the relative permittivity of the effective dielectric, the wavelength and velocity factor of the line will be given in terms of their free-space values λ_0, c_0 :

$$\lambda = \frac{\lambda_0}{\sqrt{\epsilon_{eff}}}, \quad c = \frac{c_0}{\sqrt{\epsilon_{eff}}} \quad (3.39)$$

There exist many empirical formulas for the characteristic impedance of the line and the effective dielectric constant. Hammerstad and Jensen's are some of the most accurate ones:

$$\epsilon_{eff} = \frac{\epsilon_r + 1}{2} + \frac{\epsilon_r - 1}{2} \left(1 + \frac{10}{u}\right)^{-ab}, \quad u = \frac{w}{h} \quad (3.40)$$

Where, $\epsilon_r = \epsilon/\epsilon_0$ is the relative permittivity of the dielectric and the quantities a, b are defined by:

$$a = 1 + \frac{1}{49} \ln \left[\frac{u^4 + \left(\frac{u}{52}\right)^2}{u^4 + 0.432} \right] + \frac{1}{18.7} \ln \left[1 + \left(\frac{u}{18.1}\right)^3 \right]$$

$$b = 0.564 \left(\frac{\epsilon_r - 0.9}{\epsilon_r + 3} \right)^{0.053}$$

The accuracy of these formulas is better than 0.01% for $u < 1$ and 0.03% for $u < 1000$. Similarly, the characteristic impedance is given by the empirical formula:

$$Z = \frac{\eta_0}{2\pi\sqrt{\epsilon_{eff}}} \ln \left[\frac{f(u)}{u} + \sqrt{1 + \frac{4}{u^2}} \right] \quad (3.41)$$

Where, $\eta_0 = \sqrt{\mu_0/\epsilon_0}$ and the function $f(u)$ is defined by:

$$f(u) = 6 + (2\pi - 6) \exp \left[- \left(\frac{30.666}{u} \right)^{0.7528} \right]$$

The accuracy is better than 0.2% for $0.1 \leq u \leq 100$ and $\epsilon_r < 128$. In the limit of large ratio w/h , or, $u \rightarrow \infty$, Eqs. (2.40) and (2.41) tend to those of the parallel plate line of the previous section:

$$\epsilon_{eff} \rightarrow \epsilon_r, \quad Z \rightarrow \frac{\eta_0}{\sqrt{\epsilon_r}} \frac{h}{w} = \eta \frac{h}{w}$$

Some typical substrate dielectric materials used in microstrip lines are alumina, a ceramic form of Al_2O_3 with $r = 9.8$, and RT-Duroid, a teflon composite material with $\epsilon_r = 2.2$. Practical values of the width-to-height ratio are in the range $0.1 \leq u \leq 10$ and practical values of characteristic impedances are between 10–200 ohm but in this literature I have used transmission line of 50 ohm characteristic impedance and Taconic substrate with $\epsilon_r = 2.45$. Figure 3.18 shows the dependence of Z and ϵ_{eff} on u for the two cases of $\epsilon_r = 2.2$ and $\epsilon_r = 9.8$.

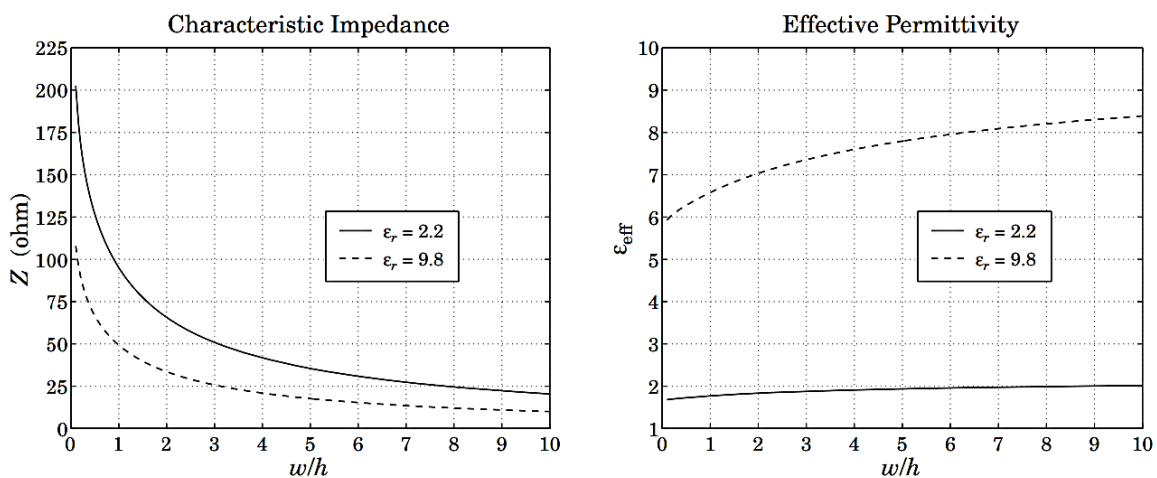


Figure 3.18: Characteristic impedance and effective permittivity of microstrip line.

3.10 Different circuit theories based on the frequency of operation

Microwave radio frequencies (RF) are electromagnetic (EM) waves that have a frequency range from around 0.3 GHz to 300 GHz with a corresponding wavelength range from 1m to 1mm. Microwave signals travel by line-of-sight and are not bent by the Earth's ionosphere unlike lower frequency signals. As well, microwave signals obey the laws of optics and can be transmitted, absorbed, or reflected depending on the transferring media types. In the late 1970s, lumped element components started to find a place in the microwave frequency range [67]. Recently, lumped element components have demonstrated the capability to operate up to 18 GHz [67]; however, the low unloaded quality factor (Q_0) realized by lumped element components results in poor insertion loss performance as the frequency increases.

For this reason, distributed microwave theory was developed as an extension to lumped element theory. Figure 3.19 illustrates the three available theories for solving any electrical problem based on its frequency of operation. Lumped element theory is a simplified circuit model used to solve low frequency problems where the effective size of a device is very small compared to the wavelength; distributed element theory is a simplified circuit model for high frequency problems where the maximum dimension of a device is comparable with the wavelength; while Maxwell's theory is a full-wave solution based on Maxwell's equations and is suitable for all electrical problems.

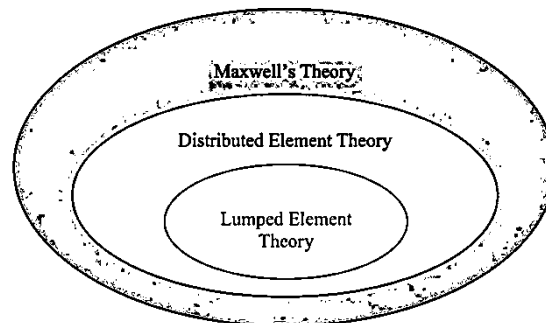


Figure 3.19: Different circuit-theories based on the frequency of operation.

Different numerical techniques based on Maxwell's equation have been developed such as the Finite Difference Time-Domain (FDTD) method, the Finite Element Method (FEM), and the Method of moments (MOM). Depending on the problem under analysis, each of those techniques has its own strength in terms of accuracy, computation time, and boundary definitions when dealing with the radiated emissions.

Distributed elements are a solution to the low Q -factor encountered by the lumped elements; however, planar distributed elements are often built using Microstrip or Stripline technologies (see Figure 3.20 and Figure 3.21, respectively) that make the physical dimensions large in comparison to the lumped elements. Both Microstrip and Stripline are planar technologies which can be fabricated using photolithography techniques. However, Microstrips are preferred because they are lighter, more compact, and easier to fabricate. Stripline supports a pure transverse ElectroMagnetic (TEM) mode which allows better noise immunity. Microstrip supports a quasi-TEM mode or a hybrid mode that is due to the inhomogeneous

medium surrounding the transmission line (i.e. dielectric material below and air above the transmission line).

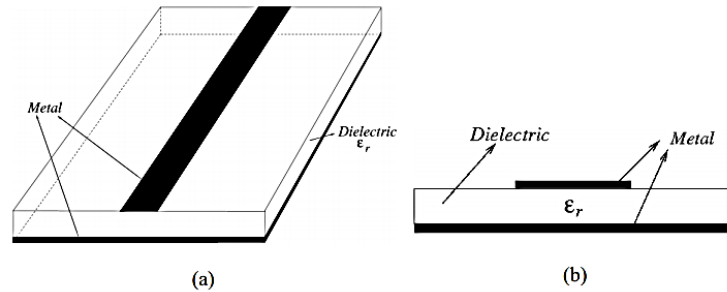


Figure 3.20: Microstrip transmission line: (a) 3D view; (b) 2D side view.

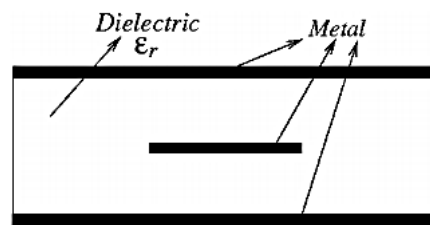


Figure 3.21: Stripline cross-section.

The diversity of applications and operational environments has led to high production volumes of microwave front-ends including but not limited to:

- i. Packaging,
- ii. Antennas, and
- iii. Microwave filters.

Each of these components is capable of degrading the performance of a system and needs individual attention while designing the system.

3.11 Conventional Filter Design

There are two methods to make the conventional designs. They are named as the image parameter method and the insertion loss method. Those will be briefly described one by one. Then the implementation of the microstrip filter will be described.

3.10.1 Filter Design by the Image Parameter Method

The image parameter method of filter design involves the specification of passband and stopband characteristics for a cascade of simple two-port networks, and so is related in concept to the periodic structures. The method is relatively simple but has the disadvantage that an arbitrary frequency response cannot be incorporated into the design. This is in contrast to the insertion loss method, which is the subject of the following section. Nevertheless, the image parameter method is useful for simple filters, and it provides a link between infinite periodic structures and practical filter design. The image parameter method also finds application in solid-state traveling-wave amplifier design.

- **Image Impedances and Transfer Functions for Two-Port Networks**

Consider the arbitrary two-port network shown in figure 4.4, where the network is specified by its ABCD parameters. Note that the reference direction for the current at port 2 has been chosen according to the convention for ABCD parameters. The image impedances, Z_{i1} and Z_{i2} , are defined for this network as follows:

Z_{i1} = input impedance at port 1 when port 2 is terminated with Z_{i2}

Z_{i2} = input impedance at port 2 when port 1 is terminated with Z_{i1}

Thus both ports are matched when terminated in their image impedances. We can derive expressions for the image impedances in terms of the ABCD parameters of the network.

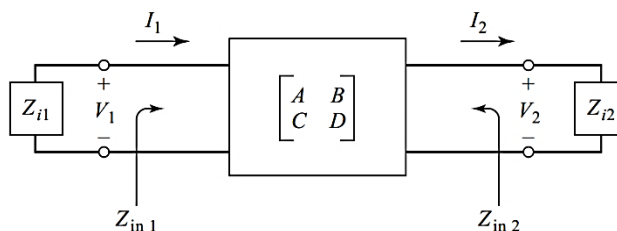


Figure 3.22: A two-port network terminated in its image impedances.

The port voltages and currents are related as

$$V_1 = AV_2 + BI_2$$

$$I_1 = CV_2 + DI_2$$

The input impedance at port 1, with port 2 terminated in Z_{i2} , is

$$Z_{in1} = \frac{V_1}{I_1} = \frac{AV_2 + BI_2}{CV_2 + DI_2} = \frac{AZ_{i2} + B}{CZ_{i2} + D}$$

Since $V_2 = Z_{i2}I_2$ and $AD - BC = 1$ for a reciprocal network, here obtains

$$V_2 = DV_1 - BI_1$$

$$I_2 = -CV_1 + AI_1$$

Then the input impedance at port 2, with port 1 terminated in Z_{i1} , can be found as

$$Z_{in2} = \frac{-V_2}{I_2} = \frac{DV_1 - BI_1}{-CV_1 + AI_1} = \frac{DZ_{i1} + B}{CZ_{i1} + A}$$

since $V_1 = -Z_{i1}I_1$, $Z_{in1} = Z_{i1}$ and $Z_{in2} = Z_{i2}$ are desired.

Solving for Z_{i1} and Z_{i2} gives

$$Z_{i1} = \sqrt{\frac{AB}{CD}}$$

$$Z_{i2} = \sqrt{\frac{BD}{AC}}$$

If the network is symmetric, then $A = D$ and $Z_{i1} = Z_{i2}$ as expected. Now consider the voltage transfer function for a two-port network terminated in its image impedances. With reference to Figure 3.23 the output voltage at port 2 can be expressed as

$$V_2 = DV_1 - BI_1 = \left(D - \frac{B}{Z_{i1}}\right)V_1$$

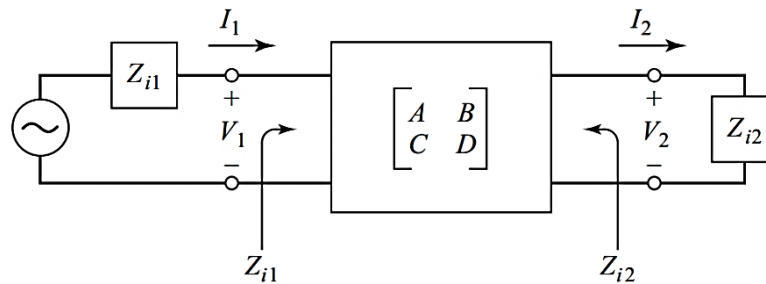


Figure 3.23: A two-port network terminated in its image impedances and driven with a voltage generator.

The voltage ratio is

$$\frac{V_2}{V_1} = \sqrt{\frac{D}{A}}(\sqrt{AD} - \sqrt{BC})$$

Similarly, the current ratio is,

$$\frac{I_2}{I_1} = \sqrt{\frac{A}{D}}(\sqrt{AD} - \sqrt{BC})$$

The factor $\sqrt{D/A}$ can be interpreted as a transformer turns ratio. Apart from this factor, we can define a propagation factor for the network as

$$e^{-\gamma} = \sqrt{AD} - \sqrt{BC}$$

Where, $\gamma = \alpha + j\beta$

$$e^{\gamma} = \sqrt{AD} + \sqrt{BC}$$

$$\cosh \gamma = (e^{\gamma} + e^{-\gamma})/2 = \sqrt{AD}$$

Two important types of two-port networks are the T and π circuits, which can be made in symmetric form.

- **Constant-k Filter Sections**

We can now develop low-pass and high-pass filter sections. First consider the T-network shown in Figure 3.6. Intuitively, we can see that this is a low-pass filter network because the series inductors and shunt capacitor tend to block high-frequency signals while passing low frequency signals. Comparing with the results given in Table 8.1, we have $Z_1 = j\omega L$ and $Z_2 = 1/j\omega C$, so the image impedance is

$$Z_{iT} = \sqrt{\frac{L}{C}} \sqrt{1 - \frac{\omega^2 LC}{4}}$$

If we define a cutoff frequency, ω_c , as

$$\omega_c = \frac{2}{\sqrt{LC}}$$

and a nominal characteristic impedance, R_0 , as

$$R_0 = \sqrt{\frac{L}{C}} = k$$

$$Z_{iT} = R_0 \sqrt{1 - \frac{\omega^2}{\omega_c^2}}$$

Then $Z_{iT} = R_0$ for $\omega = 0$

The propagation factor is,

$$e^\gamma = 1 - \frac{2\omega^2}{\omega_c^2} + \frac{2\omega}{\omega_c} \sqrt{\frac{\omega^2}{\omega_c^2} - 1}$$

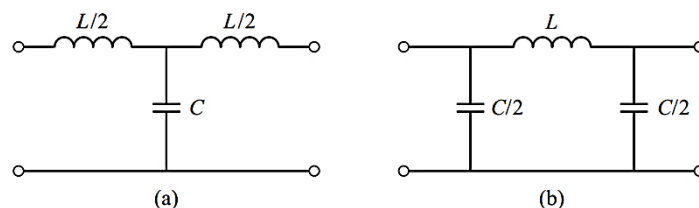


Figure 3.24: Low-pass constant- k filter sections in T and π forms. (a) T-section. (b) π - section.

Now consider two frequency regions:

1. For $\omega < \omega_c$: This is the passband of the filter section. Equation for Z_{iT} shows that Z_{iT} is real and equation for e^γ shows that γ is imaginary, since $\omega^2/\omega_c^2 - 1$ is negative and $|e^\gamma| = 1$:

$$|e^\gamma|^2 = \left(1 - \frac{2\omega^2}{\omega_c^2}\right)^2 + \frac{4\omega^2}{\omega_c^2} \left(1 - \frac{\omega^2}{\omega_c^2}\right) = 1$$

2. For $\omega > \omega_c$: This is the stopband of the filter section. Equation for Z_{iT} shows that Z_{iT} is imaginary, and equation for e^γ shows that e^γ is real and $-1 < e^\gamma < 0$ (as seen from the limits as $\omega \rightarrow \omega_c$ and $\omega \rightarrow \infty$). The attenuation rate for $\omega \gg \omega_c$ is 40 dB/decade. Typical phase and attenuation constants are sketched in Figure 3.7. Observe that the attenuation, α , is zero or relatively small near the cutoff frequency, although $\alpha \rightarrow \infty$ as

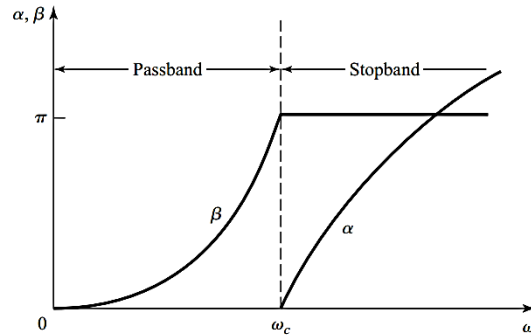


Figure 3.25: Typical passband and stopband characteristics of the low-pass constant- k sections of Figure 3.6.

For the low-pass π -network of Figure 8.9, we have that $Z_1 = j\omega L$ and $Z_2 = 1/j\omega C$, so the propagation factor is the same as that for the low-pass T-network. The cutoff frequency, ω_c , and nominal characteristic impedance, R_0 , are the same as the corresponding quantities for the T-network. At $\omega = 0$ $Z_{iT} = Z_{i\pi} = R_0$, where $Z_{i\pi}$ is the image impedance of the low-pass π -network, but Z_{iT} and $Z_{i\pi}$ are generally not equal at other frequencies.

High-pass constant- k sections are shown in Figure 3.8; we see that the positions of the inductors and capacitors are reversed from those in the low-pass prototype. The design equations are easily shown to be

$$R_0 = \sqrt{\frac{L}{C}} \quad \text{and} \quad \omega_c = \frac{1}{2\sqrt{LC}}$$

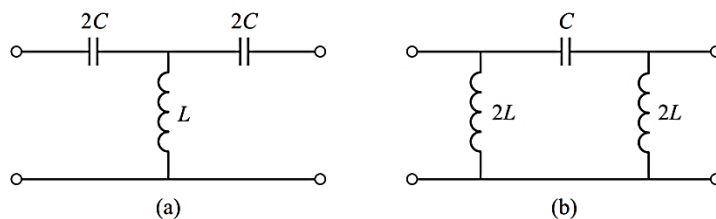


Figure 3.26: High-pass constant- k filter sections in T and π forms. (a) T-section. (b) π -section.

• m -Derived Filter Sections

As shown in Figure 3.27 the impedances Z_1 and Z_2 in a constant- k T-section are replaced with Z_1' and Z_2' .

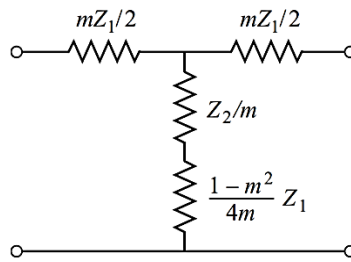


Figure 3.27: Development of an m -derived filter section from a constant- k section.

The replaced equation is,

$$Z'_1 = mZ_1$$

Then it has chosen Z_2 to obtain the same value of Z_{iT} as for the constant- k section. It shows the following equation

$$Z_{iT} = \sqrt{mZ_1Z'_2 + \frac{m^2Z_1^2}{4}}$$

And solution for Z'_2 gives,

$$Z'_2 = \frac{Z_2}{m} + \frac{Z_1}{4m} - \frac{mZ_1}{4} = \frac{Z_2}{m} + \frac{(1-m^2)}{4m}Z_1$$

For a low-pass filter, we have $Z_1 = j\omega L$ and $Z_2 = 1/j\omega C$. The m -derived components as

$$Z'_1 = j\omega Lm$$

$$Z'_2 = \frac{1}{j\omega Cm} + \frac{(1-m^2)}{4m}j\omega L$$

$$e^\gamma = 1 + \frac{Z'_1}{Z'_2} + \sqrt{\frac{Z'_1}{Z'_2} \left(1 + \frac{Z'_1}{4Z'_2} \right)}$$

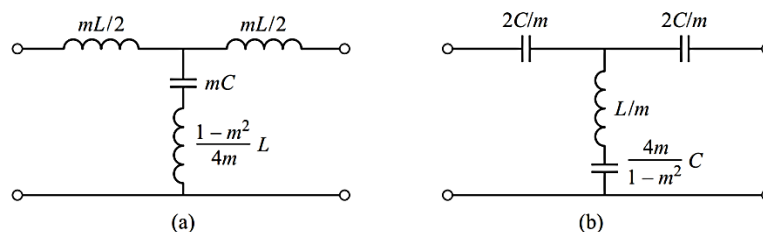


Figure 3.28: m -Derived filter sections. (a) Low-pass T-section. (b) High-pass T-section.

If we restrict $0 < m < 1$, then these results show that e^γ is real and $|e^\gamma| > 1$ for $\omega > \omega_c$. Thus the stopband begins at $\omega = \omega_c$, as for the constant- k section. However, when $\omega = \omega_\infty$, where

$$\omega_\infty = \frac{\omega_c}{\sqrt{1-m^2}}$$

The denominators vanish and e^γ becomes infinite, implying infinite attenuation. Physically, this pole in the attenuation characteristic is caused by the resonance of the series LC resonator in the shunt arm of the T; this is easily verified by showing that the resonant frequency of this LC resonator is ω_∞ . Note that the equation of ω_∞ indicates that $\omega_\infty > \omega_c$, so infinite attenuation occurs after the cutoff frequency, ω_c , as illustrated in Figure 3.29. The position of the pole at ω_∞ can be controlled with the value of m .

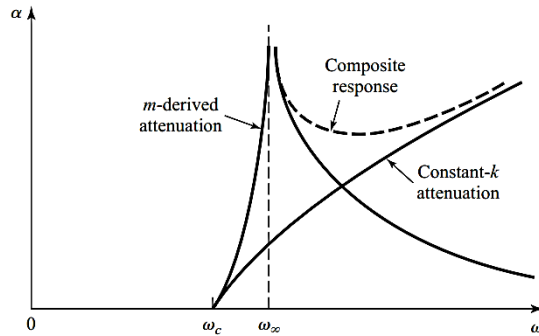


Figure 3.29: Typical attenuation responses for constant-k , m -derived, and composite filters.

• **Composite Filters**

By combining in cascade the constant-k, m-derived sharp cutoff and the m -derived matching sections we can realize a filter with the desired attenuation and matching properties.

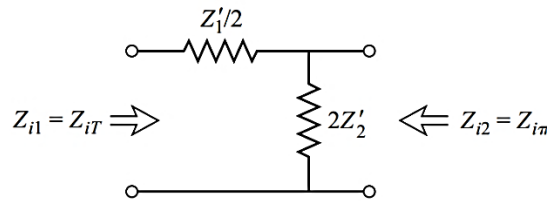


Figure 3.30: A bisected π -section used to match $Z_{i\pi}$ to Z_{iT}

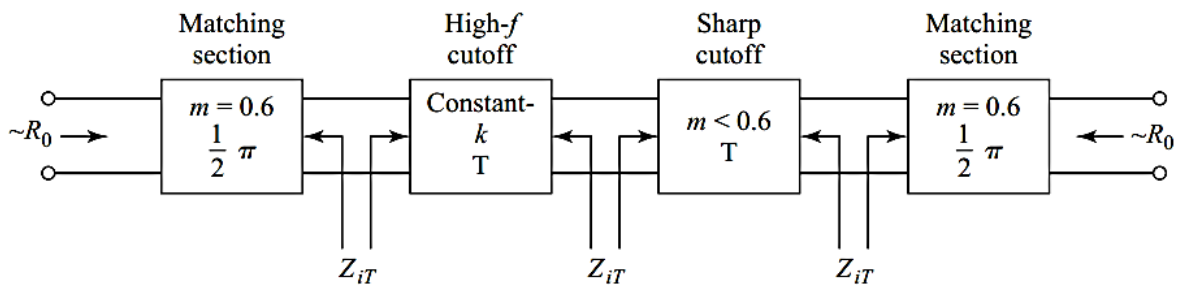


Figure 3.31: The final four-stage composite filter.

This type of design is called a composite filter, and is shown in Figure 3.31. The sharp-cutoff section, with $m < 0.6$, places an attenuation pole near the cutoff frequency to provide a sharp attenuation response; the constant-k section provides high attenuation further in to the stopband. The bisected- π sections at the ends of the filter match the nominal source and load impedance, R_0 , to the internal image impedances, Z_{iT} , of the constant-k and m-derived sections..

3.10.2 Filter Design by the Insertion Loss Method

The image parameter method of the previous section may yield a usable filter response for some applications, but there is no methodical way of improving the design. The insertion loss method, however, allows a high degree of control over the passband and stop-band amplitude and phase characteristics, with a systematic way to synthesize a desired response. The necessary design trade-offs can be evaluated to best meet the application requirements. If, for example, a minimum insertion loss is most important, a binomial response could be used; a Chebyshev response would satisfy a requirement for the sharpest cutoff. If it is possible to sacrifice the attenuation rate, a better phase response can be obtained by using a linear phase filter design. In addition, in all cases, the insertion loss method allows filter performance to be improved in a straightforward manner, at the expense of a higher order filter. For the filter prototypes to be discussed below, the order of the filter is equal to the number of reactive elements.

In the insertion loss method a filter response is defined by its insertion loss, or power loss ratio, P_{LR} :

$$P_{LR} = \frac{\text{Power available from the source}}{\text{Power delivered to load}} = \frac{P_{inc}}{P_{load}} = \frac{1}{1 - |\Gamma(\omega)|^2}$$

Observe that this quantity is the reciprocal of $|S_{12}|^2$ if both load and source are matched. The insertion loss (IL) in dB is

$$IL = 10 \log P_{LR}$$

$$P_{LR} = 1 + \frac{M(\omega^2)}{N(\omega^2)}$$

where M and N are real polynomials in ω^2 . The practical filter responses are described below.

- **Maximally flat:**

This characteristic is also called the binomial or Butterworth response, and is optimum in the sense that it provides the flattest possible passband response for a given filter complexity, or order. For a low-pass filter, it is specified by

$$P_{LR} = 1 + k^2 \left(\frac{\omega}{\omega_c} \right)^{2N}$$

where N is the order of the filter and ω_c is the cutoff frequency. The passband extends from $\omega=0$ to $\omega=\omega_c$; at the band edge the power loss ratio is $1 + k^2$. If we choose this as the -3 dB point, as is common, we have $k=1$, which we will assume from now on. For $\omega > \omega_c$, the attenuation increases monotonically with frequency, as shown in Figure 3.14. For $\omega \gg \omega_c$, $P_{LR} \cong k^2 (\omega/\omega_c)^{2N}$, which shows that the insertion loss increases at the rate of $20N$ dB/decade. Like the binomial response for multi section quarter-wave matching transformers, the first $(2N - 1)$ derivatives of the equation of P_{LR} are zero at $\omega = 0$.

- **Equal ripple:**

If a Chebyshev polynomial is used to specify the insertion loss of an Nth-order low-pass filter as

$$P_{LR} = 1 + k^2 T_N^2 \left(\frac{\omega}{\omega_c} \right)$$

then a sharper cutoff will result, although the passband response will have ripples of amplitude $1 + k^2$, as shown in Figure 4.14, since $T_N(x)$ oscillates between ± 1 for $|x| \leq 1$. Thus, k^2 determines the passband ripple level. For large x , $T_N(x) \cong \frac{1}{2}(2x)^{2N}$, so for $\omega \gg \omega_c$ the insertion loss becomes

$$P_{LR} \cong \frac{k^2}{4} \left(\frac{2\omega}{\omega_c} \right)^{2N}$$

which also increases at the rate of $20 N$ dB/decade.

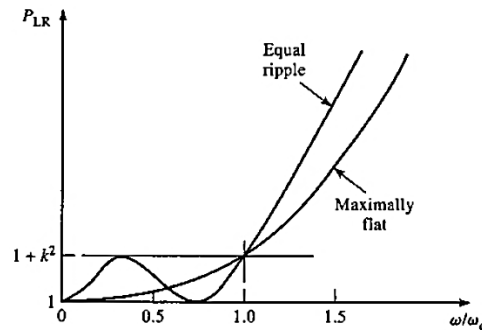


Figure 3.32: Maximally flat and equal-ripple low-pass filter responses ($N = 3$).

- **Elliptic function:**

The maximally flat and equal-ripple responses both have monotonically increasing attenuation in the stopband. In many applications, it is adequate to specify a minimum stopband attenuation, in which case a better cutoff rate can be obtained. Such filters are called elliptic function filters, and they have equal-ripple responses in the pass band as well as in the stopband, as shown in Figure 3.15. The maximum attenuation in the pass-band, A_{\max} , can be specified, as well as the minimum attenuation in the stopband, A_{\min} . Elliptic function filters are difficult to synthesize, so we will not consider them further.

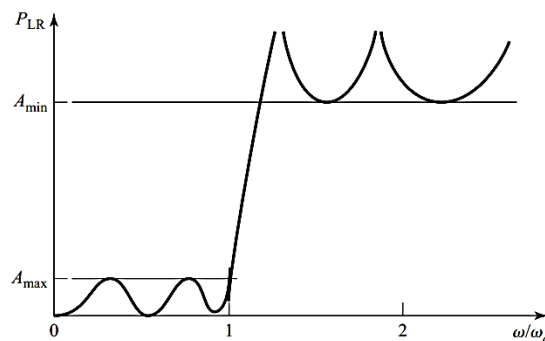


Figure 3.33: Elliptic function low-pass filter response.

- **Linear phase:**

The above filters specify the amplitude response, but in some applications it is important to have a linear phase response in the passband to avoid signal distortion. Since a sharp-cutoff response is generally incompatible with a good phase response, the phase response of a filter must be deliberately synthesized, usually resulting in an inferior attenuation characteristic. A linear phase characteristic can be achieved with the following phase response:

$$\phi(\omega) = A\omega \left[1 + p \left(\frac{\omega}{\omega_c} \right)^{2N} \right]$$

Where $\phi(\omega)$ is the phase of the voltage transfer function of the filter, and p is a constant. A related quantity is the group delay, defined as

$$\tau_d = \frac{d\phi}{d\omega} = \left[1 + p(2N + 1) \left(\frac{\omega}{\omega_c} \right)^{2N} \right]$$

Which shows that the group delay for a linear phase filter is a maximally flat function.

More general filter specifications can be obtained, but the above cases are the most common. We will next discuss the design of low-pass filter prototypes that are normalized in terms of impedance and frequency; this normalization simplifies the design of filters for arbitrary frequency, impedance, and the type (low-pass, high-pass, bandpass, or bandstop). The low-pass prototypes are then scaled to the desired frequency and impedance, and the lumped-element components replaced with distributed circuit elements for implementation at microwave frequencies. This design process is illustrated in Figure 3.34.

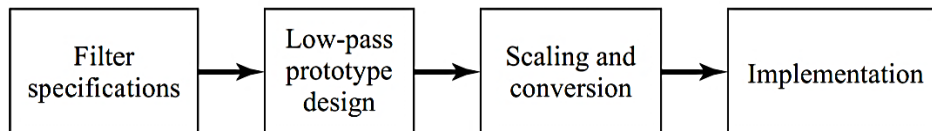


Figure 3.34: The process of filter design by the insertion loss method.

3.10.3 Filter Implementation

The lumped-element filter designs generally work well at low frequencies, but two problems arise at higher RF and microwave frequencies. First, lumped-element inductors and capacitors are generally available only for a limited range of values, and can be difficult to implement at microwave frequencies. Distributed elements, such as open-circuited or short-circuited transmission line stubs, are often used to approximate ideal lumped elements. In addition, at microwave frequencies the distances between filter components is not negligible. The first problem is treated with Richards' transformation, which can be used to convert lumped elements to transmission line sections. Kuroda's identities can then be used to physically separate filter elements by using transmission line sections. Because such additional transmission line sections do not affect the filter response, this type of design is called redundant filter synthesis. It is possible to design microwave filters that take advantage of these sections to improve the filter response; such non-redundant synthesis does not have a lumped-element counterpart.

- **Richards' Transformation**

This is the first step to make lumped element into RF element. This transformation converts inductor and capacitor element into stubs. The working principle is described below,

The transformation,

$$\Omega = \tan \beta l = \tan \left(\frac{\omega l}{v_p} \right) \quad (3.42)$$

maps the ω plane to the Ω plane, which repeats with a period of $\omega l/v_p = 2\pi$. This transformation was introduced by P. Richards [68] to synthesize an LC network using open- and short-circuited transmission line stubs. Thus, if we replace the frequency variable ω with Ω , we can write the reactance of an inductor as

$$jX_L = j\Omega L = jL \tan \beta l \quad (3.43)$$

and the susceptance of a capacitor as

$$jB_C = j\Omega C = jC \tan \beta l \quad (3.44)$$

These results indicate that an inductor can be replaced with a short-circuited stub of length β and characteristic impedance L , while a capacitor can be replaced with an open-circuited stub of length β and characteristic impedance $1/C$. A unity filter impedance is assumed. Cutoff occurs at a unity frequency for a low-pass filter prototype; to obtain the same cutoff frequency for the Richards'-transformed filter, (4.1) shows that

$$\Omega = 1 = \tan \beta l$$

which gives a stub length of $l = \lambda/8$, where λ is the wavelength of the line at the cutoff frequency, ω_c . At the frequency $\omega_0 = 2\omega_c$, the lines will be $\lambda/4$ long, and an attenuation pole will occur. At frequencies away from ω_c , the impedances of the stubs will no longer match the original lumped-element impedances, and the filter response will differ from the desired prototype response. In addition, the response will be periodic in frequency, repeating every $4\omega_c$.

In principle, then, Richards' transformation allows the inductors and capacitors of a lumped-element filter to be replaced with short-circuited and open-circuited transmission line stubs, as illustrated in Figure 3.35. Since the electrical lengths of all the stubs are the same ($\lambda/8$ at ω_c), these lines are called *commensurate* lines.

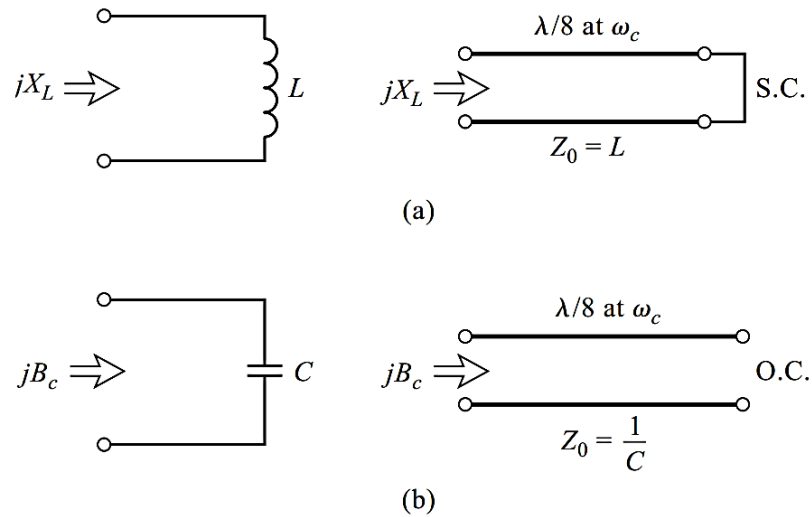


Figure 3.35: Richards' transformation. (a) For an inductor to a short-circuited stub. (b) For a capacitor to an open-circuited stub.

- **Kuroda's Identities**

The four Kuroda identities use redundant transmission line sections to achieve a more practical microwave filter implementation by performing any of the following operations:

- Physically separate transmission line stubs
- Transform series stubs into shunt stubs, or vice versa
- Change impractical characteristic impedances into more realizable values

The additional transmission line sections are called unit elements and are $\lambda/8$ long at ω_c ; the unit elements are thus commensurate with the stubs used to implement the inductors and capacitors of the prototype design. The four Kuroda identities are illustrated in Figure 3.36, where each box represents a unit element, or transmission line, of the indicated characteristic impedance and length ($\lambda/8$ at ω_c). The inductors and capacitors represent short-circuit and open-circuit stubs, respectively.

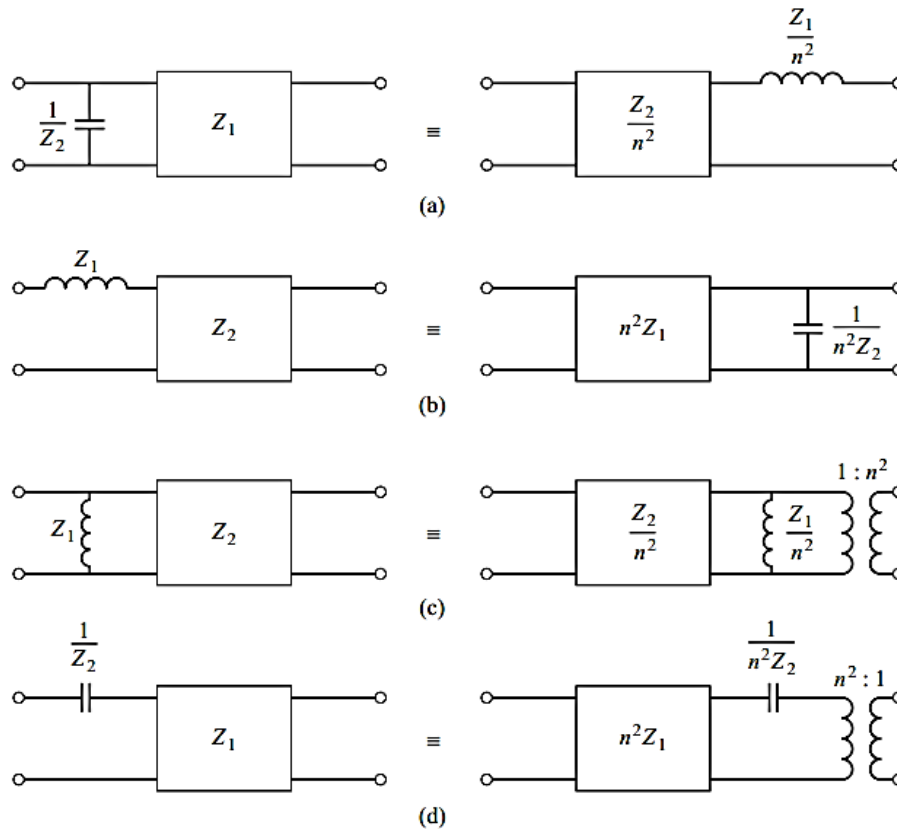


Figure 3.36: The Four Kuroda Identities ($n^2 = 1 + Z_2/Z_1$)

3.11 Low-Pass Filter Design Procedure Using Stubs

- **Maximally Flat Low-pass Filter Prototype**

The process of making low-pass filter can be extended to find the element values for filters with an arbitrary number of elements, N , but clearly this is not practical for large N . For a normalized low-pass design, where the source impedance is 1 and the cutoff frequency is $\omega_c = 1$ rad/sec, however, the element values for the ladder-type circuits of Figure 3.37 can be tabulated. Table 3.1 gives such element values for maximally flat low-pass filter prototypes for $N = 1$ to 10. These data can be used with either of the ladder circuits of Figure 3.39 in the following way. The element values are numbered from g_0 at the generator impedance to g_{N+1} at the load impedance for a filter having N reactive elements.

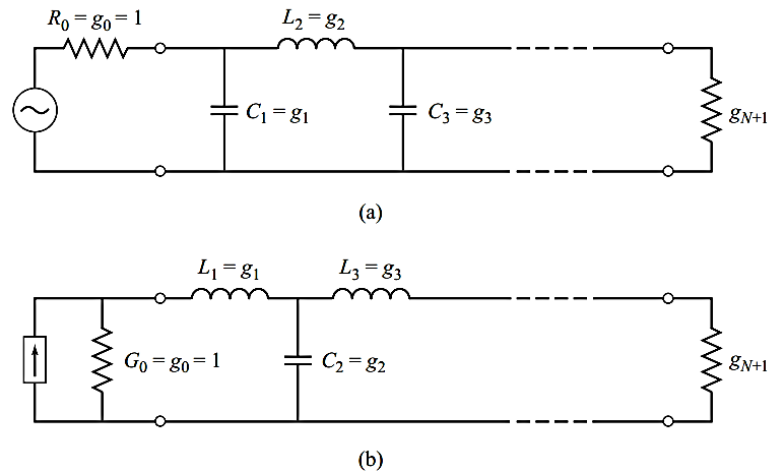


Figure 3.37: Ladder circuits for low-pass filter prototypes and their element definitions. (a) Prototype beginning with a shunt element. (b) Prototype beginning with a series element.

The elements alternate between series and shunt connections, and g_k has the following definition:

g_0 = generator resistance (figure 3.37a), generator conductance (figure 3.37b)

g_k ($k=1$ to N) = inductance for series inductors, capacitance for shunt capacitors

g_{N+1} = load resistance if g_N is a shunt capacitor, load conductance if g_N is a series inductor

Then the circuits of Figure 3.37 can be considered as the dual of each other, and both will give the same filter response.

Finally, as a matter of practical design procedure, it will be necessary to determine the size, or order, of the filter. This is usually dictated by a specification on the insertion loss at some frequency in the stopband of the filter. Figure 4.20 shows the attenuation characteristics for various N versus normalized frequency. If a filter with $N > 10$ is required, a good result can usually be obtained by cascading two designs of lower order.

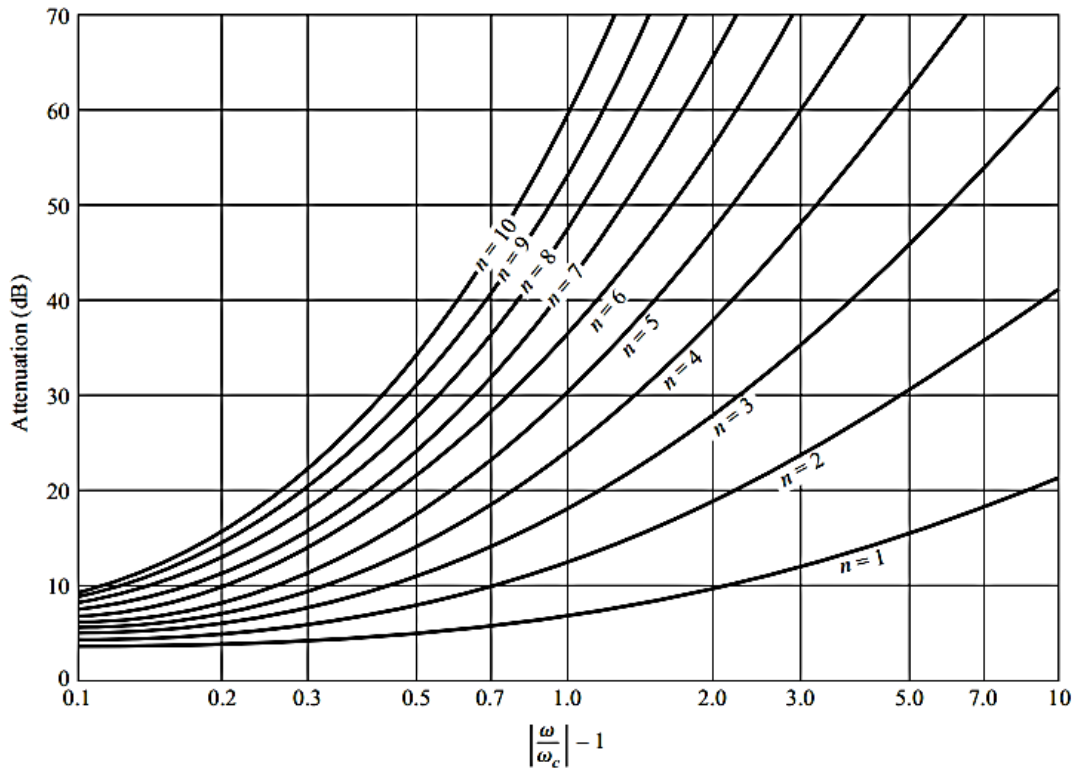


Figure 3.38: Attenuation versus normalized frequency for maximally flat filter prototypes.

Table 3.1: Element values for maximally flat, low-pass filter prototypes ($g_0=1$, $\omega_c=1$, $N=1$ to 10)

| N | g_1 | g_2 | g_3 | g_4 | g_5 | g_6 | g_7 | g_8 | g_9 | g_{10} | g_{11} |
|-----|--------|--------|--------|--------|--------|--------|--------|--------|--------|----------|----------|
| 1 | 2.0000 | 1.0000 | | | | | | | | | |
| 2 | 1.4142 | 1.4142 | 1.0000 | | | | | | | | |
| 3 | 1.0000 | 2.0000 | 1.0000 | 1.0000 | | | | | | | |
| 4 | 0.7654 | 1.8478 | 1.8478 | 0.7654 | 1.0000 | | | | | | |
| 5 | 0.6180 | 1.6180 | 2.0000 | 1.6180 | 0.6180 | 1.0000 | | | | | |
| 6 | 0.5176 | 1.4142 | 1.9318 | 1.9318 | 1.4142 | 0.5176 | 1.0000 | | | | |
| 7 | 0.4450 | 1.2470 | 1.8019 | 2.0000 | 1.8019 | 1.2470 | 0.4450 | 1.0000 | | | |
| 8 | 0.3902 | 1.1111 | 1.6629 | 1.9615 | 1.9615 | 1.6629 | 1.1111 | 0.3902 | 1.0000 | | |
| 9 | 0.3473 | 1.0000 | 1.5321 | 1.8794 | 2.0000 | 1.8794 | 1.5321 | 1.0000 | 0.3473 | 1.0000 | |
| 10 | 0.3129 | 0.9080 | 1.4142 | 1.7820 | 1.9754 | 1.9754 | 1.7820 | 1.4142 | 0.9080 | 0.3129 | 1.0000 |

• Equal-Ripple Low-Pass Filter Prototype

Tables exist for designing equal-ripple low-pass filters with a normalized source impedance and cutoff frequency ($\omega_c = 1$ rad/sec), and these can be applied to either of the ladder circuits of Figure 3.39. This design data depends on the specified passband ripple level; Table 3.2 lists element values for normalized low-pass filter prototypes having 0.5 or 3.0 dB ripple for $N = 1$ to 10. Notice that the load impedance $g_{N+1} \neq 1$ for even N . If the stopband attenuation is specified, the curves in Figure 3.39 can be used to determine the necessary value of N for these ripple values.

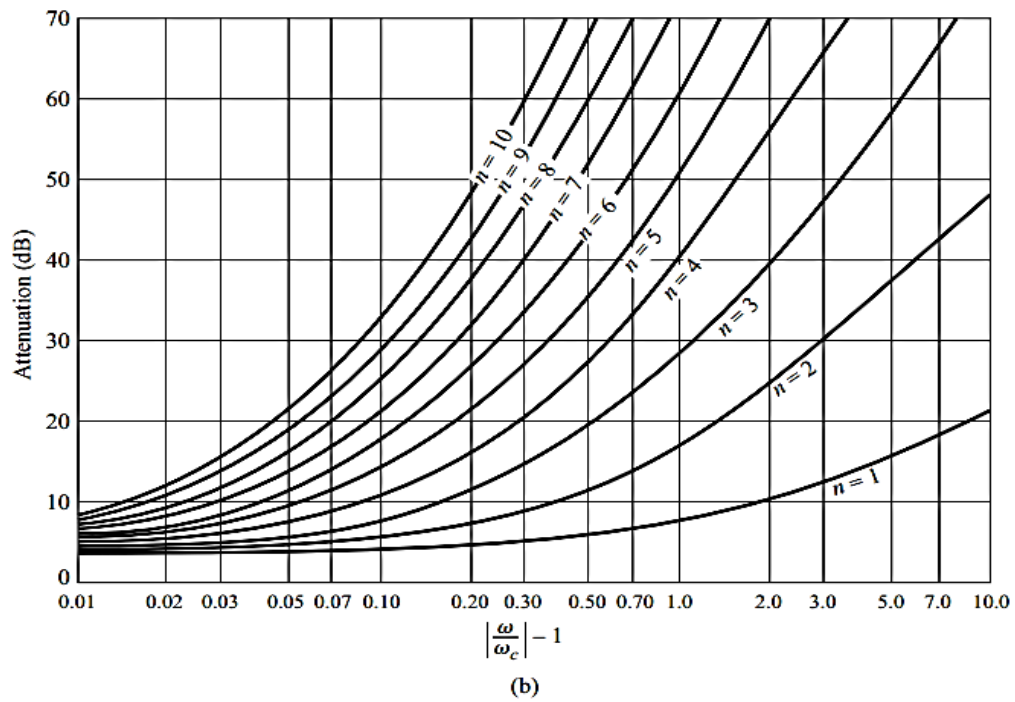
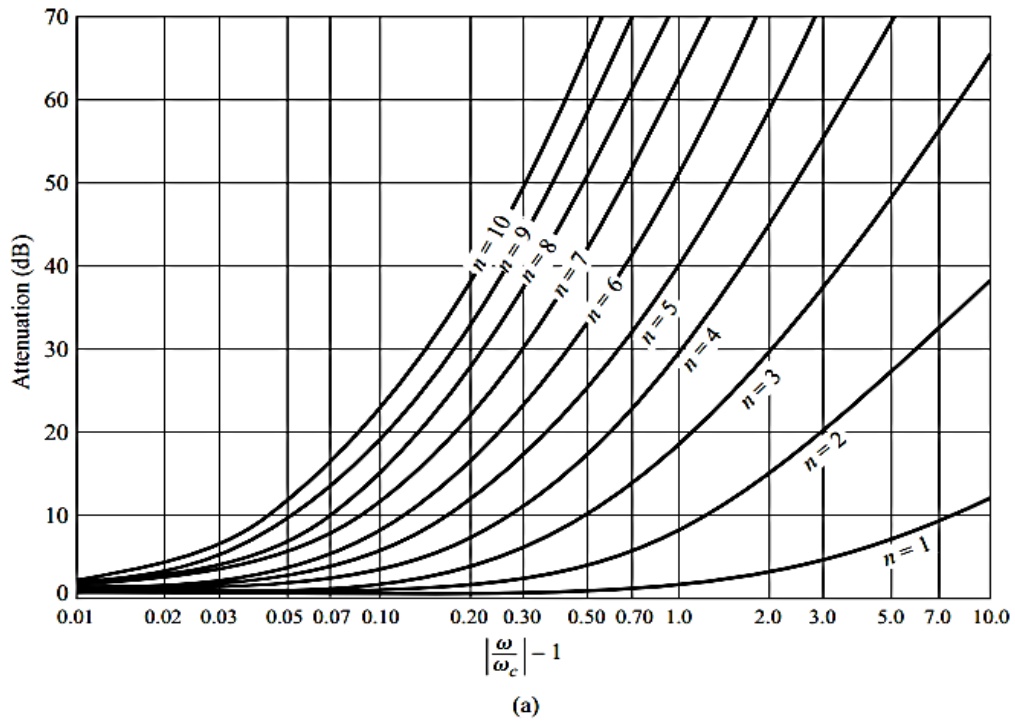


Figure 3.39: Attenuation versus normalized frequency for equal-ripple filter prototypes. (a) 0.5 dB ripple level. (b) 3.0 dB ripple level.

Table 3.2: Element Values for Equal-Ripple Low-Pass Filter Prototypes ($g_0=1$, $\omega_c=1$, $N=1$ to 10, 0.5 dB and 3.0 dB ripple)

| 0.5 dB Ripple | | | | | | | | | | | |
|---------------|--------|--------|--------|--------|--------|--------|--------|--------|--------|----------|----------|
| N | g_1 | g_2 | g_3 | g_4 | g_5 | g_6 | g_7 | g_8 | g_9 | g_{10} | g_{11} |
| 1 | 0.6986 | 1.0000 | | | | | | | | | |
| 2 | 1.4029 | 0.7071 | 1.9841 | | | | | | | | |
| 3 | 1.5963 | 1.0967 | 1.5963 | 1.0000 | | | | | | | |
| 4 | 1.6703 | 1.1926 | 2.3661 | 0.8419 | 1.9841 | | | | | | |
| 5 | 1.7058 | 1.2296 | 2.5408 | 1.2296 | 1.7058 | 1.0000 | | | | | |
| 6 | 1.7254 | 1.2479 | 2.6064 | 1.3137 | 2.4758 | 0.8696 | 1.9841 | | | | |
| 7 | 1.7372 | 1.2583 | 2.6381 | 1.3444 | 2.6381 | 1.2583 | 1.7372 | 1.0000 | | | |
| 8 | 1.7451 | 1.2647 | 2.6564 | 1.3590 | 2.6964 | 1.3389 | 2.5093 | 0.8796 | 1.9841 | | |
| 9 | 1.7504 | 1.2690 | 2.6678 | 1.3673 | 2.7239 | 1.3673 | 2.6678 | 1.2690 | 1.7504 | 1.0000 | |
| 10 | 1.7543 | 1.2721 | 2.6754 | 1.3725 | 2.7392 | 1.3806 | 2.7231 | 1.3485 | 2.5239 | 0.8842 | 1.9841 |
| 3.0 dB Ripple | | | | | | | | | | | |
| N | g_1 | g_2 | g_3 | g_4 | g_5 | g_6 | g_7 | g_8 | g_9 | g_{10} | g_{11} |
| 1 | 1.9953 | 1.0000 | | | | | | | | | |
| 2 | 3.1013 | 0.5339 | 5.8095 | | | | | | | | |
| 3 | 3.3487 | 0.7117 | 3.3487 | 1.0000 | | | | | | | |
| 4 | 3.4389 | 0.7483 | 4.3471 | 0.5920 | 5.8095 | | | | | | |
| 5 | 3.4817 | 0.7618 | 4.5381 | 0.7618 | 3.4817 | 1.0000 | | | | | |
| 6 | 3.5045 | 0.7685 | 4.6061 | 0.7929 | 4.4641 | 0.6033 | 5.8095 | | | | |
| 7 | 3.5182 | 0.7723 | 4.6386 | 0.8039 | 4.6386 | 0.7723 | 3.5182 | 1.0000 | | | |
| 8 | 3.5277 | 0.7745 | 4.6575 | 0.8089 | 4.6990 | 0.8018 | 4.4990 | 0.6073 | 5.8095 | | |
| 9 | 3.5340 | 0.7760 | 4.6692 | 0.8118 | 4.7272 | 0.8118 | 4.6692 | 0.7760 | 3.5340 | 1.0000 | |
| 10 | 3.5384 | 0.7771 | 4.6768 | 0.8136 | 4.7425 | 0.8164 | 4.7260 | 0.8051 | 4.5142 | 0.6091 | 5.8095 |

- **Example of Low-pass filter design:**

To design a low-pass filter for fabrication using microstrip lines. Let, the following steps are considered. The specifications include a cutoff frequency of 4 GHz, an impedance of 50 ohm, and a third-order 3 dB equal-ripple passband response. Firstly, the normalized low-pass prototype element values are taken from Table 3.2. They are:

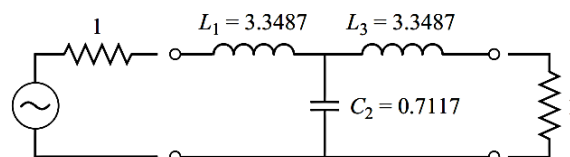
$$g_1 = 3.3487 = L_1$$

$$g_2 = 0.7117 = C_2$$

$$g_3 = 3.3487 = L_3$$

$$g_4 = 1.0000 = R_L$$

with the lumped-element circuit shown in Figure 3.40.



(a)

Figure 3.40: Filter design procedure. Lumped-element low-pass filter prototype.

Now, here use Richards' transformations to convert series inductors to series stubs, and shunt capacitors to shunt stubs, as shown in Figure 3.41. The characteristic impedance of a series stub (inductor) is L , and the characteristic impedance of a shunt stub (capacitor) is $1/C$. For

commensurate line synthesis, all stubs are $\lambda/8$ long at $\omega = \omega_c$. (It is usually most convenient to work with normalized quantities until the last step in the design.)

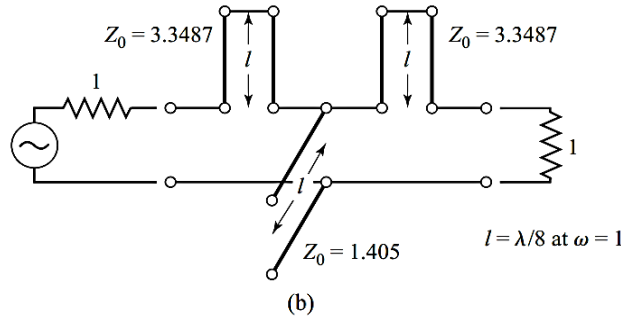


Figure 3.41: Using Richards' transformations to convert inductors and capacitors to series and shunt stubs.

The series stubs of Figure 3.41 would be very difficult to implement in microstrip line form, so we will use one of the Kuroda identities to convert these to shunt stubs. First we add unit elements at either end of the filter, as shown in Figure 3.42.

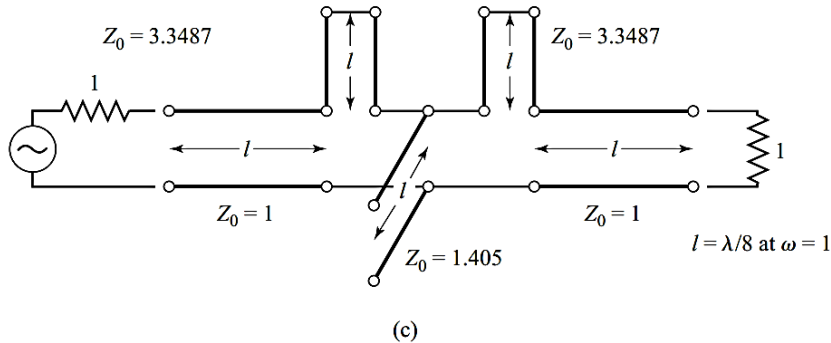


Figure 3.42: Adding unit elements at the ends of the filter.

These redundant elements do not affect filter performance since they are matched to the source and load ($Z_0 = 1$). Then we can apply Kuroda identity (b) from figure 4.20 to both ends of the filter. In both cases we have that

$$n^2 = 1 + \frac{Z_2}{Z_1} = 1 + \frac{1}{3.3487} = 1.299$$

The result is shown in Figure 3.43.

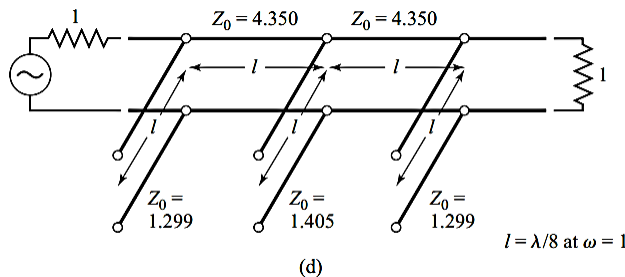


Figure 3.43: Applying the second Kuroda identity.

Finally, we impedance and frequency scale the circuit, which simply involves multiplying the normalized characteristic impedances by 50 ohm and choosing the line and stub lengths to be $\lambda/8$ at 4 GHz. The final circuit is shown in Figure 3.44,

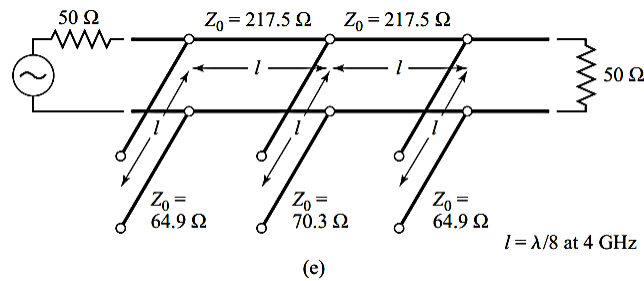


Figure 3.44: After impedance and frequency scaling of the design.

with a microstrip layout in Figure 3.45.

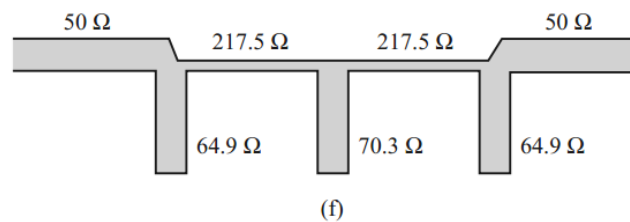


Figure 3.45: Microstrip fabrication of the final filter.

The calculated amplitude response of this filter is plotted in Figure 3.46, along with the response of the lumped-element version.

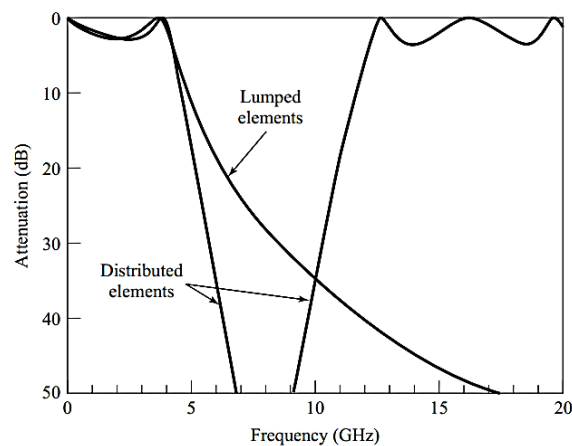


Figure 3.46: Amplitude responses of lumped-element and distributed-element low-pass filter.

Note that the pass-band characteristics are very similar up to 4 GHz, but the distributed-element filter has a sharper cutoff. Also notice that the distributed-element filter has a response that repeats every 16 GHz, as a result of the periodic nature of Richards' transformation.

3.12 Stepped-Impedance Low-Pass Filters

A relatively easy way to implement low-pass filters in microstrip or stripline is to use alternating sections of very high and very low characteristic impedance lines. Such filters are usually referred to as stepped-impedance, or hi-Z, low-Z filters, and are popular because they are easier to design and take up less space than a similar low-pass filter using stubs. Because of the approximations involved, however, their electrical performance is not as good, so the use of such filters is usually limited to applications where a sharp cutoff is not required.

In [57], the stepped impedance trace for crosstalk reduction was presented. Here, if the victim trace is a low-frequency or DC trace, one may employ a stepped impedance LPF configuration (i.e. using elements of alternating high and low impedance of the trace). Length l_{Hi} of the high impedance (Z_H) element can be calculated using the electrical length defined as,

$$\beta l_{Hi} = \frac{LR_0}{Z_H} \quad (3.45)$$

Where $\beta = 2\pi/\lambda$, λ corresponds to the cut-off frequency of the LPF, and R_0 represents the feed trace characteristic impedance. Similarly, length l_{Li} of the low impedance element (Z_L) can be calculated as,

$$\beta l_{Li} = \frac{CZ_L}{R_0} \quad (3.46)$$

where L and C are the normalized lumped element values for the inductors and capacitors respectively. The width of the elements is chosen corresponding to impedances Z_H and Z_L . Here, Z_H and Z_L are usually set to the highest and lowest characteristic impedance values that can be practically fabricated. It is worth mentioning that the difference between the two impedances should be as high as possible for excellent filter performance (i.e. sharp cut-off). However, in this case, sharp cutoff is not an essential requirement. Figure 4.24 illustrates an example of a 6 elements LPF design. Here, $Z_H = 120 \Omega$, $Z_L = 20 \Omega$, and $R_0 = 50 \Omega$, $d = 0.158$ cm, $\epsilon_r = 4.2$, $\tan \delta = 0.02$ and copper conductors of 0.5 mil thickness were chosen. Also, a cut-off frequency of 2 GHz was selected. The calculated values using (4.4) and (4.5) are given in Table 3.3.

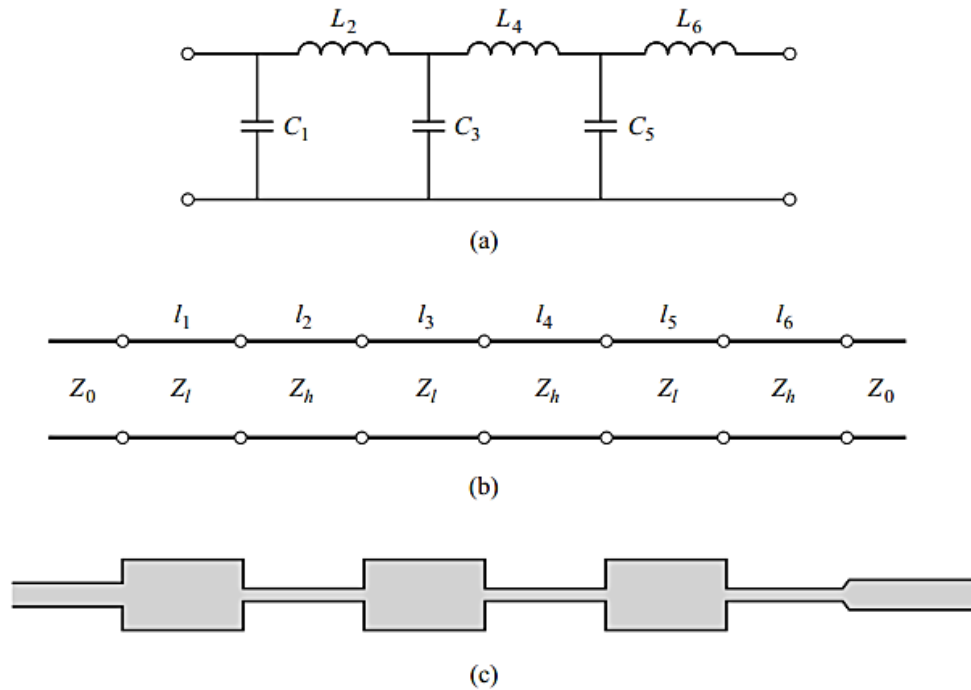


Figure 3.47: 6 element (a) Low-pass filter prototype circuit. (b) Stepped-impedance implementation. (c) Microstrip layout of final filter.

Table 3.3: 6 Elements Stepped Impedance LPF Design.

| Element Value | Impedance (Ohm) | Electrical Length | Length (mm) | Width (mm) |
|---------------|-----------------|-------------------|-------------|------------|
| $C_1=0.517$ | $Z_L=20$ | 11.8 | 2.05 | 11.3 |
| $L_2=1.414$ | $Z_H=120$ | 33.8 | 6.63 | 0.428 |
| $C_3=1.932$ | $Z_L=20$ | 44.3 | 7.69 | 11.3 |
| $L_4=1.932$ | $Z_H=120$ | 46.1 | 9.04 | 0.428 |
| $C_5=1.414$ | $Z_L=20$ | 32.4 | 5.63 | 11.3 |
| $L_6=0.517$ | $Z_H=120$ | 12.3 | 2.41 | 0.428 |

Figure 3.47 shows the calculated amplitude response of the filter, with and without losses. The effect of loss is to increase the passband attenuation to about 1 dB at 2 GHz. The response of the corresponding lumped-element filter is also shown in Figure 3.48. The passband characteristic is similar to that of the stepped impedance filter, but the lumped-element filter gives more attenuation at higher frequencies. This is because the stepped-impedance filter elements depart significantly from the lumped-element values at higher frequencies. The stepped-impedance filter may have other passbands at higher frequencies, but the response will not be perfectly periodic because the lines are not commensurate.

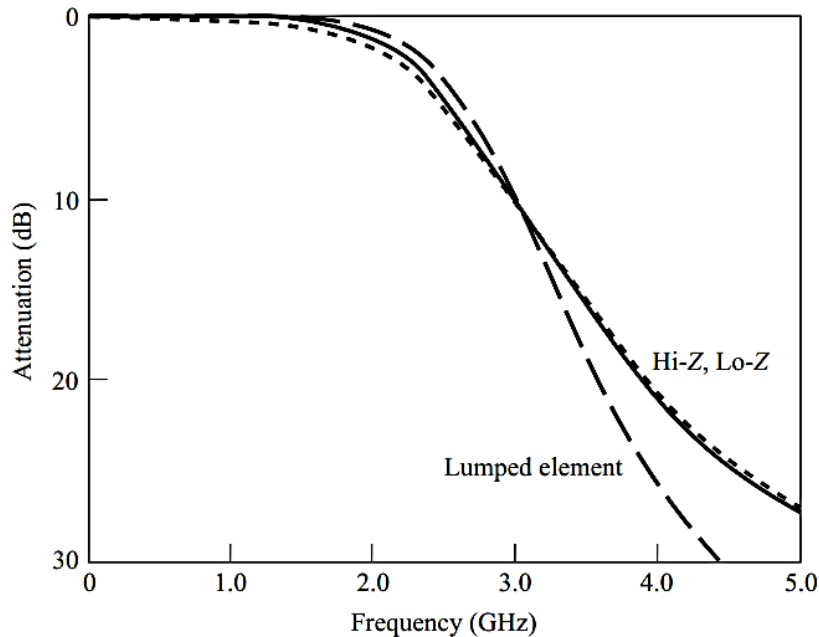


Figure 3.48: Amplitude response of the stepped-impedance low-pass filter, with (dotted line) and without (solid line) losses. The comparison with lumped-element filter is also shown in figure.

3.13 Conclusions

To understand the properties of EBGs the theory of EBG structures and various shapes of EBGs have been reviewed in short extent. Since they are also periodic in nature all theories of periodic structures hold true for EBGs. Two port networks, ABCD parameter and S-parameter theories are also analyzed for understanding the design and simulation. Then there have been shortly described about microwave and its range, application and the major terms. This chapter gives the better understanding of the phenomenon of EBG structures and wave propagation in periodic media. Then transmission line model has been presented by which anyone can understand about its working principle.

In this chapter, the theory of the conventional filter and two of the designs and their characteristics were also investigated. The stepped impedance design is easier and better performing than stubbed low-pass filter design. One drawback is that the open-circuited stub design has higher radiated emissions as compared to the stepped impedance design. Our main purpose of this thesis is to design new low-pass filter using electromagnetic bandgap structure to reduce the complexity of the calculations and design procedure. The design of the low-pass filter using electromagnetic bandgap structure is chosen for simplifying the designs and the procedures and optimizes the amplitude response.

Chapter-4

EBGS assisted T-line for LPF

4.1 Microstrip Lines

4.1.1 Microstrip Structure

The general structure of a microstrip is illustrated in Figure 4.1. A conducting strip (microstrip line) with a width W and a thickness t is on the top of a dielectric substrate that has a relative dielectric constant ϵ_r and a thickness h , and the bottom of the substrate is a ground (conducting) plane.

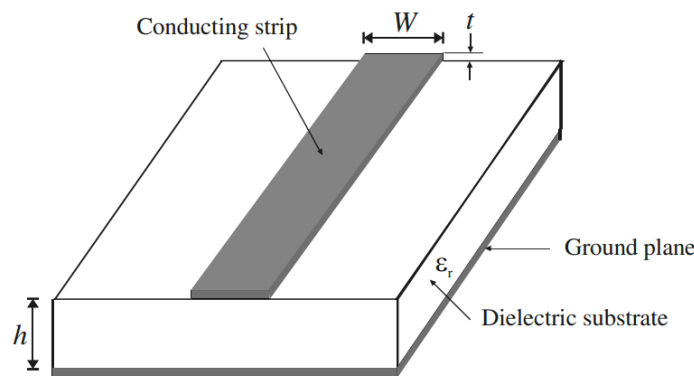


Figure 4.1: General microstrip structure.

4.1.2 Waves in Microstrips

The fields in the microstrip extend within two media—air above and dielectric below—so that the structure is inhomogeneous. Due to this inhomogeneous nature, the microstrip does not support a pure TEM wave. This is because that a pure TEM wave has only transverse components, and its propagation velocity depends only on the material properties, namely the permittivity ϵ and the permeability μ . However, with the presence of the two guided-wave media (the dielectric substrate and the air), the waves in a microstrip line will have non-vanished longitudinal components of electric and magnetic fields, and their propagation velocities will depend not only on the material properties, but also on the physical dimensions of the microstrip.

4.2 Definition of Electromagnetic Bandgap Structure (EBGS)

Periodic structures are abundant in nature, which have fascinated artists and scientists alike. When they interact with electromagnetic waves, exciting phenomena appear and amazing features result. In particular, characteristics such as frequency stop bands, passbands, and band gaps could be identified. Reviewing the literature, one observes that various terminologies have been used depending on the domain of the applications. These applications are seen in filter designs, gratings, frequency selective surfaces (FSS), photonic

crystals and photonic band gaps (PBG) etc. We classify them under the broad terminology of “Electromagnetic Band Gap (EBG)” structures. Generally speaking, electromagnetic band gap structures are defined as artificial periodic (or sometimes non-periodic) objects that prevent/assist the propagation of electromagnetic waves in a specified band of frequency for all incident angles and all polarization states.

4.3 Analysis methods for EBG structures

To analyze unique features of EBG structures, various methods have been implemented. These methods can be put into three categories: (1) lumped element model, (2) periodic transmission line method, and (3) full wave numerical methods. The lumped element model is the simplest one that describes the EBG structure as an LC resonant circuit [58], as shown in Figure 4.2. The values of the inductance L and capacitance C are determined by the EBG geometry and its resonance behavior is used to explain the band gap feature of the EBG structure. This model is simple to understand, but the results are not very accurate because of the simplified approximation of L and C .

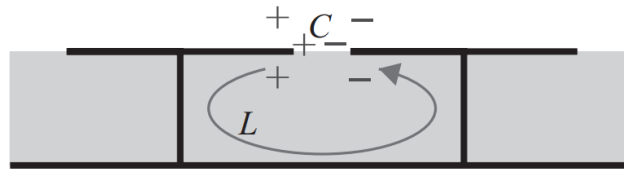


Figure 4.2: Lumped LC model for EBG analysis.

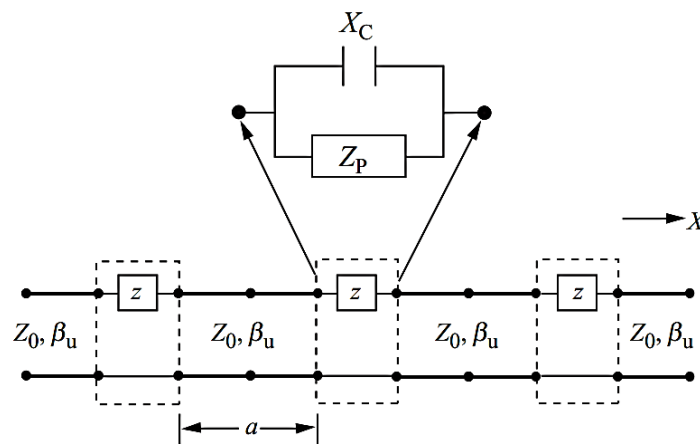


Figure 4.3: Periodic transmission line method for EBG analysis [36].

The periodic transmission line method is another popularly used technique to analyze EBG structures [36]. Figure 4.3 depicts a transmission line model of EBG structures, where Z_P is the impedance for each periodic element and X_C is the coupling capacitor. The Floquet periodic boundary condition is considered in this approach. After analyzing the cascaded transmission line, the dispersion curve can be readily obtained, which provides more information than the lumped element method. The surface wave modes, leaky wave modes, left- and right-hand regions, and band gaps can be easily identified from the dispersion curve. However, a difficulty in this method is how to accurately obtain the equivalent Z_P and X_C values of the EBG structures.

4.4 Analysis methods for Dumbbell Shaped DGS structures

The center frequency of the stopband of a PBG is approximately calculated by the well-known formula of Bragg's condition. Using this formula, the period for any stopband frequency can be determined. The theory of DGS is different from PBGS. At DGS, the dimensions of the dumbbell shaped slot (DGS unit cell) control the current paths on the ground plane hence the equivalent inductance and capacitance of the ground. Figure 4.4 shows the unit cell of a dumbbell shaped DGS. It is composed of two larger slots connected by a narrow vertical slot. The larger slot is a square patterned PBG element. On the other hand narrower vertical slot is a rectangular patterned PBG element.

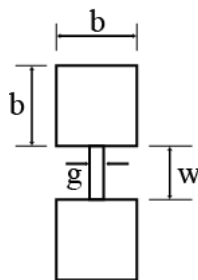


Figure 4.4: Geometry of a unit cell of a dumbbell shape DGS. The arm length of a larger square patterned slot is 'b'. The vertical rectangular slot has width, w and gap g.

The unit cell is etched in the ground plane of a standard 50 ohm transmission line. In order to investigate the frequency characteristics of the unit DGS cell, few structures having different 'b' and 'g' are simulated. All simulation results in one-pole LPF characteristics, which is obvious. There are two frequency properties; one is pole location, another is the existence of cut-off frequencies. Employing DGS section increases the effective permittivity and hence effective inductance. Cut-off frequency is mainly dependent on the etched larger square patterned slot that depends on the value of 'b'. The pole location mainly depends on the gap distance 'g'. Two parameters 'b' and 'g' are studied to observe the frequency characteristics.

The lumped LC equivalent model can be expressed as [33]:

$$C = \frac{\omega_c}{Z_0 g_1} \left[\frac{1}{\omega_0^2 - \omega_c^2} \right]$$

$$L = \frac{1}{4\pi^2 f_0^2 C}$$

Where, f_0 is the frequency of the attenuation pole, ω_c is the angular cutoff frequency, Z_0 is the characteristic impedance of the line, and g_1 is the admittance value of the Butterworth low pass filter response.

The equivalent circuit of DGS unit cell is shown in Figure 4.5.

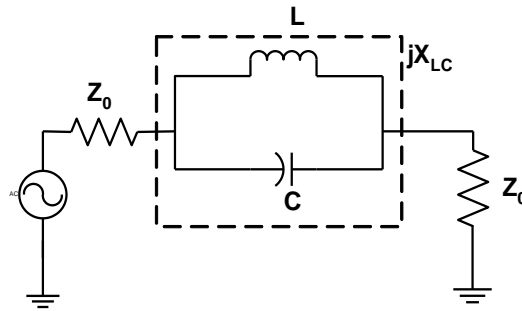


Figure 4.5: The equivalent circuit of dumbbell shaped DGS unit.

4.5 Uniform PBG (UPBG) Configurations Applied To Microstrip Lines

In modern microwave devices, microstrip transmission lines are most common. Therefore, in the following sections, the investigation is concentrated into only on PBG assisted microstrip transmission line. To derive the characteristic performance of PBG assisted lines it is more logical to use scattering parameters (S-parameters) instead of showing K- β diagram. S-parameters are universally accepted format of device characterizations. Moreover, commercially available software tool Zealand IE3D will be used to design and to extract S-parameters for all designs due to the flexibility of Zealand IE3D. Zealand IE3D is a method of moment (MOM) based full-wave analysis tool, hence very accurate.

The perturbation in the ground plane of any microstrip transmission line in the form of PBGS creates stopband that is useful for suppression of surface waves, leakage, and spurious transmission and to improve the performance of antennas, filter and other microwave devices and components. The stopband characteristic is highly influenced by the shape, size and the period of the PBGSs located on the ground plane. Therefore, it is useful to see the performance of the standard 50-ohm microstrip transmission line on PBGSs. The lines will be investigated to see the performance of three rows of uniform PBG structure as [43]. In this section, uniform circular and square patterned PBGS will be investigated. It is well known that the EM field is highly concentrated under the microstrip line. Under this consideration, one dimensional (1-D) uniform PBGS (one line) will be investigated and compared the result with 2-D structure (three lines). Finally 1-D PBGS will be used as two structures yield similar performances.

4.5.1 Design of Microstrip Transmission Line over Uniform PBGS (uniform circular PBGS)

With the inclusion of PBGSs the dispersion characteristics of a transmission line change. At first a microstrip transmission line with the unperturbed ground plane is designed that does not provide any stopband characteristics. Then the effect is observed on the dispersion characteristics in the form of scattering parameters matrices versus frequency by perturbing the ground plane with uniform circular PBGSs.

- **Designing equation**

In the PBG engineering it is a conventional rule to use Bragg's condition [60] to calculate the central stopband frequency provided by PBGSs. Under this condition, inter-cell separation (known as period) is approximately equal to half wavelength of the stopband central frequency. From the inter-cell separation, the size of the PBG element is calculated on the basis of Filling factor (FF).

The geometry of the design is patterned under 50 ohm transmission line are designed by using "Taconic Substrate" in which relative dielectric constant $\epsilon_r = 2.45$, Thickness, $h=31\text{mil}$ or 0.787mm . Using Personal Computer Aided Antenna Design 5.0 (PCAAD) software the values of transmission line width, $w = 0.2263\text{ cm}$ and effective dielectric constant, $\epsilon_{eff} = 2.068$ has been found.

We know that,

$$\lambda_0 = \frac{300\text{ (mm)}}{f_c\text{ (GHz)}}$$

$$\lambda_g = \frac{\lambda_0}{\sqrt{\epsilon_{eff}}}$$

$$a = \frac{\lambda_g}{2}$$

For $f_c = 10\text{ GHz}$,

$$\lambda_0 = \frac{300}{10} = 30\text{ mm}$$

$$\lambda_g = \frac{\lambda_0}{\sqrt{\epsilon_{eff}}} = \frac{30}{2.068} = 20.86\text{ mm}$$

Now,

$$a = \frac{\lambda_g}{2} = \frac{20.86}{2} = 10.43\text{ mm}$$

Filling factor, $FF = \frac{r}{a}$

Where, r = radius of circular PBGS, a = inter-element spacing.

The center frequency of the stopband is calculated approximately with the following expression:

$$\beta a = \pi$$

Where, a is the period of the PBG pattern, and β is the wave number in the dielectric slab and is defined by expression:

$$\beta = \frac{2\pi f_0}{c} \sqrt{\epsilon_{eff}}$$

Where,

f_0 = the center frequency of the stopband

ϵ_{eff} = the effective relative permittivity of the dielectric slab

c = the speed of light in free space

- **Designs of Uniform Circular PBGSs**

The following different microstrip transmission lines are designed. All the PBGSs are designed at the stopband central frequency of 10 GHz.

1. **Standard 50-ohm transmission line:** In this case the ground plane is fully unperturbed. A standard 50 ohm line is realized on Taconic substrate having dielectric constant of 2.45 and height of 31 mils.
2. **2-D uniform circular elements in the ground plane:** Here three PBG structures under 50 ohm transmission lines with FF of 0.125, 0.25 and 0.45 are designed to produce the same result of [43]. This design gives the idea of optimum value of FF to be 0.25. The geometry of a three rows (2-D) uniform hole patterned PBGSs in the ground plane of a 50 ohm transmission line is shown in Figure 4.6.

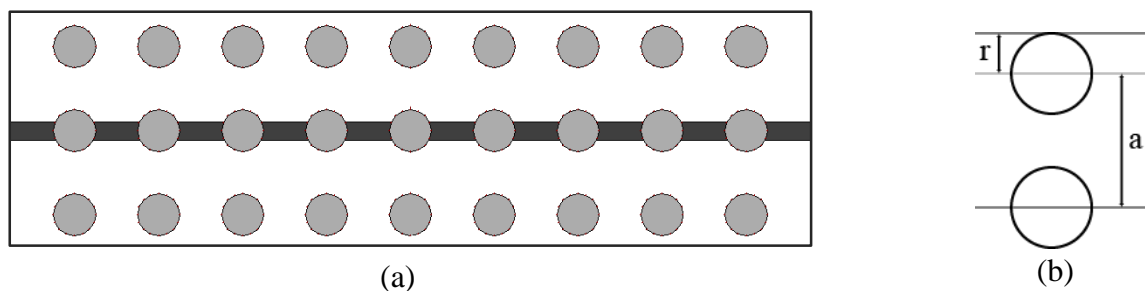


Figure 4.6: (a) Geometry of a 50-ohm microstrip transmission line where 2-D (three lines) uniform circular PBGSs are etched in the ground plane. (b) The filling factor (FF) explanation ($FF = r/a$).

1-D uniform circular PBGSs with FF of 0.25: This design will yield the performance to consider 1-D PBGSs that replace 2-D PBGSs. The geometry of 1-D uniform hole patterned PBGSs is shown in Figure 4.7. In this design only one row of PBG elements are etched in the ground plane just under the 50 ohm transmission line.

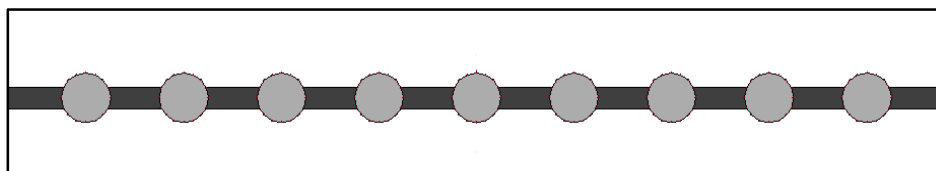


Figure 4.7: Geometry of a standard 50-ohm transmission line with 1-D uniform circular PBGSs etched in the ground plane.

- **Designs of Uniform Square Patterned PBGSs**

Uniform square patterned PBGSs will also be designed. Here three rows and one row PBGSs will be designed and their performances will be compared. It will be useful to replace three rows PBGSs by 1-D PBGSs. On the basis of the availability of the materials for the fabrications Taconic substrate with $\epsilon_r = 2.45$ and height (h) = 31 mils is used in the simulation.

1. **2-D Uniform Square Patterned PBGSs**

The conventional uniform square patterned PBGSs are shown in Figure 4.8. Three lines of total 27 PBG elements are etched under the standard 50-ohm transmission line. The FF is taken to be 0.5.

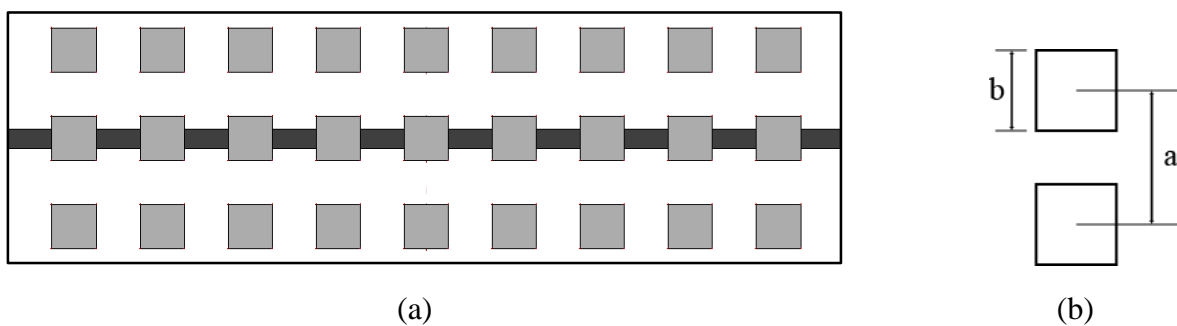


Figure 4.8: (a) 2-D (three lines) of square patterned PBGSs under standard 50 ohm transmission line. Substrates: $\epsilon_r = 2.45$ and height (h) = 31 mils and $\tan \delta = 0.002$. The inter-element spacing, $a = 10.43$ mm, element width and length, $b = 5.215$ mm. (b) The filling factor (FF) explanation ($FF = b/a$).

2. **1-D square patterned PBGSs**

The geometry of 1-D (one line) circular patterned PBGSs is shown in Figure 4.9. Here only 9 PBG elements are etched in the ground plane.

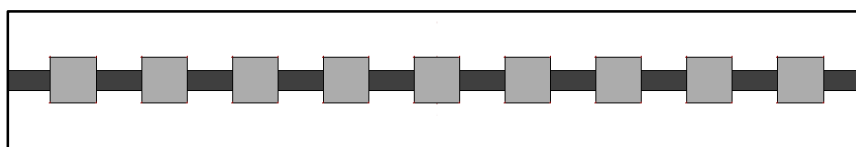


Figure 4.9: 1-D square patterned periodic structures under standard 50-ohm transmission line. The substrate is Taconic having dielectric constant of 2.45 and height of 31 mils. The inter-element spacing, $a = 10.43$ mm, element width and length, $b = 5.215$ mm.

- **Designs of Uniform Dumbbell shaped Defected Ground Structures (DGSs)**

Uniform dumbbell shaped DGSs will also be designed. Here one row dumbbell shaped DGSs will be designed. On the basis of the availability of the materials for the fabrications Taconic substrate with $\epsilon_r = 2.45$ and height (h) = 31 mils is used in the simulation. The bigger slot dimension is 205×205 mil or (5.21×5.21 mm) and narrow slot dimension is 50×200 mil or (1.27×5.08 mm)

1. 1-D Dumbbell shaped DGSs

The geometry of 1-D (one line) Dumbbell shaped DGSs is shown in Fig. 4.10. Here only 9 DGS elements are etched in the ground plane.

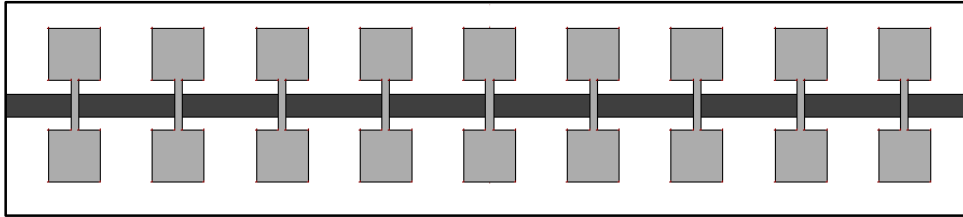


Figure 4.10: 1-D Dumbbell shaped DGSs patterned periodic structures under standard 50-ohm transmission line. The substrate is Taconic having dielectric constant of 2.45 and height of 31 mils. The inter-element spacing, $a = 10.43$ mm, element width and length, $b = 5.215$ mm.

4.5.2 Results

An ideal transmission line as well as transmission lines having circular and square patterned uniform PBGSs in the ground plane have been investigated. The performances have been analyzed of the lines in terms of 10 dB return loss bandwidth, 20 dB rejection bands, ripple heights in passband, depth of the stopband and maximum value of return loss.

- **The Ideal Transmission line:**

The S-parameters of the designs have been investigated to conceive the idea of 1-D PBGSs in lieu of 2-D PBGSs, optimized FF and the influence of number of PBGSs on the dispersion characteristics of the microstrip transmission line. The Taconic substrate is used in the simulation for the ideal and uniform structured PBGSs. The simulated S-parameters performances of an ideal transmission line are shown in Fig. 4.11. The insertion loss is approximately zero dB throughout the whole frequency range from 0 to 14 GHz.

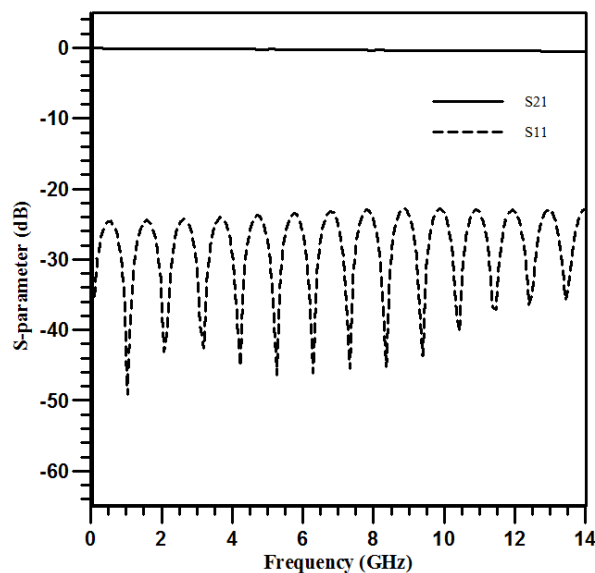


Fig. 4.11: IE3D simulated S-parameters versus frequency of an ideal 50-ohm transmission line. The substrate is Taconic having height of 31 mils and the dielectric constant is 2.45

It can be seen from the graph that the signal is transmitting between two ports of transmission line with negligible loss. Therefore within the whole range of frequencies (0-14 GHz) there is no stopband. The return loss performance of the ideal microstrip line over the whole frequency range is also excellent and >10 dB. Obviously the S-parameters performance shown in Figure 4.11 characterizes an ideal transmission line.

- **The Transmission Line with 2-D (three lines) Uniform Circular PBGS**

At first, small uniform and circular holes have been introduced in the ground plane to observe their effects on the performance of a standard 50 ohm transmission line. The radius of the uniform circular PBGSs are 2.6075 mm and the period is 10.43 mm. The S-parameters performance is shown in Fig. 4.12. It can be seen from the figure that this design provides wider passband and deeper stopband. The 10 dB return loss bandwidth is found to be 6.31 GHz; the 20 dB rejection bandwidth is 4.35 GHz. The ripple height along the passband is negligible. But around cut-off frequencies ripples are observed. The center frequency is found to be shifted around 10.06 GHz resulting in 1% frequency deviations from the design frequency. The maximum value of isolation is found to be 61.6 dB.

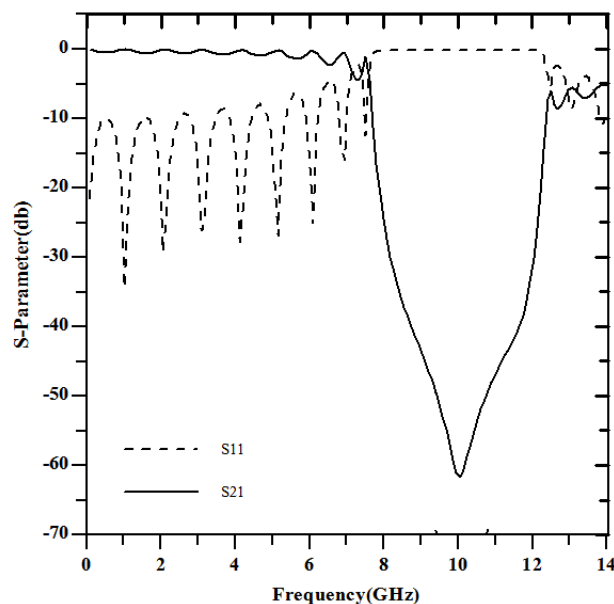


Figure 4.12: Simulated S-parameter performances of a standard 50-ohm transmission line perturbed by 2-D (three lines) uniform circular PBGSs in the ground plane. The substrate is Taconic having height of 31 mils and dielectric constant of 2.45. The uniform circular PBGSs are of 2.6075 mm and the period is 10.43 mm (FF=0.25).

- **The Transmission Line with 1-D Uniform Circular PBGSs**

It is mentioned that 0.25 is the optimum FF for Taconic with dielectric constant of 2.45 and height of 31 mils. Based on this value a microstrip transmission line with 1-D uniform circular PBGSs has also been investigated. The simulation result is shown in Fig. 4.13.

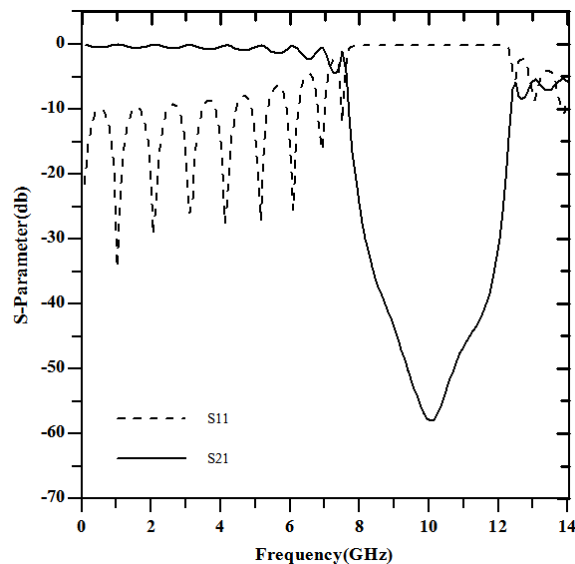


Figure 4.13: Simulated S-parameter performances of a standard 50 ohm transmission line perturbed by 1-D (one line) uniform circular PBGSs in the ground plane.

From the Fig. 4.13, it can be seen that return loss performance, stopband characteristics and ripple height for this design is similar as 2-D design. A negligible difference in the value of maximum isolation is observed. In the case of three rows of uniform circular PBGSs the maximum isolation is found to be approximately 61.6 dB. On the other hand, one row of uniform circular PBGS provides approximately 61.46 dB

From this figures (Figure 4.12 and 4.13) it is very clear that 1-D PBGSs and 2-D PBGSs provide very similar performances.

- **The Transmission Line with 2-D Uniform rectangular PBGSs**

The S-parameters performances of uniform square patterned PBGSs have also been analyzed. The simulated and measured S-parameters performances of three lines (2-D) uniform square patterned PBGSs are shown in Figure 4.14.

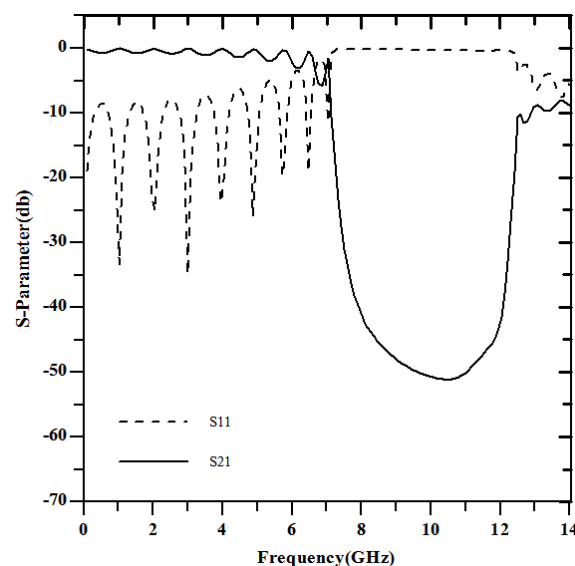


Figure 4.14: S-parameters performances of three lines uniform square-patterned PBG structures. The substrate is Taconic having dielectric constant of 2.45 and height of 31 mils. The inter-element spacing is 10.43 mm and FF is 0.5.

At first, small uniform and rectangular holes have been introduced in the ground plane to observe their effects on the performance of a standard 50 ohm transmission line. The both length of the uniform rectangular PBGSs are 5.215 mm and the period is 10.43 mm.

It can be seen from the figure that this design provides wider passband and deeper stopband. The 20 dB rejection bandwidth is 5.12 GHz. The ripple height along the passband is negligible. But around cut-off frequencies ripples are observed. The center frequency is found to be shifted around 10.41 GHz resulting in 4% frequency deviations from the design frequency. The maximum value of isolation is found to be 51.1 dB.

- **The Transmission Line with 1-D Uniform rectangular PBGSs**

It is mentioned that 0.5 is the optimum FF for Taconic with dielectric constant of 2.45 and height of 31 mils. Based on this value a microstrip transmission line with 1-D uniform rectangular PBGSs has also been investigated. The simulation result is shown in Fig. 4.15.

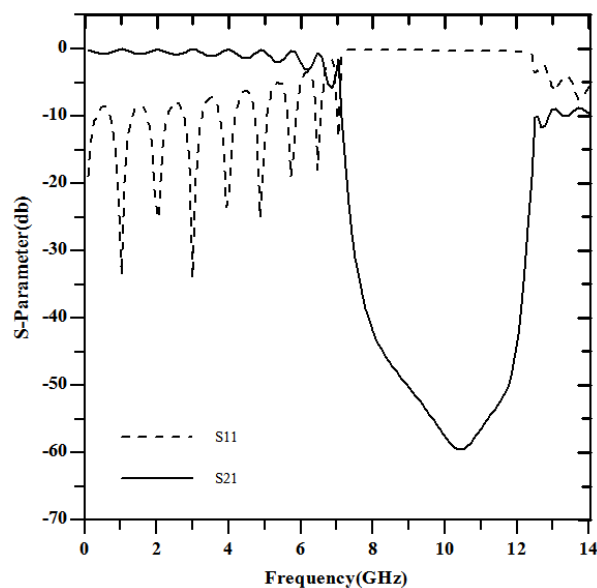


Figure 4.15: Simulated S-parameter performances of a standard 50 ohm transmission line perturbed by 1-D (one line) uniform rectangular PBGSs in the ground plane.

From the Fig. 4.15, it can be seen that return loss performance, stopband characteristics and ripple height for this design is similar as 2-D design. A small difference in the value of maximum isolation is observed. In the case of three rows of uniform rectangular PBGSs the maximum isolation is found to be approximately 51.1 dB. On the other hand, one row of uniform rectangular PBGS provides approximately 59.5 dB.

- **The Transmission Line with 1-D Uniform Dumbbell shaped DGSs**

It is mentioned that 0.5 is the optimum FF of larger slot of DGS for Taconic with dielectric constant of 2.45 and height of 31 mils. Based on this value a microstrip transmission line with 1-D uniform Dumbbell shaped DGSs has been investigated. The simulation result is shown in Fig. 4.16.

It can be seen from the figure that this design provides wider passband and deeper stopband. The 20 dB rejection bandwidth is 3.66 GHz. The ripple height along the passband is not negligible in this time. The maximum value of isolation is found to be 41.1 dB. It looks like a low pass filter but a observable harmonics is shown before 10 GHz frequency.

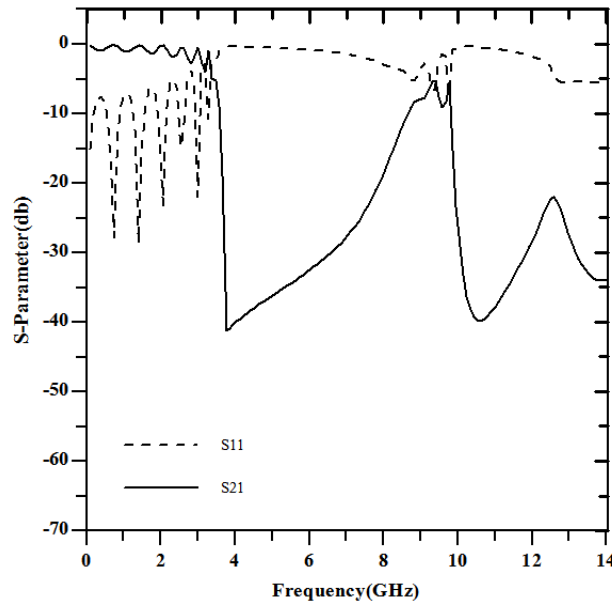


Figure 4.16: S-parameters performances of three lines uniform Dumbbell shaped DGS structures. The substrate is Taconic having dielectric constant of 2.45 and height of 31 mils. The inter-element spacing is 10.43 mm and FF with respect to larger element is 0.5.

4.6 Compactness

DGS plays a vital role to make the compact size structures. To make this understand an example is given in this section. For example, the conventional square patterned DGS structure beneath the transmission line makes the center frequency near about 10GHz and cutoff frequency near about 7GHz. For the lower the cutoff frequency a change is required for the design. According to the theory, it is necessary to change the filling factor (FF) either by reducing EBG areas or by increasing the interval between two EBG structures. Figure 4.17 is the design of square patterned 1-D EBG structure followed the figure 5.9. The change is that the filling factors i.e., the interval between two EBG structures are increased.

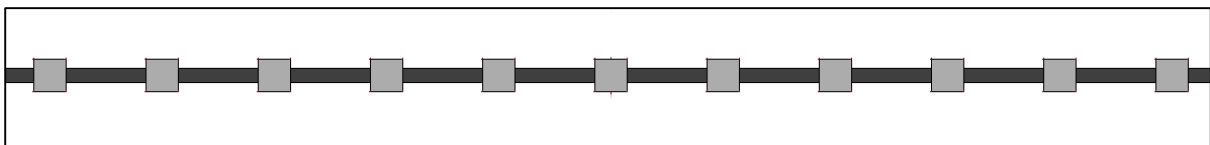


Figure 4.17: 1-D square patterned periodic structures under standard 50-ohm transmission line. The substrate is Taconic having dielectric constant of 2.45 and height of 31 mils. The inter-element spacing, $a = 20.86$ mm, element width and length, $b = 5.215$ mm.

The graphical representation of the insertion loss performances of a standard 50 ohm transmission line perturbed by 1-D (one line) uniform rectangular PBGSs vs. Dumbbell shaped DGS is shown below,

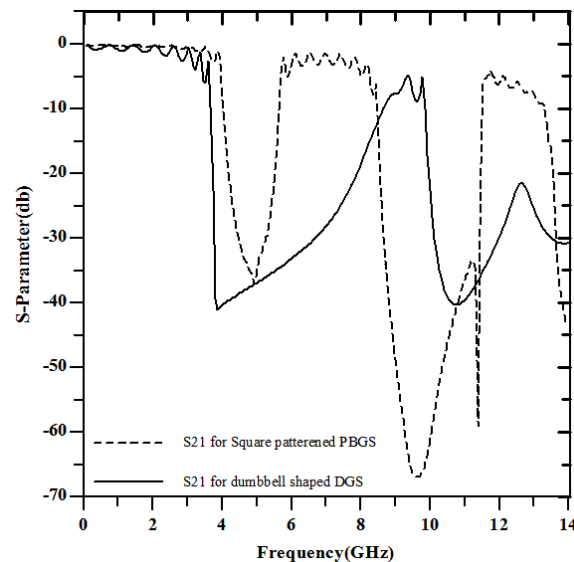


Figure 4.18: Simulated insertion loss performances of a standard 50 ohm transmission line perturbed by 1-D (one line) uniform rectangular PBGSs vs. Dumbbell shaped DGS in the ground plane. The inter-element distance is $a = 822$ mils (PBGSs) and 411 mils (DGSs).

The main drawbacks of that PBGS structure are:

1. Total size of the structure size is 200% increase from the conventional structure (figure 4.9)
2. Stop band is not too wide.
3. Harmonics after 6GHz is not negligible.

From the result of uniform DGSs it can be seen that the DGSs make the same result with cutoff frequency near about 4 GHz by the compact way and also gives wider stop band than that PBGS structure. Analyzing figure 4.18, a thing is clear that DGSs are miniaturized the total designs. And this DGSs give the significant performance.

4.7 Conclusion

Firstly, the transmission line model has been presented. To understand the properties of PBGSs the theory of PBG structures and dumbbell shaped DGS structures has been presented in short extent. Since they are also periodic in nature all theories of periodic structures hold true for PBGSs.

Uniform circular, square shaped PBGSs and dumbbell shaped DGSs have been analyzed. All designs have been investigated with FF of 0.25 for circular PBGSs and 0.5 for both rectangular PBGSs and dumbbell shaped DGSs is considered to be the optimum value of FF. Three rows and one row uniform PBGSs are studied to replace 2-D PBG elements by 1-D PBG elements for both the shapes. Both the designs provide very similar performances. Throughout whole investigations, it is preferred to use 1-D PBGSs rather than 2-D PBGSs.

Chapter-5

Non-uniform EBGs for LPF

5.1 Introduction

In chapter 4, uniform circular, rectangular patterned PBGSs and dumbbell shaped DGSs with optimum FFs and the numbers of PBG/DGS elements have been addressed. High passband ripples and poor passband matching are the two serious problems of conventional uniform PBGSs. In this chapter non-uniform PBGSs with Binomial and *Chebyshev* distributions are investigated. How proposed PBGS and dumbbell shaped DGS improves these two problems and simplifies the filter synthesis are demonstrated. The aperiodicity of non-uniform structure is realized by Binomial and *Chebyshev* distribution. The non-uniformities of the chirped PBG elements are realized by implementing Binomial and *Chebyshev* distribution in calculating the amplitudes of PBG elements.

In this chapter, novel DGS structures in the form of non-uniform distributions of different patterns (e.g., circular, rectangular, dumbbell shaped, etc.) are proposed to investigate the improvement in S-parameters performance and it will be seen if they can be used as an ideal LPF. While the uniform distribution of the circular patterned PBG [43] is hindered with high passband ripples near the cut-off frequency, the non-uniform distributions in the forms of Binomial and *Chebyshev* polynomials yield superior performances by suppressing passband ripples and producing distinct wide stopbands. The novelty of the proposition is that Binomial and *Chebyshev* polynomials are exploited to control the LPF response and selectivity. Hence the filter synthesis is substantially relaxed in the present approach. Also the depth of passband return loss, selectivity and the ripples can be controlled with the side-lobe level index of *Chebyshev* polynomial. Since the passband ripple height increases with the FF, the uniform circular patterned PBG limits the wideband applications. Using the non-uniform distribution of PBG patterns, both passband ripple and stop bandwidth problems are alleviated and the selectivity of the stopband of planar PBGSs increases.

5.2 Theory of Non-uniform 1-D Microstrip PBGSs

5.2.1 Binomial Distribution

Binomial distribution is the determination of the probability distribution for the discrete number of successes in an independent sequence of experiments. The coefficients of the polynomial are determined by the expression (5.1).

$$(1 + x)^{N-1} = 1 + (N - 1)x + \frac{(N - 1)(N - 2)}{2!}x^2 + \frac{(N - 1)(N - 2)(N - 3)}{3!}x^3 + \dots \quad (5.1)$$

The positive coefficients of the series expansion for different values of N are expressed in terms of the Pascal's triangle [76].

| | | | | | | | | | | |
|---|----|----|-----|-----|-----|-----|-----|----|----|---|
| | | | | 1 | | | | | | |
| | | | | 1 | | 1 | | | | |
| | | | 1 | | 2 | | 1 | | | |
| | | 1 | | 3 | | 3 | | 1 | | |
| | 1 | | 4 | | 6 | | 4 | | 1 | |
| | 1 | 5 | | 10 | | 10 | | 5 | 1 | |
| | 1 | 6 | 15 | | 20 | | 15 | 6 | 1 | |
| | 1 | 7 | 21 | 35 | | 35 | 21 | 7 | 1 | |
| | 1 | 8 | 28 | 56 | 70 | | 56 | 28 | 8 | 1 |
| | 1 | 9 | 36 | 84 | 126 | 126 | 84 | 36 | 9 | 1 |
| 1 | 10 | 45 | 120 | 210 | 252 | 210 | 120 | 45 | 10 | 1 |

Figure 5.1: Pascal's Triangle.

If the values of N represent the numbers of elements in an array, the coefficients of the expansion represent the relative amplitudes of the elements. Generally, this type of array suffers from practical limitation of bandwidth and efficiency due to the abrupt change in amplitude tapering between adjacent elements. In this work the dimensions of the circular PBGSs are varied proportionally to the relative amplitudes of the polynomial.

5.2.2 Chebyshev Distribution

Instead of maximally flat passband characteristics, an equally useful characteristic is one that may permit the transmission coefficient to vary with minute ripples over the stopband. This provides a considerable increase in bandwidth with respect to Binomial distribution. This equal-ripple characteristic is obtained by making the distribution according to Chebyshev polynomial. The basic properties of the polynomials [61] are expressed as follows:

$$T_m(z) = 2zT_{m-1}(z) - T_{m-2}(z) \quad (5.2)$$

where $T_m(z)$ is expressed as:

$$T_m(z) = \cos[m\cos^{-1}(z)] \text{ for } |z| \leq 1 \quad (5.3)$$

The coefficients of the polynomial are determined for any prescribed side lobe level. The amplitudes of 10 element PBGSs according to *Chebyshev* equations are determined as follows:

0.36 0.49 0.71 0.78 1 1 0.78 0.71 0.49 0.36

The amplitude 1 is for the two center elements of the 10-element array and the rest elements follow suit. For PBG design the elements are varied proportionally to the relative amplitudes, respectively.

5.3 Design of LPF Using 1-D Microstrip PBGSs

5.3.1 Design Principles

To understand the design of non-uniform distribution, the principle is described by *Chebyshev* distribution. Figure 5.2 and Figure 5.3 show different varieties—a *uniform* circular and *non-uniform* circular patterned planar PBGSs on microstrip substrates respectively. As can be seen in the figures, the uniform and the non-uniform circular patterns are etched with a period ‘ a ’ on the ground plane of standard microstrip transmission lines. The important design parameters to achieve a stopband characteristic are the period ‘ a ’ and the filling factor ‘ r/a ’. For the uniform circular patterned PBG, the circles are of the same radius ‘ r_0 ’ and period ‘ a ’. For non-uniform patterned PBGSs, the central elements have the largest radii of ‘ r_0 ’ and the radii of the adjacent circles decrease proportionally to the amplitude coefficients of the polynomials. For *Chebyshev* distribution, the area of the PBG patterns will vary proportionally to the coefficients of the polynomial for a particular side-lobe level (voltage ratio). Here two distinct relationships are proposed between the amplitudes of the coefficients of the polynomials and the physical dimensions of the PBG circles. They are: (1) polynomial coefficient’s amplitude \propto the radius of the PBG circle (r), called Type-A, and (2) polynomial coefficient’s amplitude \propto the area of the PBG circle (πr^2); called Type-B. The investigations are carried out with the two types of PBG configurations with circular patterns and the respective results are produced in this section. For all the designs the center frequency of the stopband is calculated approximately with the equation of Bragg’s condition.

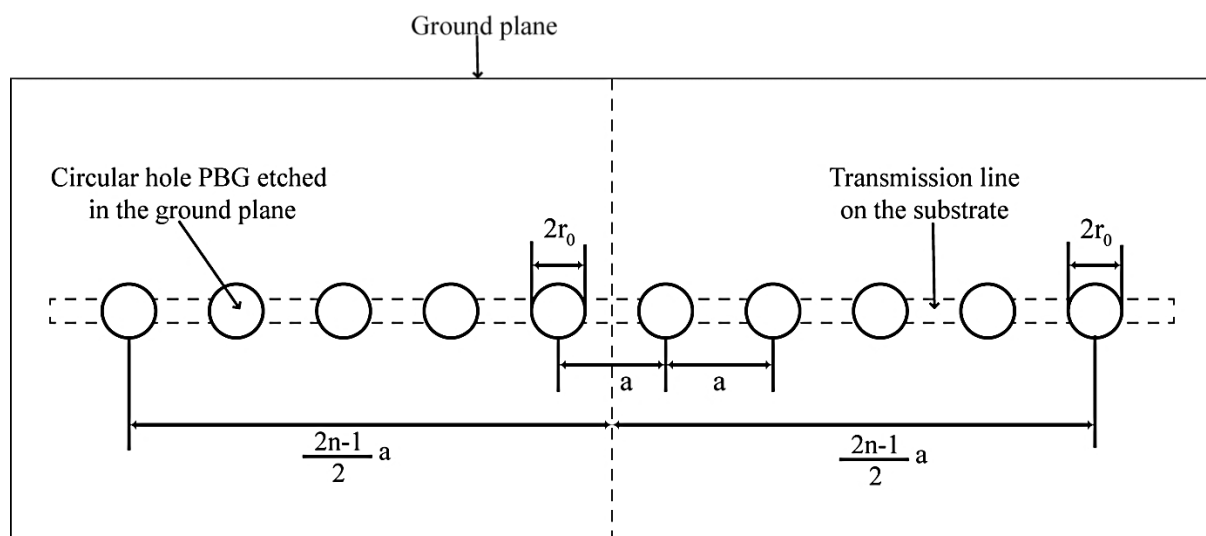


Figure 5.2: Geometry of circular uniform PBGS. The PBG elements are having radius of r_0 etched in the ground plane.

For an N-element PBG patterns, the n-th element’s location from the center of the PBG period can be derived from the following equation:

$$d_n = \begin{cases} \frac{2n-1}{2}a & \text{for even } N \\ (n-1)a & \text{for odd } N \end{cases} \quad (5.4)$$

Figure 5.2 and Figure 5.3 show such distribution for even N .

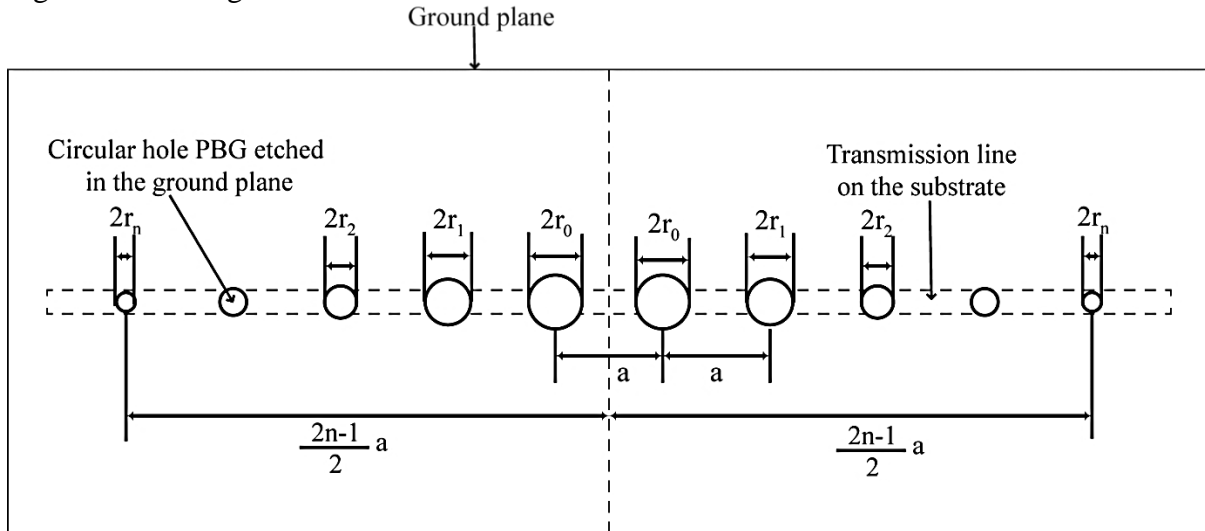


Figure 5.3: Geometry of circular non-uniform PBGSs etched in the ground plane. The central two elements have largest value and the remaining PBGS follow *Chebyshev* distribution.

5.3.2 Non-Uniform PBG Structures

1. Design-1 (Binomial Distribution over circular PBGSs):

The geometry of one lined circular patterned PBGSs using binomial distribution below the 50 ohm transmission line is shown in figure 5.4. The length of line is 100 mm and width is 2.263 mm. Here only 8 EBG elements are etched in ground plane and the filling factors are variable. The non-uniform circular patterned PBGS elements have the period of 10.43 mm. For the radius of non-uniform circular patterned PBGSs, we have used the coefficient of the Binomial distribution for 8 element PBGSs. We have applied Binomial distribution on the radius (r) of every DGS. For $N=8$ the coefficients are 0.03, 0.2, 0.6, 1, 0.6, 0.2, 0.03 and the radius (r) of the PBGSs are taken 0.08, 1.05, 1.57, 2.61, 1.57, 1.05, 0.08 mm.

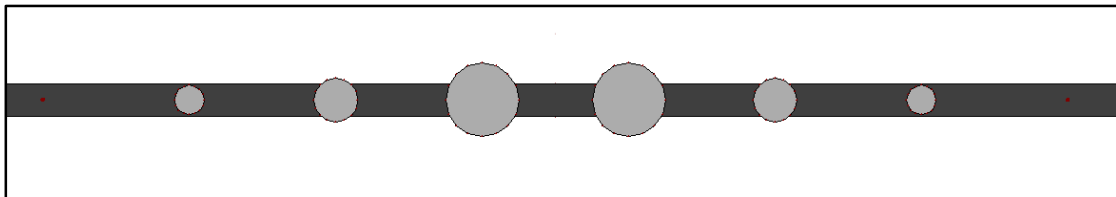


Figure 5.4: Geometry of a binomially distributed circular patterned PBGS designed by varying the radius of PBGSs etched in the ground plane. The period of PBGS is 10.43 mm and the substrate is Taconic with dielectric constant= 2.45 and height= 31 mils.

2. Design-2 (Binomial Distribution over rectangular PBGSs):

The geometry of one lined rectangular patterned PBGSs using binomial distribution below the 50 ohm transmission line is shown in figure 5.5. The length of line is 100 mm and width

is 2.263 mm. Here also 8 EBG elements are etched in ground plane and the filing factors are also variable. The non-uniform circular patterned PBGS elements have the period of 10.43 mm. For the arms of non-uniform rectangular patterned PBGSs, we have used the coefficient of the Binomial distribution for 8 element PBGSs. We have applied Binomial distribution on the arms of every rectangular patterned PBGS. For $N=8$ the coefficients are 0.03, 0.2, 0.6, 1, 0.6, 0.2, 0.03 and the arm of the PBGSs are taken 0.08, 1.05, 1.57, 2.61, 1.57, 1.05, 0.08 mm.

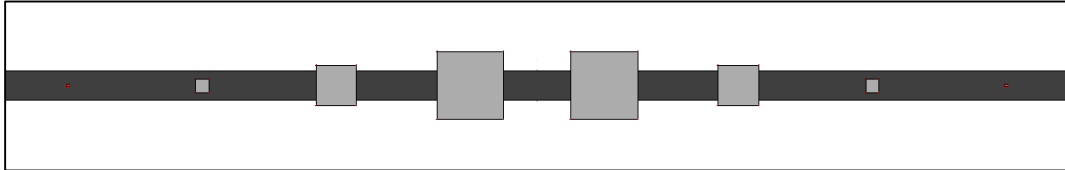


Figure 5.5: Geometry of a binomially distributed rectangular patterned PBGS designed by varying the arm lengths of PBGSs etched in the ground plane. The period of PBGS is 10.43 mm and the substrate is Taconic with dielectric constant= 2.45 and height= 31 mils.

3. Design-3 (*Chebyshev* Distribution over circular PBGSs):

The geometry of one lined circular patterned PBGSs using *Chebyshev* distribution below the 50 ohm transmission line is shown in figure 5.6. The length of line is 100 mm and width is 2.263 mm. Here 9 EBG elements are etched in the ground plane and the filing factors are variable. The non-uniform circular patterned PBGS elements have the period of 10.43 mm. For the radius of non-uniform circular patterned PBGSs, we have used the coefficient of the *Chebyshev* distribution for 9 element PBGSs. We have applied Binomial distribution on the radius (r) of every PBGS. For $N=9$ the coefficients are 0.36 0.49, 0.71, 0.78, 1, 0.78, 0.71, 0.49, 0.36 and the radius (r) of the PBGSs are taken 0.94, 1.28, 1.86, 2.04, 2.61, 2.04, 1.86, 1.28, 0.94 mm. The FF of the central element is 0.25.

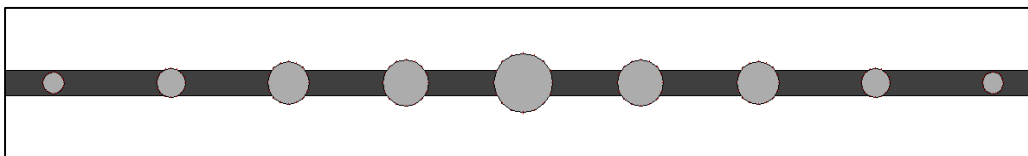


Figure 5.6: Geometry of a *Chebyshev* distributed circular patterned PBGS designed by varying the radius of PBGSs etched in the ground plane. The period of PBGS is 10.43 mm and the substrate is Taconic with dielectric constant= 2.45 and height= 31 mils.

4. Design-4 (*Chebyshev* Distribution over rectangular PBGSs):

The geometry of one lined rectangular patterned PBGSs using binomial distribution below the 50 ohm transmission line is shown in figure 5.7. The length of line is 100 mm and width is 2.263 mm. Here also 9 EBG elements are etched in ground plane and the filing factors are also variable. The non-uniform circular patterned PBGS elements have the period of 10.43 mm. For the arms of non-uniform rectangular patterned PBGSs, we have used the coefficient of the Binomial distribution for 9 element PBGSs. We have applied Binomial distribution on the arms of every rectangular patterned PBGS. For $N=9$ the coefficients are 0.36 0.49, 0.71,

0.78, 1, 0.78, 0.71, 0.49, 0.36 and the arm of the PBGSs are taken 0.94, 1.28, 1.86, 2.04, 2.61, 2.04, 1.86, 1.28, 0.94 mm.

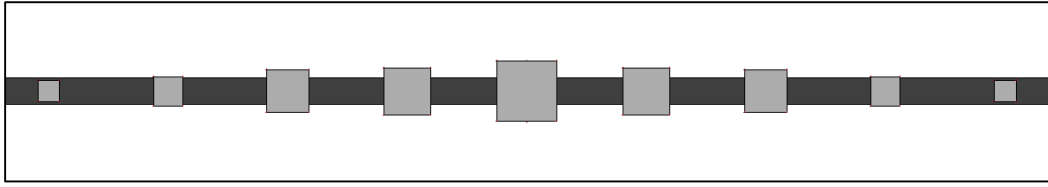


Figure 5.7: Geometry of a *Chebyshev* distributed rectangular patterned PBGS designed by varying the arm lengths of PBGSs etched in the ground plane. The period of PBGS is 10.43 mm and the substrate is Taconic with dielectric constant= 2.45 and height= 31 mils.

5.3.3 Results of Non-Uniform PBG Structures

The microstrip transmission lines to be investigated are: (a) non-uniform PBG elements with binomial distributions and (b) non-uniform PBG elements with *Chebyshev* distributions. The performances of all the designs are investigated in terms of 10 GHz center frequency under the consideration of negligible ripples in the passband.

1. Design-1 (Binomial Distribution over circular PBGSs):

The S-parameters performance of PBGSs that are resulted in accordance with the binomial distribution is shown in Figure 5.8.

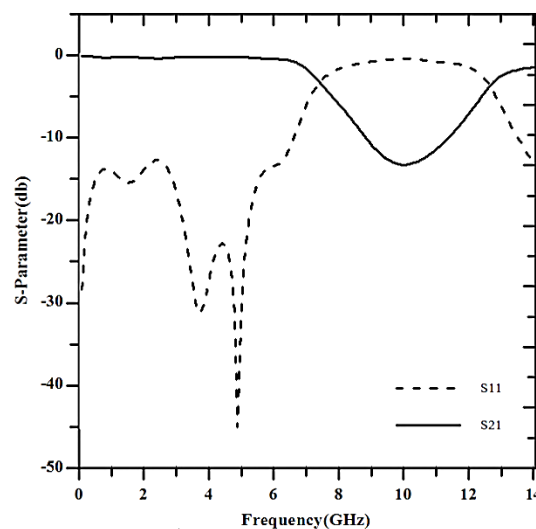


Figure 5.8: S-parameters performance of a transmission line over binomially distributed circular patterned PBGS according to design 1.

It can be seen that the transmission of signal in the passband is uniform ensuring minimum ripple height. The 10 dB passband return loss BW is found to be 6.88 GHz and the 20 dB rejection bandwidth is not found with maximum isolation of 13.26 dB.

2. Design-2 (Binomial Distribution over rectangular PBGSs):

The S-parameters performance of PBGSs that are resulted in accordance with the binomial distribution is shown in Figure 5.9.

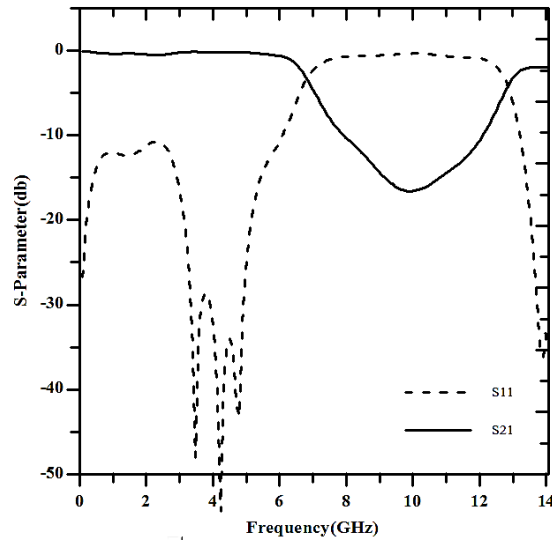


Figure 5.9: S-parameters performance of a transmission line over binomially distributed rectangular patterned PBGS according to design 2.

It can be seen that the transmission of signal in the passband is uniform ensuring minimum ripple height. The 10 dB passband return loss BW is found to be 7.12 GHz and the 20 dB rejection bandwidth is not found with maximum isolation of 16.59 dB.

3. Design-3 (*Chebyshev* Distribution over circular PBGSs):

The S-parameters performance of PBGSs that are resulted in accordance with the *Chebyshev* distribution is shown in Figure 5.10.

It can be seen that the transmission of signal in the passband is uniform ensuring minimum ripple height. The 10 dB passband return loss BW is found to be 4.6 GHz and the 20 dB rejection bandwidth is not found with maximum isolation of 19.07 dB.

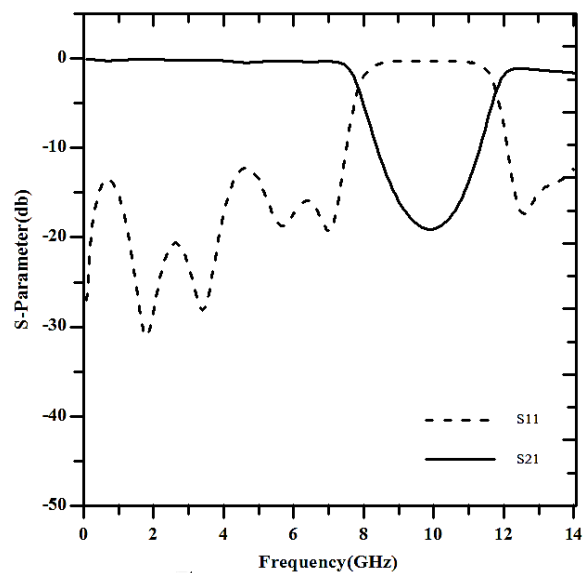


Figure 5.10: S-parameters performance of a transmission line over *Chebyshev* distributed circular patterned PBGS according to design 3.

4. Design-4 (*Chebyshev* Distribution over rectangular PBGSs):

The S-parameters performance of PBGSs that are resulted in accordance with the *Chebyshev* distribution is shown in Figure 5.11.

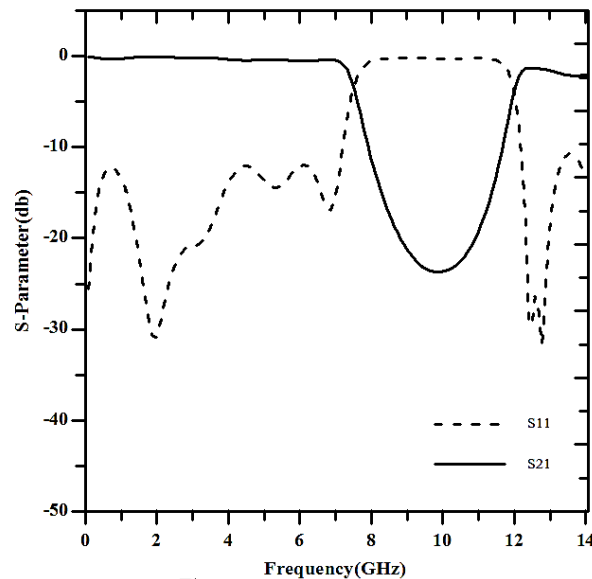


Figure 5.11: S-parameters performance of a transmission line over *Chebyshev* distributed rectangular patterned PBGS according to design 4.

It can be seen that the transmission of the signal in the passband is uniform ensuring minimum ripple height. The 10 dB passband return loss BW is found to be 4.98 GHz and the 20 dB rejection bandwidth is 2.1 GHz with maximum isolation of 23.7 dB.

So, from those above designs and their results describes that if a low pass filter is needed to establish, it is highly recommended to increase maximum isolation above 20 dB and the rejection bandwidth. So, dumbbell shape defected ground structures is chosen to fulfill the requirements of the LPFs. In the next portion there is an elaborate discussion about novel dumbbell shaped DGS and hybrid dumbbell shaped DGS which contains both dumbbell shaped DGS and regular PBGS structures in the same structure.

5.3.4 Non-Uniform Dumbbell Shaped Defected Ground Structures

The conventional DGSs provide better performances than the conventional PBGSs. Especially in terms of wider stopband the conventional DGSs stems significant improvement over the regular conventional PBGSs. Therefore there is a scope to find the performance of DGSs with non-uniform distribution. As Binomial distribution provides abrupt transition in size so attention will be confined to *Chebyshev* distribution. DGSs with *Chebyshev* distribution will provide better performance over the conventional DGSs reported in the literature.

❖ Parametric Studies

The influences of different dimensions of dumbbell shaped DGS unit cell are presented here. The investigation of some parametric studies over different dimensions of dumbbell shaped DGS are described in the literature [62]. According to the literature here is investigated the parametric studies with some other different values.

▪ Influence of Dimension of Larger Slot:

The dimensions of larger square slot had been varied by making $b = 180, 200, 220$ and 240 mils. The gap and width were maintained constant for all designs having $g = 30$ mils and $w=200$ mils. The insertion loss performances of these four designs are shown in Figure 5.12. For the darker one $b=180$ mils, for the lighter one $b=240$ mils.

The cut-off frequencies are different for different dimensions. When the dimension is larger, the series inductance increases and the cut-off frequency decreases. The gap capacitance remains constant for the fixed dimension of the narrow slot. It is seen that the attenuation pole locations are also changed. This arises from the fact that the parallel combination of variable series inductance and constant shunt capacitance are always different due to changes in dimension of larger slot. The location of the attenuation pole is the resonant frequency of an LC circuit.

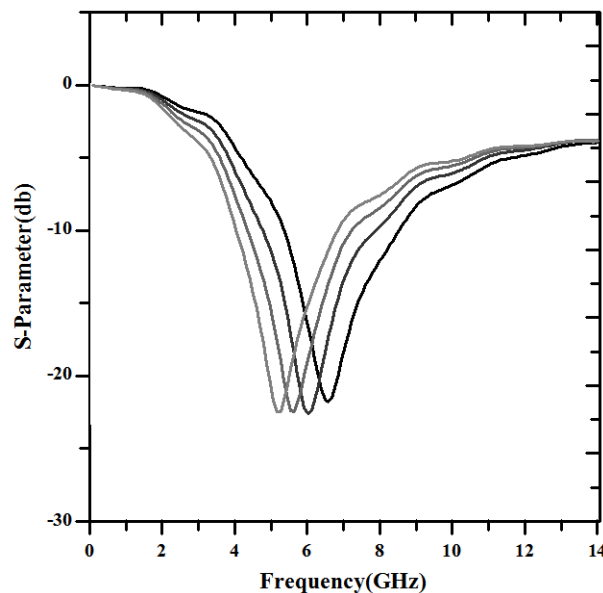


Figure 5.12: Insertion loss performance of a unit cell of dumbbell shaped DGS with variable larger slots of 240, 220, 200 and 180 mils respectively.

▪ Influence of the Gap Distance of Narrow Slot:

Gap distances were varied by making $g = 20, 30, 40$ and 50 mils. The dimension of the larger slot, $b = 104$ mils and the width of the narrow slot, $w = 50$ in all four designs. The Insertion loss performances are shown in Figure 5.13. For the darker one, $g = 20$ mils, for the lighter one, $g = 50$ mils.

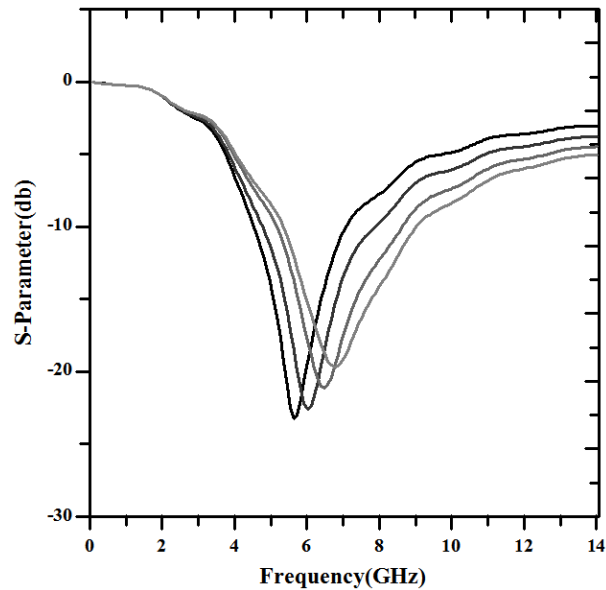


Figure 5.13: Insertion loss performance of a unit cell of dumbbell shaped DGS with variable gap distances of 20, 30, 40 and 50 mils respectively.

It can be seen that the cut-off frequencies are approximately same. That means the gap distance has no significant influence on the series inductance. Rather, it controls the pole location. As the gap distance is increased the gap capacitance decreases and hence the pole location moves up to a higher frequency.

▪ **Influence of width:**

The width of the narrow slot was varied. The effect of increasing the width is supposed to provide more capacitance as the increase in dimension of the slot is perpendicular to the microstrip line. On the other hand the inductive effect will also be significant. It is seen that both the pole location and the cut-off frequencies are influenced by the width of the narrow slot as expected. Increasing width enhances the inductive and capacitive effect. The insertion loss performances with different widths of a unit DGS cell are shown in Figure 5.14.

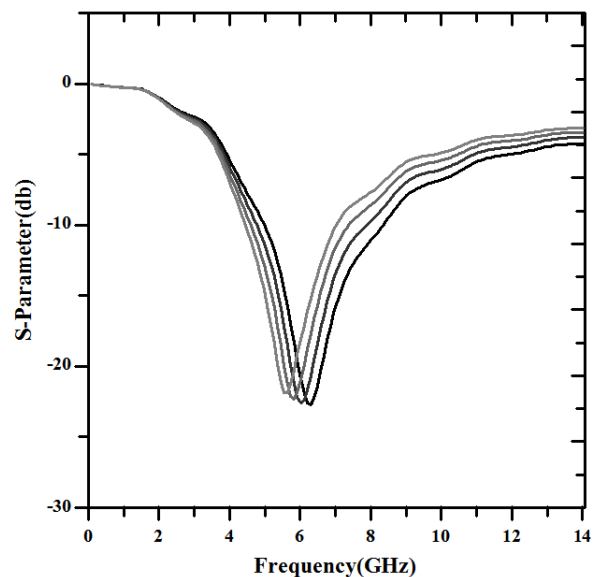


Figure 5.14: Insertion loss performance of a unit cell of dumbbell shaped DGS with variable width of narrow slots of 240, 220, 200 and 180 mils respectively.

For the darker one $b=180$ mils, for the lighter one $b=240$ mils. Based on these parametric studies the next investigation will be preceded. The objective is to describe some novel dumbbell shaped DGSs and hybrid DGSs with the help of the above studies.

❖ Novel Dumbbell shaped DGSs and Hybrid DGSs

It is started from a conventional 1-D square patterned periodic dumbbell shaped DGS structure based on Bragg's condition [60]. The original design is modified to achieve the performance of a LPF. The following designs are investigated.

- **Design-1 (Binomial Distribution over larger slot lengths and narrow slot widths of dumbbell shaped DGSs):**

In design 1, Taconic substrate having dielectric constant 2.45 and height of 31 mils have used. The geometry of LPF designed by non-uniform dumbbell shaped DGS is shown in figure 6.15. The PBGS elements of the DGS are square in size and each PBGS has both arm's length is calculated to be 205 mils corresponding to $FF=0.5$ to analyse S-parameter performance. The non-uniform dumbbell shaped DGS elements have the period of 411 mils. The length and width of the narrow slot are 30 and 200 respectively. For the width of the narrow slot of non-uniform dumbbell shaped DGS, the coefficient of the Binomial distribution for 7 element DGSs have used. Binomial distribution on the length (b) of every DGS has applied. For $N=7$ the coefficients are 1, 0.75, 0.3, 0.05 and the length (b) of the PBGSs are taken 205, 153.75, 61.5, 6.15 mils. The FF of the central element is 0.5 for both PBGS and narrow slot of the DGS. The design is shown in Figure 5.15.

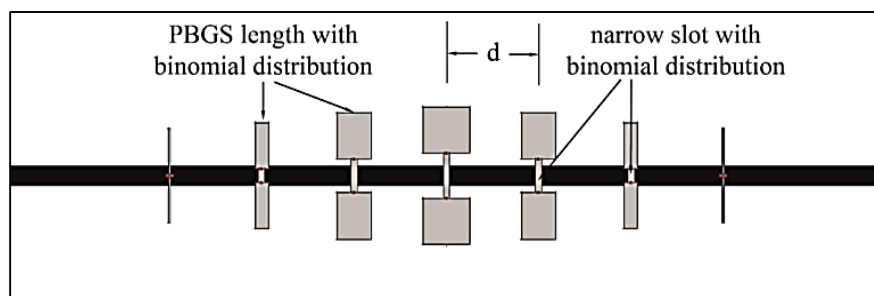


Figure 5.15: Geometry of a Binomially distributed LPF designed by varying narrow slot width (w) and length (b) of PBGS of dumbbell shaped DGS etched in the ground plane. The period of DGS is $d = 411$ mil and the substrate is Taconic with dielectric constant= 2.45 and height= 31 mils.

- **Design-2 (Binomial Distribution over larger slot lengths of dumbbell shaped DGSs):**

In design 2 the areas of narrow slots (30×100) have kept constant. The FF of the central element is 0.5 for PBGS of the DGS. The other design pattern is similar as design 1. The design is shown in Figure 5.16.

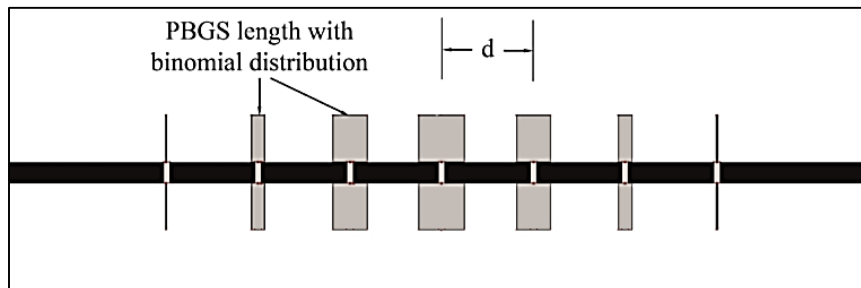


Figure 5.16: Geometry of a Binomially distributed LPF designed by varying length (b) of PBGS of the dumbbell shaped DGS etched in the ground plane. The period of DGS is $d = 411$ mil and the substrate is Taconic with dielectric constant = 2.45 and height = 31 mils.

- **Design-3 (Binomial Distribution over narrow slot widths of dumbbell shaped DGSs):**

In design 3 here, Binomial distribution on the narrow slot width (w) of every DGS has applied. For $N=7$ the coefficients are 1, 0.75, 0.3, 0.05 and the width (w) of the narrow slot are taken 200, 150, 60, 10 mils. The FF of the central element is 0.5 for both larger slots of the DGS. The design is shown in Figure 5.17.

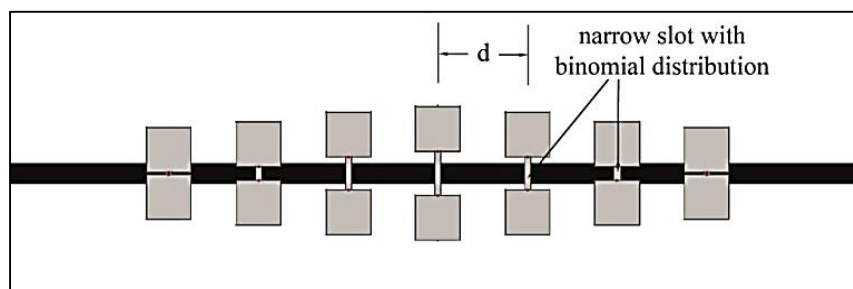


Figure 5.17: Geometry of a Binomial distributed LPF designed by varying narrow slot width (w) of the DGS etched in the ground plane. The period of DGS is $d = 411$ mil and the substrate is Taconic with dielectric constant = 2.45 and height = 31 mils.

- **Design-4 (Binomial Distribution over larger slot length and narrow slot widths of dumbbell shaped DGSs and interleaved PBGSs):**

In design 4, the dumbbell shaped DGS pattern is followed by design 1. But the square PBGSs have been interleaved that is 1-D in nature and the square PBGSs are reduced by Binomial distribution. The arm lengths of square PBGS are taken as 200, 120, 40, 6 mils for the coefficients of 1, 0.6, 0.2, 0.03 for $N=8$ as of Binomial distributions. With a view to generating low pass filter (LPF), this interleaved PBGS will be useful. The combined design of the PBGS - DGS is shown in Figure 5.18.

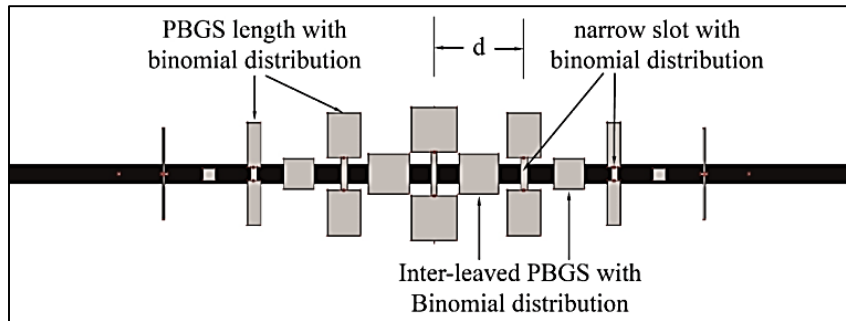


Figure 5.18: Geometry of a Binomially distributed LPF designed by varying both length (b) of PBGS and width (w) of the narrow slot of the dumbbell shaped DGS and interleaved square PBGS etched in the ground plane. The period of dumbbell shaped DGS is $d = 411$ mil for both DGS and interleaved PBGS and the substrate is Taconic with dielectric constant = 2.45 and height = 31 mils.

- **Design-5 (Binomial Distribution over larger slot and narrow slot widths of dumbbell shaped DGSs and lengths of interleaved PBGSs):**

The design 5 is different from previous designs. The widths (a) of PBGSs and the width of narrow slot of the dumbbell shaped DBGs and lengths of the interleaved PBGSs are changed by Binomial distribution. The widths (a) of PBGSs of dumbbell shaped DGSs are 200, 150, 60, 10 mils with lengths (b) were kept constant. The lengths of those EBGS are 205, 153.75, 61.5, 6.15 mils. For PBGS of dumbbell shaped DGS the filling factor of the central element has kept 0.48 and for interleaved PBGS the filling factor has kept 0.5. The narrow slots have designed similar as Design 1. The combined design of the PBGS - DGS is shown in Figure 5.19.

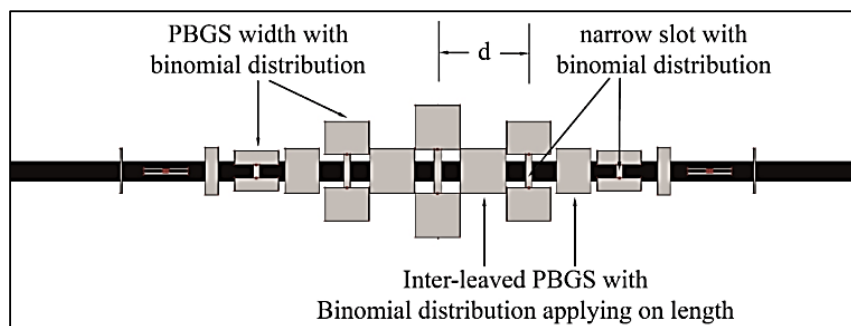


Figure 5.19: Geometry of a Binomially distributed LPF designed by varying both width (a) of PBGS and width (w) of the narrow slot of the dumbbell shaped DGS and lengths of the interleaved PBGS etched in the ground plane. The period of dumbbell shaped DGS is $d = 411$ mils for both DGS and interleaved PBGS and the substrate is Taconic with dielectric constant = 2.45 and height = 31 mils.

- **Design-6 (Chebyshev Distribution over larger slot lengths and narrow slot widths of dumbbell shaped DGSs):**

In design 6, Taconic substrate having dielectric constant 2.45 and height of 31 mils have used. The geometry of LPF designed by non-uniform dumbbell shaped DGS is shown in figure 5.20. The PBGS elements of the DGS are square in size and each PBGS has both arm's length is calculated to be 200 mils to analyse S-parameter performance. The non-uniform dumbbell shaped DGS elements have the period of 411 mils. The length and width of the narrow slot of the centre element is 30 and 200 respectively. For the width of the narrow slots and length of larger slots of non-uniform dumbbell shaped DGSs, the coefficient of the *Chebyshev* distribution for 9 element DGSs have used. *Chebyshev* distributions on the length (b) of every DGS have applied. For $N=9$ the coefficients are 0.36 0.49, 0.71, 0.78, 1, 0.78, 0.71, 0.49, 0.36 and the length (b) of the PBGSs are taken 72, 98, 142, 156, 200, 156, 142, 98, 72 mils. The design is shown in Figure 6.20.

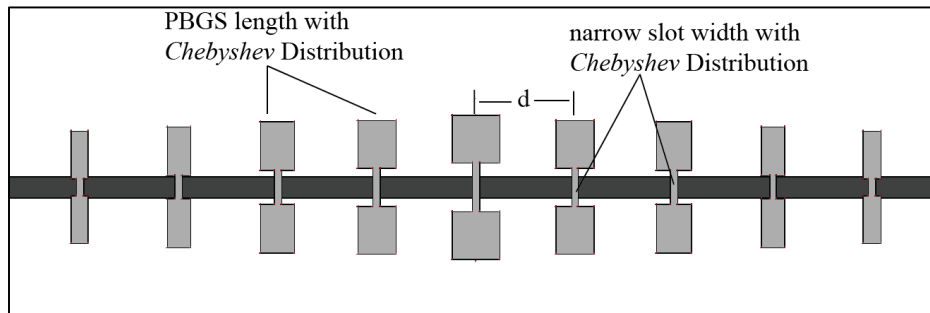


Figure 5.20: Geometry of a *Chebyshev* distributed LPF designed by varying narrow slot widths (w) and lengths (b) of larger slots of dumbbell shaped DGS etched in the ground plane. The period of DGS is $d = 411\text{mil}$ and the substrate is Taconic with dielectric constant= 2.45 and height= 31 mils.

- **Design-7 (Chebyshev Distribution over larger slot lengths and narrow slot widths of dumbbell shaped DGSs and interleaved PBGSs):**

In design 7, the dumbbell shaped DGS pattern is followed by design 6. But the interleaved square PBGSs are reduced by *Chebyshev* distribution. The arm lengths of square PBGS are taken as 72, 98, 142, 156, 200, 200, 156, 142, 98, 72 mils for the coefficients of 0.36 0.49, 0.71, 0.78, 1, 1, 0.78, 0.71, 0.49, 0.36 for $N=10$ as of *Chebyshev* distributions. With a view to generating low pass filter (LPF), this interleaved PBGS will be useful. The combined design of the PBGS - DGS is shown in Figure 5.21.

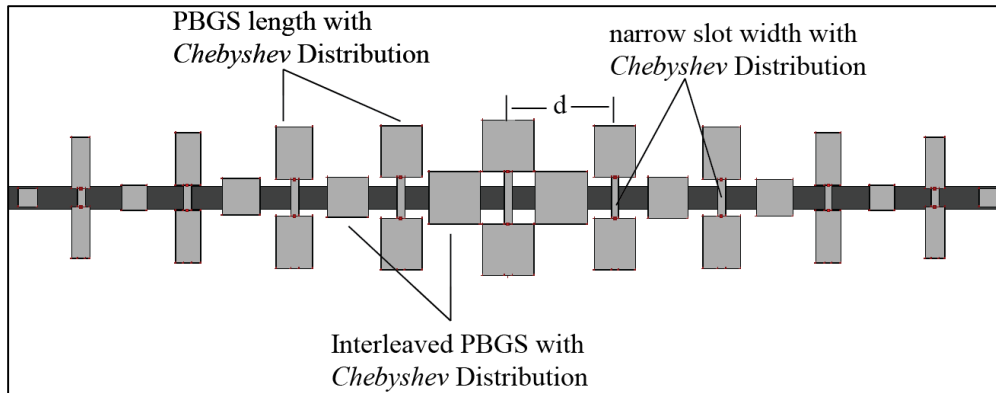


Figure 5.21: Geometry of a *Chebyshev* distributed LPF designed by varying both length (b) of PBGS and width (w) of the narrow slot of the dumbbell shaped DGS and interleaved square PGBS etched in the ground plane. The period of dumbbell shaped DGS is $d = 411$ mil for both DGS and interleaved PBGS and the substrate is Taconic with dielectric constant= 2.45 and height= 31 mils.

- **Design-8 (Chebyshev Distribution over larger slot lengths and narrow slot widths of dumbbell shaped DGSs and lengths of interleaved PBGSs):**

In design 8, the dumbbell shaped DGS pattern is followed by design 7. But the lengths of square PBGSs are reduced by *Chebyshev* distribution. The arm lengths of square PBGSs are taken as 72, 98, 142, 156, 200, 200, 156, 142, 98, 72 mils for the coefficients of 0.36 0.49, 0.71, 0.78, 1, 1, 0.78, 0.71, 0.49, 0.36 for $N=10$ as of *Chebyshev* distributions. Widths of the interleaved PBGSs are remaining constant. The combined design of the PBGS - DGS is shown in Figure 5.22.

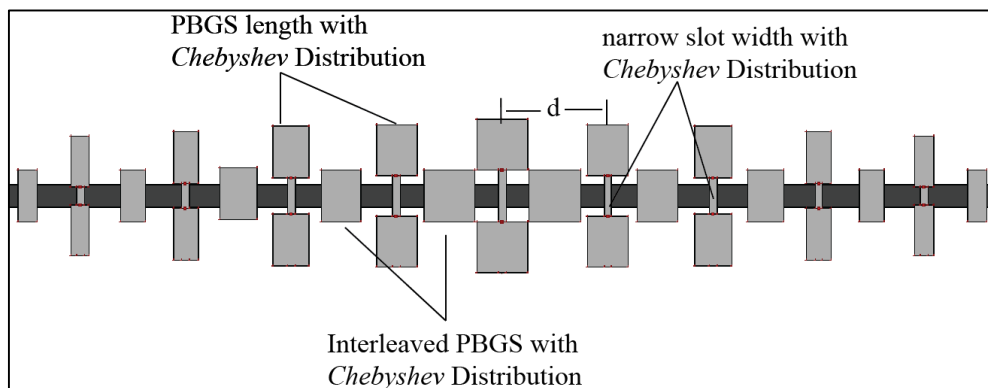


Figure 5.22: Geometry of a *Chebyshev* distributed LPF designed by varying both length (b) of PBGS and width (w) of the narrow slot of the dumbbell shaped DGS and varying length of interleaved square PGBS etched in the ground plane. The period of dumbbell shaped DGS is $d = 411$ mil for both DGS and interleaved PBGS and the substrate is Taconic with dielectric constant= 2.45 and height= 31 mils.

- **Design-9 (Chebyshev Distribution over larger slot lengths and narrow slot widths of dumbbell shaped DGSs and widths of interleaved PBGSs):**

In design 9, the dumbbell shaped DGS pattern is followed by design 7. But the widths of square PBGSs are reduced by *Chebyshev* distribution. The arm lengths of square PBGSs are taken as 72, 98, 142, 156, 200, 200, 156, 142, 98, 72 mils for the coefficients of 0.36 0.49, 0.71, 0.78, 1, 1, 0.78, 0.71, 0.49, 0.36 for $N=10$ as of *Chebyshev* distributions. Lengths of the interleaved PBGSs are remaining constant. The combined design of the PBGS - DGS is shown in Figure 5.23.

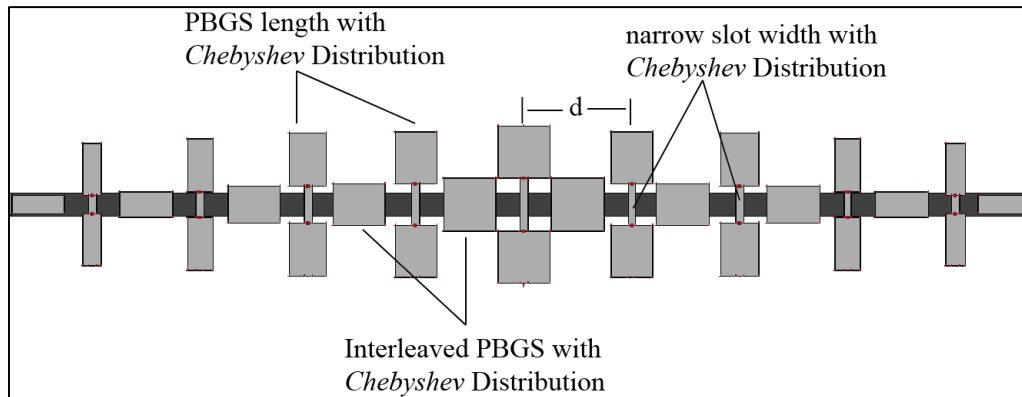


Figure 5.23: Geometry of a *Chebyshev* distributed LPF designed by varying both length (b) of PBGS and width (w) of the narrow slot of the dumbbell shaped DGS and varying width of interleaved square PGBS etched in the ground plane. The period of dumbbell shaped DGS is $d = 411$ mil for both DGS and interleaved PBGS and the substrate is Taconic with dielectric constant= 2.45 and height= 31 mils.

- **Design-10 (Chebyshev Distribution over larger slot and narrow slot widths of dumbbell shaped DGSs and widths of interleaved PBGSs):**

In design 10, the dumbbell shaped DGS pattern is followed by design 9. But the widths of the larger slot of dumbbell shaped DGSs are reduced by *Chebyshev* distribution. The widths of the larger slot of dumbbell shaped DGSs are taken as 72, 98, 142, 156, 200, 156, 142, 98, 72 mils for the coefficients of 0.36 0.49, 0.71, 0.78, 1, 0.78, 0.71, 0.49, 0.36 for $N=9$ as of *Chebyshev* distributions. The lengths of the interleaved PBGSs are remaining constant. The combined design of the PBGS - DGS is shown in Figure 5.24.

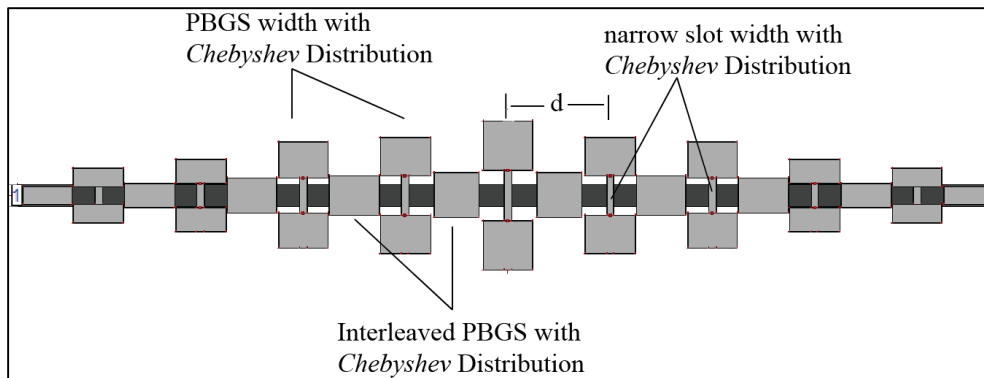


Figure 5.24: Geometry of a *Chebyshev* distributed LPF designed by varying both width (b) of larger slots and width (w) of the narrow slot of the dumbbell shaped DGS and varying width of interleaved square PBGS etched in the ground plane. The period of dumbbell shaped DGS is $d = 411$ mil for both DGS and interleaved PBGS and the substrate is Taconic with dielectric constant= 2.45 and height= 31 mils.

- **Design-11 (Chebyshev Distribution over larger slot and narrow slot widths of dumbbell shaped DGSs and lengths of interleaved PBGSs):**

In design 11, the dumbbell shaped DGS pattern is followed by design 8 and 10. The widths of the larger slot of dumbbell shaped DGSs and lengths of interleaved PBGSs are reduced by *Chebyshev* distribution. The combined design of the PBGS - DGS is shown in Figure 5.25.

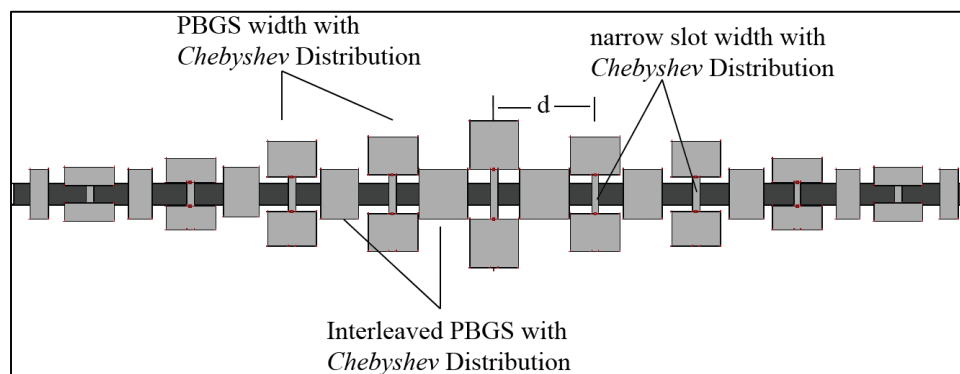


Figure 5.25: Geometry of a *Chebyshev* distributed LPF designed with varying both width (b) of larger slots and width (w) of the narrow slot of the dumbbell shaped DGS and varying lengths of interleaved square PBGSs etched in the ground plane. The period of dumbbell shaped DGS is $d = 411$ mil for both DGS and interleaved PBGS and the substrate is Taconic with dielectric constant= 2.45 and height= 31 mils.

- **Design-12 (Chebyshev Distribution over larger slot and narrow slot widths of dumbbell shaped DGSs):**

In design 12, the dumbbell shaped DGS pattern is followed by design 6. The widths of the larger slot of dumbbell shaped DGSs are reduced by *Chebyshev* distribution. The non-uniform dumbbell shaped DGS elements have the period of 411 mils. For the width of the narrow slots and larger slots of non-uniform dumbbell shaped DGSs, the coefficient of the *Chebyshev* distribution for 9 element DGSs have used. *Chebyshev* distributions on the length (b) of every DGS have applied. For $N=9$ the coefficients are 0.36, 0.49, 0.71, 0.78, 1, 0.78, 0.71, 0.49, 0.36 and the length (b) of the PBGSs are taken 72, 98, 142, 156, 200, 156, 142, 98, 72 mils. The design of the dumbbell shaped DGS is shown in Figure 5.26.

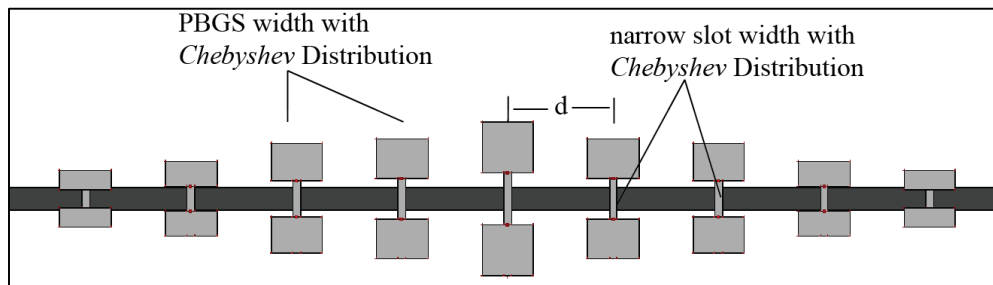


Figure 5.26: Geometry of a *Chebyshev* distributed LPF designed with varying widths (w) narrow slots and widths (b) of larger slots of dumbbell shaped DGS etched in the ground plane. The period of DGS is $d = 411$ mil and the substrate is Taconic with dielectric constant= 2.45 and height= 31 mils.

- **Design-13 (Binomial Distribution over larger slot lengths and Chebyshev distribution over narrow slot widths of dumbbell shaped DGSs with constant interleaved PBGSs):**

In design 13, Taconic substrate having dielectric constant 2.45 and height of 31 mils have used. The geometry of LPF designed by non-uniform dumbbell shaped DGS is shown in figure 5.28. The PBGS elements of the DGS are square in size and each PBGS has both arm's length is calculated to be 200 mils to analyse S-parameter performance. For the width of the narrow slots the coefficient of the *Chebyshev* distribution and widths of larger slots of non-uniform dumbbell shaped DGSs have used and the coefficient of the Binomial distribution for 7 element DGSs have used. The constant length (180 mils) inter-element PBGSs are used with the distance 411 mils. The design is shown in Figure 5.27.

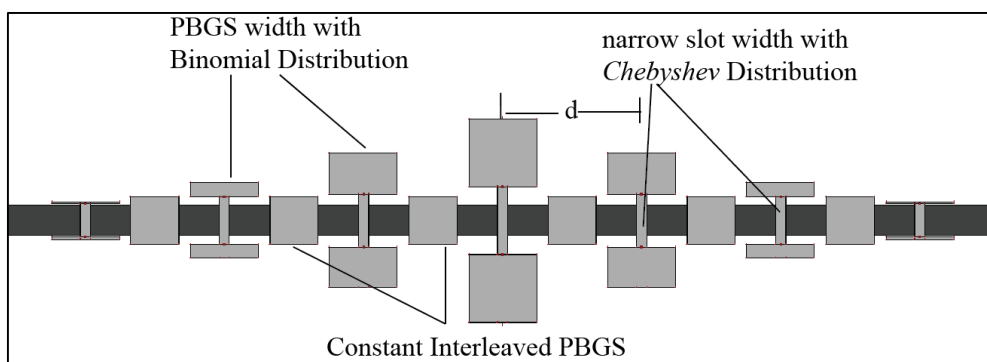


Figure 5.27: Geometry of a Binomial and *Chebyshev* distributed LPF designed by varying widths (w) narrow slots by *Chebyshev* distribution and widths (b) of larger slots of dumbbell shaped DGS by binomial distribution etched in the ground plane. The period of DGS is $d = 411$ mil and the substrate is Taconic with dielectric constant= 2.45 and height= 31 mils.

5.3.5 Simulation Results of Non-Uniform Dumbbell Shaped Defected Ground Structures

S-parameter performances of different novel designs have been investigated. Taconic substrate with dielectric constant of 2.45 and thickness of 31 mils are used in all designs. The return loss and insertion loss performances have been investigated.

- **Design-1 (Binomial Distribution over larger slot lengths and narrow slot widths of dumbbell shaped DGSs):**

The S-parameters vs. frequency of Design 1 is shown in Figure 5.28. It can be seen that the return loss curve is almost straight after 4 GHz. But it is observed that there is a ripple on the passband in the insertion loss curve of 0.5 dB height. Maximum isolation of the rejection band is -69 dB and minimum isolation is -25 dB. Pass bandwidth at 10 dB at S_{11} is 3.8 GHz and stop bandwidth at 20 dB at S_{21} is 4.4 GHz. Average 10 dB RL-BW is 3.5 GHz, 3 dB cutoff frequency is 3.8 GHz, 20 dB IL-BW is 9.5 GHz and maximum peak of IL is -45 dB.

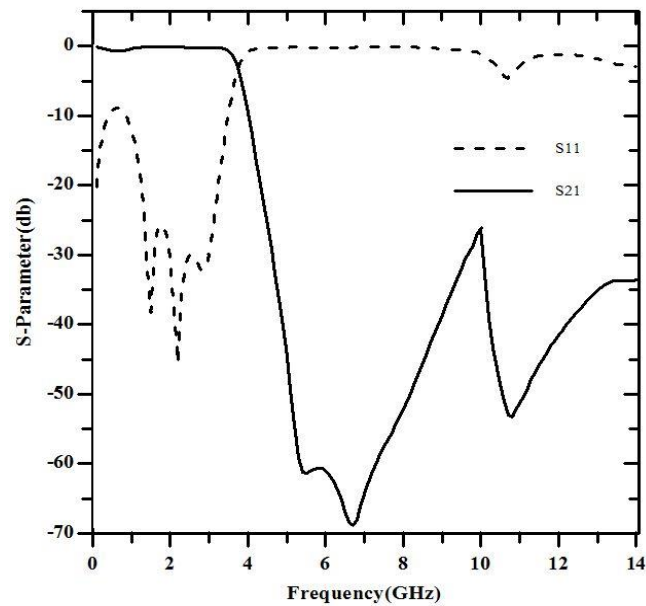


Figure 5.28: S-parameters performance of a transmission line over dumbbell shaped DGSs according to design 1. The substrate is Taconic with dielectric constant= 2.45 and height= 31 mils.

Design-2 (Binomial Distribution over larger slot lengths of dumbbell shaped DGSs):

The S-parameters vs. frequency of Design 2 is shown in Figure 5.29. It can be seen that the return loss curve is almost straight after 4GHz. But it is observed that there is a ripple on the passband in the insertion loss curve of 0.5 dB height. Maximum isolation of the rejection band is -55 dB and minimum isolation is -29 dB. The pick point is being reduced for design 2 in the IL curve. Pass bandwidth at -10 dB at S_{11} is 3.9 GHz and stop bandwidth at -20 dB at S_{21} is 4.8 GHz. Average 10 dB RL-BW is 3.8 GHz, 3 dB cutoff frequency is 4.1 GHz, 20 dB IL-BW is 9.2 GHz and maximum peak of IL is -44 dB.

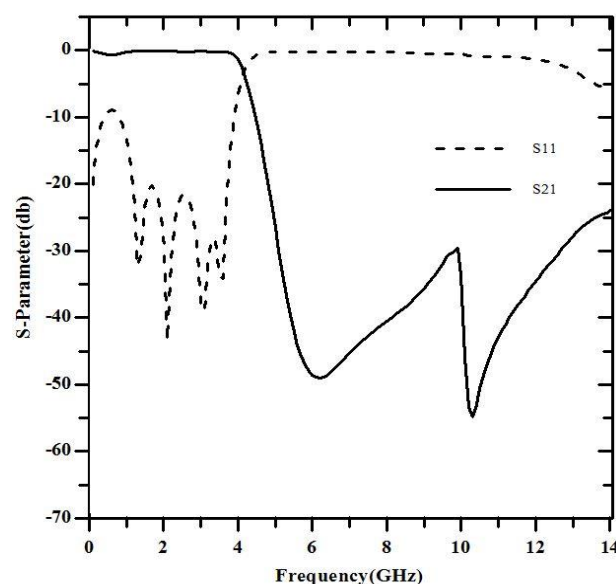


Figure 5.29: S-parameters performance of a transmission line over dumbbell shaped DGSs according to design 2. The substrate is Taconic with dielectric constant= 2.45 and height= 31 mils.

- **Design-3 (Binomial Distribution over narrow slot widths of dumbbell shaped DGSs):**

The S-parameters vs. frequency of Design 3 is shown in Figure 5.30. It can be seen that the passband ripples are of 2 dB near cut-off. Maximum isolation of the rejection band is -66 dB and minimum isolation is -34 dB. The cut-off frequency is about 4 GHz. Due to ripple of the passband in insertion loss the design is not so good enough. But it is observed that return loss curve is almost straight after 4GHz. Average 10 dB RL-BW is 3.4 GHz, 3 dB cutoff frequency is 3.6 GHz, 20 dB IL-BW is 9.9 GHz and maximum peak of IL is -35 dB.

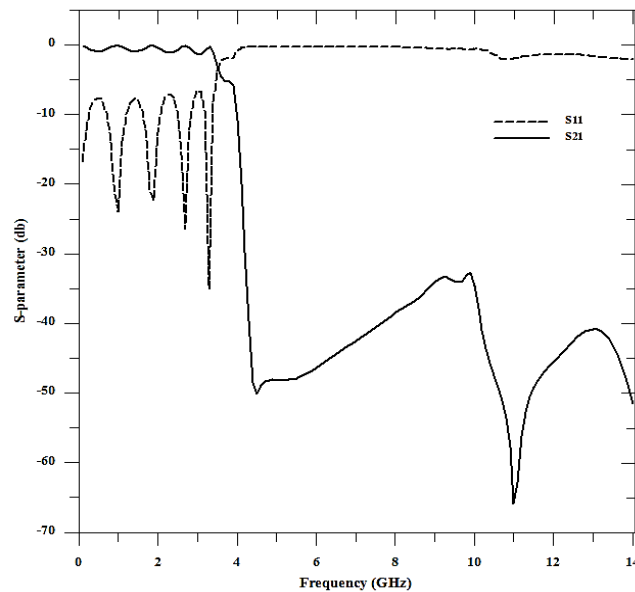


Figure 5.30: S-parameters performance of a transmission line over DGSs according to design 3. The substrate is Taconic with dielectric constant= 2.45 and height= 31 mils.

- **Design-4 (Binomial Distribution over larger slot length and narrow slot widths of dumbbell shaped DGSs and interleaved PBGSs):**

The S-parameters vs. frequency of a dumbbell shape DGS with interleaved PBGS of Design 4 is shown in Figure 5.31. Frequency shifting is found to be 1.25% at -3dB point in the IL curve. After 4 GHz the slope of the IL curve has gone down sharply. It has also observed that the RL curve is almost straight after 4.2 GHz. There is a single ripple on the passband in IL curve. Maximum isolation of the rejection band is -65 dB and minimum isolation is -31 dB. Average 10 dB RL-BW is 3.8 GHz, 3 dB cutoff frequency is 4.1 GHz, 20 db IL-BW is 9.1 GHz and maximum peak of IL is -54 dB.

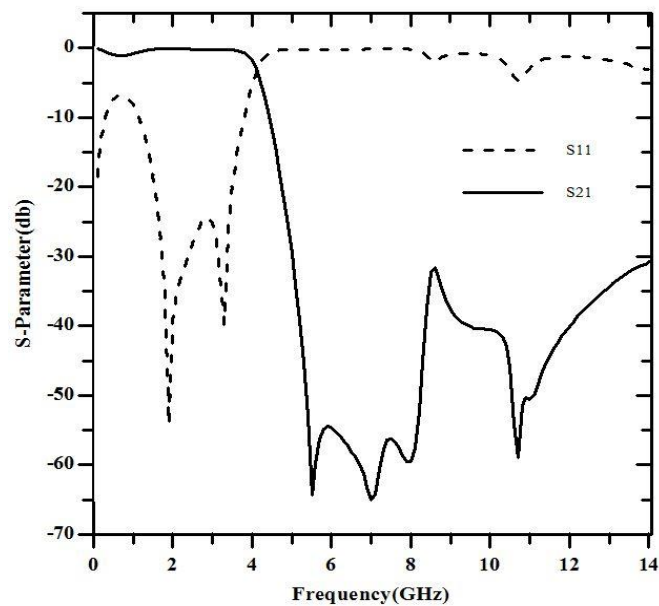


Figure 5.31: S-parameters performance of a transmission line over hybrid dumbbell shaped DGSs according to design 4. The substrate is Taconic with dielectric constant= 2.45 and height= 31 mils.

- **Design-5 (Binomial Distribution over larger slot and narrow slot widths of dumbbell shaped DGSs and lengths of interleaved PBGSs):**

The S-parameters vs. frequency of a dumbbell shape DGS with interleaved PBGS of Design 5 is shown in Figure 5.32. There is a single ripple on the passband in IL curve. Maximum isolation of the rejection band is -75 dB and minimum isolation is -28 dB. Passband of the insertion loss curve is smoother and the rejection band curves are below -20db and going down gradually. The changing of the width of PBGS of dumbbell shaped DGS and at the same time the changing of the length of interleaving PBGSs has caused a great impact on the results. Average 10 dB RL-BW is 3.7 GHz, 3 dB cutoff frequency is 4.4 GHz, 20 db IL-BW is 9 GHz and maximum peak of IL is -40 dB.

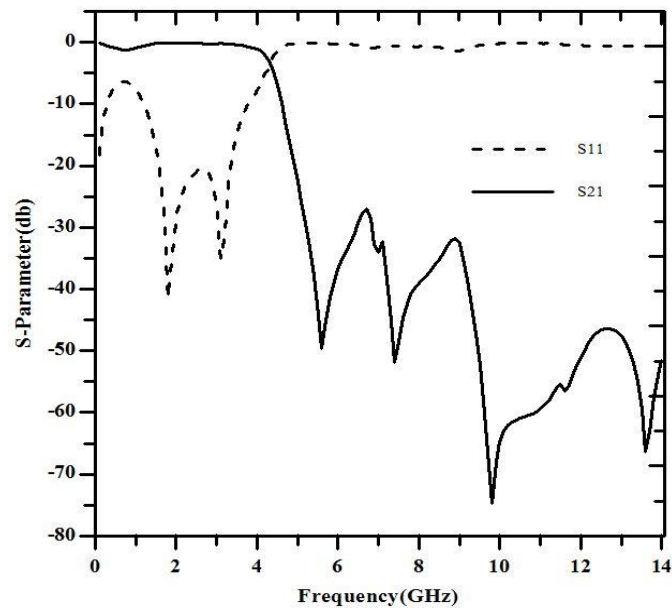


Figure 5.32: S-parameters performance of a transmission line over hybrid dumbbell shaped DGSs according to design 5. The substrate is Taconic with dielectric constant = 2.45 and height = 31 mils.

- **Design-6 (Chebyshev Distribution over larger slot lengths and narrow slot widths of dumbbell shaped DGSs):**

The S-parameters vs. frequency of Design 7 is shown in Figure 5.33. After 4 GHz the slope of the IL curve has gone down sharply. It can be seen that the return loss curve is almost straight after 4GHz. But it is observed that there is some ripple on the passband in the insertion loss curve. After 3 GHz there is an observable ripple about -2dB. Maximum isolation of the rejection band is -63 dB and minimum isolation is -28 dB. Average 10 dB RL-BW is 3.9 GHz, 3 dB cutoff frequency is 4 GHz, 20 db IL-BW is 9.2 GHz and maximum peak of IL is -45 dB.

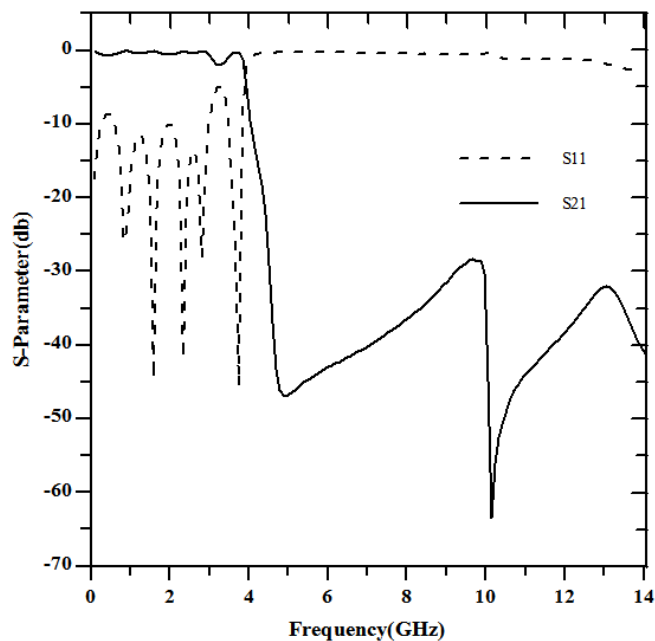


Figure 5.33: S-parameters performance of a transmission line over dumbbell shaped DGSs according to design 6. The substrate is Taconic with dielectric constant= 2.45 and height= 31 mils.

- **Design-7 (Chebyshev Distribution over larger slot lengths and narrow slot widths of dumbbell shaped DGSs and interleaved PBGSs):**

The S-parameters vs. frequency of Design 7 is shown in Figure 5.34. Frequency shifting is found to be 3.75% at -3dB point in the IL curve. After 4 GHz the slope of the IL curve has gone down sharply. It has also observed that the RL curve is almost straight after 4.9 GHz. It is observed that there is some ripple on the passband in insertion loss curve. After 3 GHz there is an observable ripple about -2dB. Maximum isolation of the rejection band is -68 dB and minimum isolation is -31 dB. Average 10 dB RL-BW is 4.1 GHz, 3 dB cutoff frequency is 4.2 GHz, 20 db IL-BW is 9.4 GHz and maximum peak of IL is -28 dB.

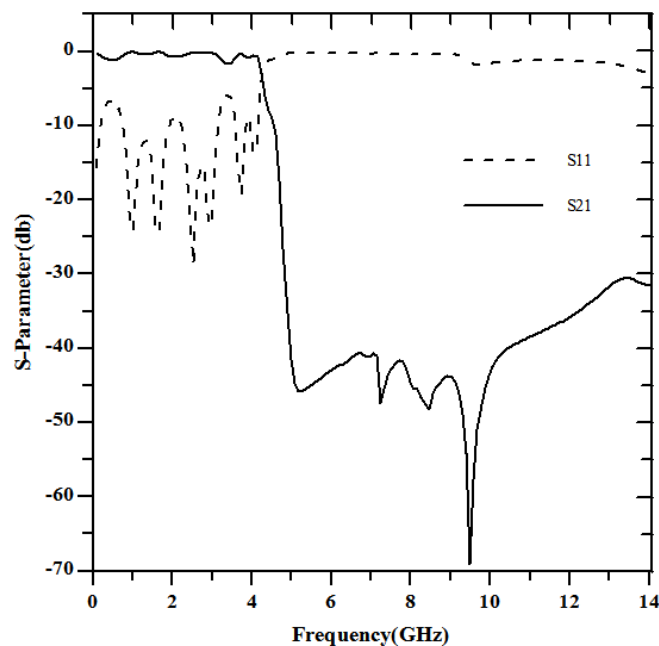


Figure 5.34: S-parameters performance of a transmission line over hybrid DGSs according to design 7. The substrate is Taconic with dielectric constant= 2.45 and height= 31 mils.

- **Design-8 (Chebyshev Distribution over larger slot lengths and narrow slot widths of dumbbell shaped DGSs and lengths of interleaved PBGSs):**

The S-parameters vs. frequency of Design 8 is shown in Figure 5.35. Frequency shifting is found to be 2.5% at -3dB point in the IL curve. After 4 GHz the slope of the IL curve has gone down sharply. It has also observed that the RL curve is almost straight after 4.5 GHz. It is observed that there is some ripple on the passband in insertion loss curve. After 3 GHz there is an observable ripple about -2dB. Maximum isolation of the rejection band is -59 dB and minimum isolation is -39 dB. Average 10 dB RL-BW is 4 GHz, 3 dB cutoff frequency is 4.1 GHz, 20 dB IL-BW is 9.4 GHz and maximum peak of IL is -36 dB.

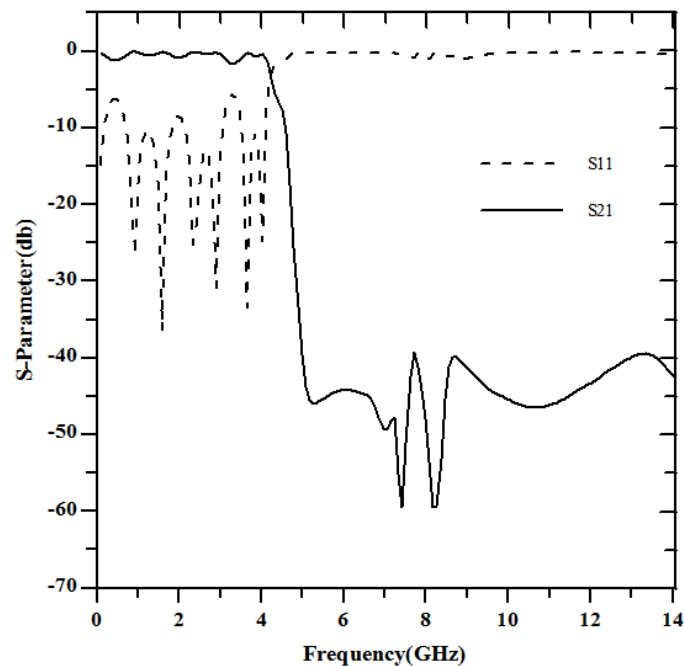


Figure 5.35: S-parameters performance of a transmission line over hybrid DGSs according to design 8. The substrate is Taconic with dielectric constant= 2.45 and height= 31 mils.

- **Design-9 (Chebyshev Distribution over larger slot lengths and narrow slot widths of dumbbell shaped DGSs and widths of interleaved PBGSs):**

The S-parameters vs. frequency of Design 9 is shown in Figure 5.36. Frequency shifting is found to be 3.75% at -3dB point in the IL curve. After 4 GHz the slope of the IL curve has gone down sharply. It has also observed that the RL curve is almost straight after 4.15 GHz. It is observed that there is some ripple on the passband in insertion loss curve. After 3 GHz there is an observable ripple about -2dB. Maximum isolation of the rejection band is -67 dB and minimum isolation is -31 dB. Average 10 dB RL-BW is 4 GHz, 3 dB cutoff frequency is 4.2 GHz, 20 db IL-BW is 9.2 GHz and maximum peak of IL is -39 dB.

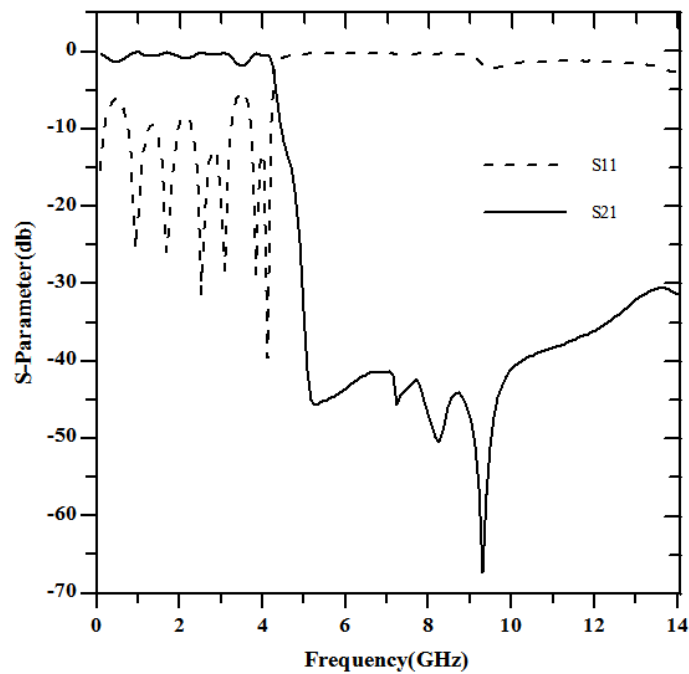


Figure 5.36: S-parameters performance of a transmission line over hybrid DGSs according to design 9. The substrate is Taconic with dielectric constant= 2.45 and height= 31 mils.

- **Design-10 (Chebyshev Distribution over larger slot and narrow slot widths of dumbbell shaped DGSs and widths of interleaved PBGSs):**

The S-parameters vs. frequency of Design 10 is shown in Figure 5.37. Frequency shifting is found to be 12.5% at -3dB point in the IL curve. After 4 GHz the slope of the IL curve has gone down sharply. It has also observed that the RL curve is almost straight after 4.5 GHz. It is observed that there is some ripple on the passband in insertion loss curve. There is an observable ripple about -2dB. Maximum isolation of the rejection band is -60 dB and minimum isolation is -34 dB. Average 10 dB RL-BW is 3.6 GHz, 3 dB cutoff frequency is 4.4 GHz, 20 dB IL-BW is 9.4 GHz and maximum peak of IL is -43 dB.

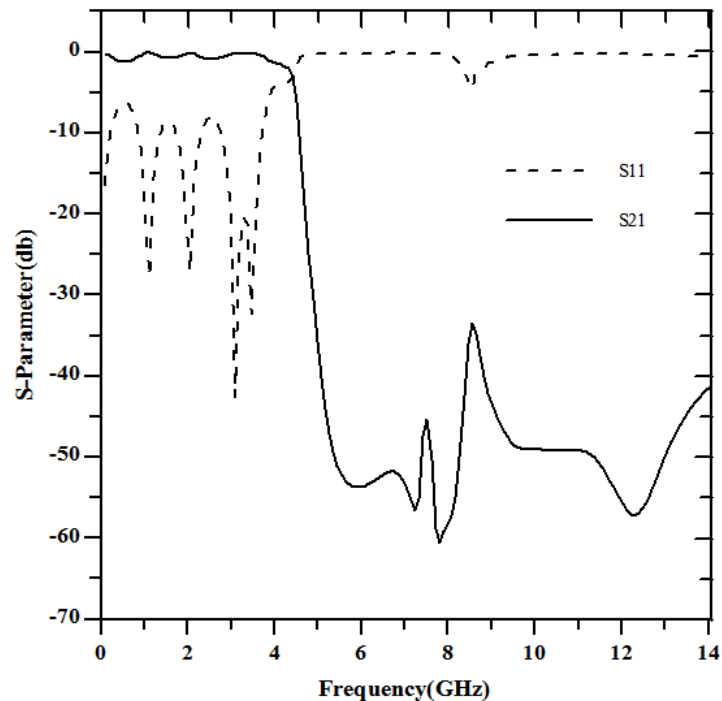


Figure 5.37: S-parameters performance of a transmission line over hybrid DGSs according to design 10. The substrate is Taconic with dielectric constant= 2.45 and height= 31 mils.

- **Design-11 (Chebyshev Distribution over larger slot and narrow slot widths of dumbbell shaped DGSs and lengths of interleaved PBGSs):**

The S-parameter performance of Design 11 is shown in Figure 5.38. Though the cutoff frequency of design 2 is 4GHz, but frequency shifting is found to be 8.7% at -3dB point in the IL curve. After 4 GHz the slope of the IL curve has gone down sharply. It has also observed that the RL curve is almost straight after 4.4 GHz. There is a -2 dB ripple on the passband in the IL curve. Maximum isolation of the rejection band is -74 dB and minimum isolation is -45 dB. In the design 2 we observe that there is an improvement of the IL curve at 10GHz. The pick point in the IL curve at 10 GHz is reduced for design 11. Average 10 dB RL-BW is 3.9 GHz, 3 dB cutoff frequency is 4.4 GHz, 20 db IL-BW is 9.4 GHz and maximum peak of IL is -38 dB.

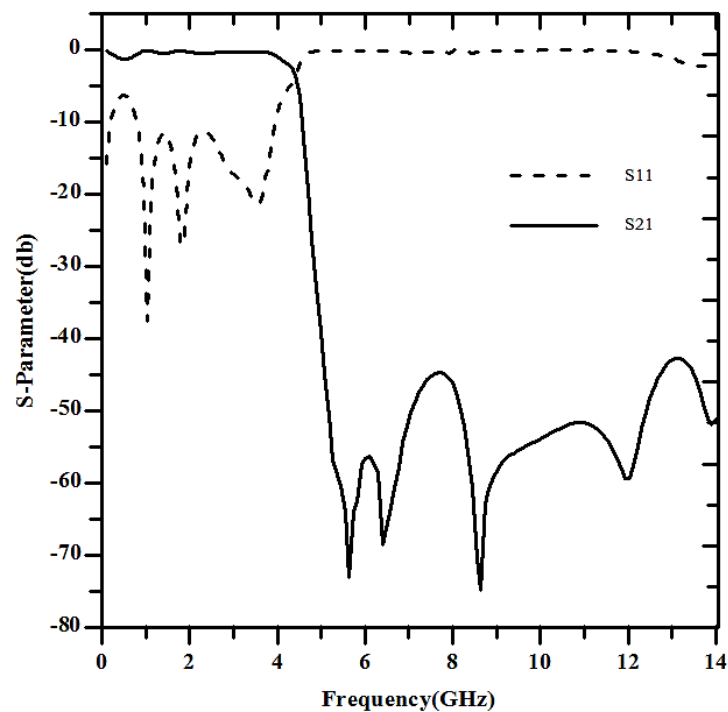


Figure 5.38: S-parameters performance of a transmission line over hybrid DGSs according to design 11. The substrate is Taconic with dielectric constant= 2.45 and height= 31 mils.

- **Design-12 (Chebyshev Distribution over larger slot and narrow slot widths of dumbbell shaped DGSs):**

The S-parameter performance of Design 12 is shown in Figure 5.39. Though the cutoff frequency of design 12 is 4GHz, but frequency shifting is found to be 2.5% at -3dB point in the IL curve. After 4 GHz the slope of the IL curve has gone down sharply. It also can be seen that the RL curve is almost straight after 4GHz. There are some very negligible ripples (less than -1dB) on the passband in the insertion loss curve. Maximum isolation of the rejection band is -62 dB and minimum isolation is -30 dB. Average 10 dB RL-BW is 3.5 GHz, 3 dB cutoff frequency is 4 GHz, 20 db IL-BW is 9.9 GHz and maximum peak of IL is -36 dB.

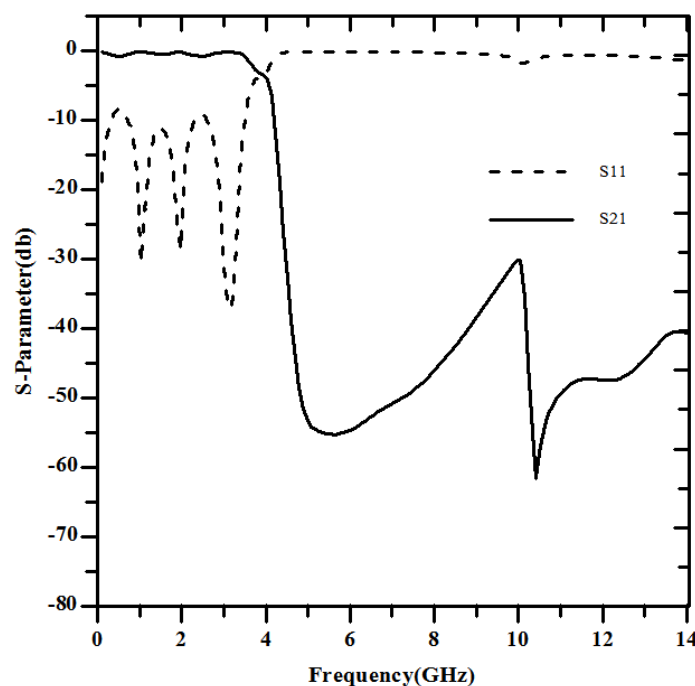


Figure 5.39: S-parameters performance of a transmission line over dumbbell shaped DGSs according to design 12. The substrate is Taconic with dielectric constant= 2.45 and height= 31 mils.

- **Design-13 (Binomial Distribution over larger slot lengths and Chebyshev distribution over narrow slot widths of dumbbell shaped DGSs with constant interleaved PBGSs):**

The S-parameters vs. frequency of Design 13 is shown in Figure 5.40. Frequency shifting is found to be 1.25% at -3dB point in the IL curve. After 4 GHz the slope of the IL curve has gone down sharply. It is observed that there is a ripple on the passband in insertion loss curve and a ripple on the return loss curve. Maximum isolation of the rejection band is -61 dB and minimum isolation is -24 dB. Average 10 dB RL-BW is 3.8 GHz, 3 dB cutoff frequency is 4.1 GHz, 20 db IL-BW is 9.3 GHz and maximum peak of IL is -35 dB.

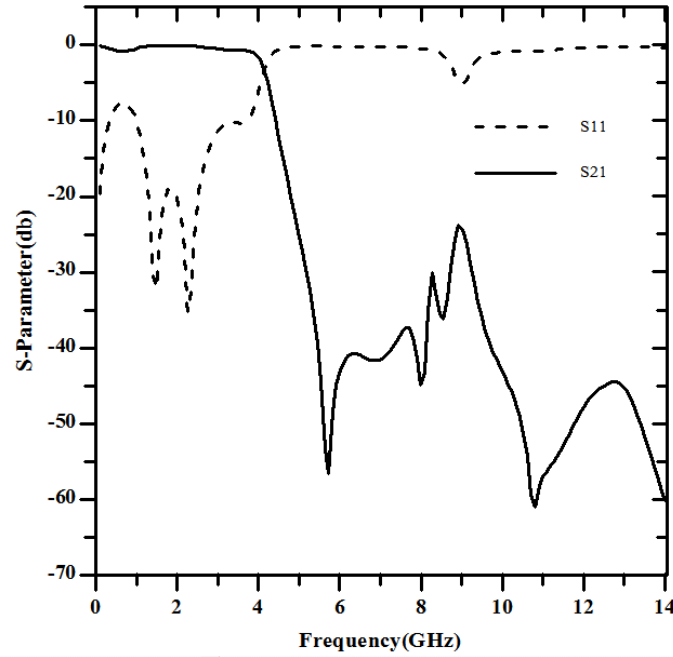
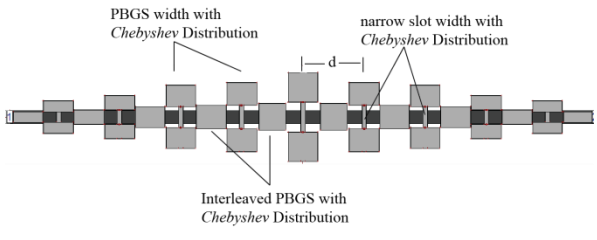
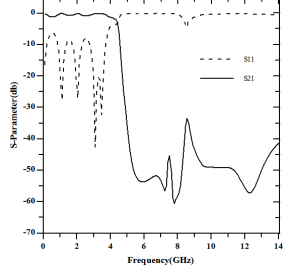
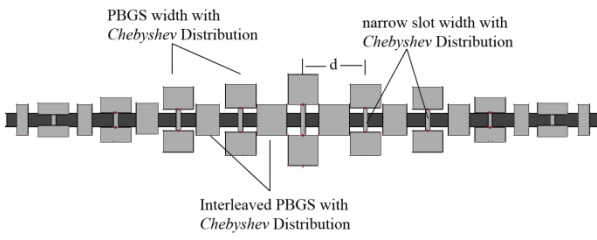
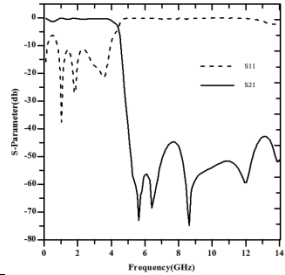
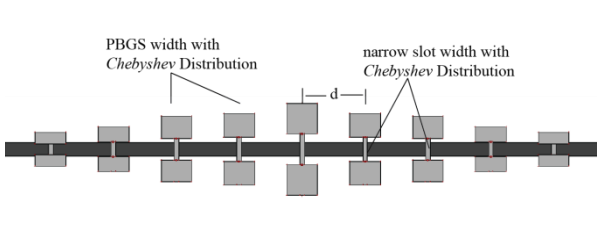
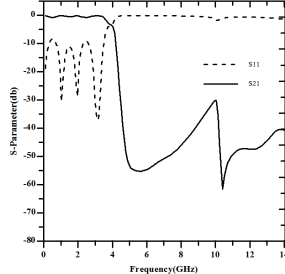


Figure 5.40: S-parameters performance of a transmission line over dumbbell shaped DGSS according to design 13. The substrate is Taconic with dielectric constant= 2.45 and height= 31 mils.

Table 5.1: Comparison of some structures with their S-Parameter performances.

| No | Designs | S-Parameter Performance | Remarks |
|----|---------|-------------------------|--|
| 1. | | | 10 dB RL-BW = 3.8 GHz 20 dB IL-BW= 9.2 GHz Maximum ripple height= 0.5 dB |
| 2. | | | 10 dB RL-BW = 3.8 GHz 20 dB IL-BW= 9.1 GHz Maximum ripple height = 0.5dB |
| 3. | | | 10 dB RL-BW = 3.7 GHz 20 dB IL-BW = 9 GHz Maximum ripple height = 1 dB |

| | | | |
|----|--|---|---|
| 4. |  |  | <p>10 dB RL-BW = 3.6 GHz 20 dB IL-BW = 9.4 GHz Maximum ripple height = 1.8 dB</p> |
| 5. |  |  | <p>10 dB RL-BW = 3.9 GHz 20 dB IL-BW = 9.4 GHz Maximum ripple height = 2 dB</p> |
| 6. |  |  | <p>10 dB RL-BW = 3.5 GHz 20 dB IL-BW = 9.9 GHz Maximum ripple height = 1 dB</p> |

5.4 Conclusion

In this chapter the frequency properties of the unit cell of a dumbbell shaped DGS and the whole novel structures based upon the properties have been investigated. In DGS the dimension of larger square patterned slots, controls the cutoff frequencies and the gap distance controls the location of attenuation pole. Another set of regular PBGSs have been inserted in between modified DGS. Various hybrid PBG-DGS designs have been etched in the ground plane of a standard 50-ohm transmission line to develop low-pass filter. At first, few structures are investigated to yield better LPF performance in terms of passband return loss BW, ripple free transmission and wider stopband. The binomially distributed structures show better performance than the *Chebyshev* structures. Binomial and *Chebyshev* distributed PBG structures do not show the low pass filter performance due to no significant stopband is found. The modified dumbbell shaped DGS and hybrid DGS shows the wider stopband and the smoother passband as of the LPF properties.

These novel designs provide the impressive LPFs. The wider stopband can be used to mitigate the surface wave problem and suppression of spurious and leakage transmission. This structure can also find potential application in RF front-ends to isolate transmitters from receiver modules.

Chapter-6

Conclusions and Future Works

6.1 Conclusions

The work presented in this thesis has been concerned with PBG assisted low-pass filters. Recently PBG engineering has been an especial area in microwave engineering. PBGSs are found to be very attractive in different microwave devices and components. The open literatures have been surveyed thoroughly to find their applications including their limitations. PBGSs are periodic in nature. PBG theories have been reviewed to understand the passband-stopband natures and their performances. The depth and width of the stopband depend on a few factors like FFs, number of elements, periods and substrate properties. Uniform circular and square patterned PBGSs and dumbbell shaped DGS have been investigated. The stopband-passband properties are reported by S-parameters performances. Different shapes of the EBG elements and structures have been shown. Three rows of circular and rectangular uniform PBGSs under the standard 50-ohm transmission line have been simulated. Comparing with the result of one row circular uniform circular PBGSs it is found that those three rows of uniform circular PBGSs and one row of uniform circular PBGSs yield very identical S-parameters performances. So 1-D PBGSs have been used in whole investigation.

In chapter 4 it is seen that the conventional hole patterned PBGSs suffer from the constrained optimized value of FF in the application as a low-pass filter. In this work a lot of efforts are devoted to finding a novel configuration of PBG elements to replace the conventional hole patterned PBG elements. Their filtering properties have been mentioned in details to see the improved performance over the conventional hole patterned PBG elements. The conventional hole patterned PBGSs are found to have poor performance mainly in the passband and their performances are hindered by the limiting value of FF.

The alternatives in the form of hole and ring patterned PBGSs with non-uniform amplitudes based on Binomial and Chebyshev distributions have been proposed. Standard 50-ohm transmission lines are simulated on Binomially distributed PBGSs having $FF = 0.3, 0.4$ and 0.5 at $9, 10.5$ and 12 GHz respectively. From all these simulations it is seen that the Binomially distributed PBGSs provide better results than uniform circular PBGSs. It is observed that 0.4 may be considered as the approximate value of optimized FF. It is better to note down there is still scope to investigate the value of optimum FF within the intermediate values ranging from 0.4 to 0.5 . The present research has also revealed the frequency dependence of the performance. It is important to note that frequency shifting is a common feature of PBG structures. The center frequency is controlled by the period of the PBG lattice structure that is determined from the Bragg's condition. So frequency shifting can be optimized by the proper choice of period of PBGSs. In the simulation results, conductor loss,

substrate loss and the loss due to connectors are not included. Above all, all the simulations have been done on an infinite ground plane (ignoring truncation). All the structures are fabricated using a milling machine. So there are fabrication errors. This type of error may cause variations in size and period of the lattice structures resulting in the variation in the magnitude of S-parameters and the frequency of interests.

Microstrip lines perturbed by PBG structures with Chebyshev distribution have been designed and analyzed at 9, 10.5 and 12 GHz for FF = 0.3, 0.4 and 0.5 respectively. Total nine designs have been investigated from which the approximate value of optimum FF for Chebyshev distribution of PBGSs can be obtained. In terms of passband ripple height, isolation, passband return loss BW and stopband it can be concluded that 0.4 is the approximate value of optimum filling factor. The frequency dependence of the performance of Chebyshev distributed PBG structured transmission line has been investigated. It is observed that the maximum rejection bandwidth is obtained at 9 GHz and the maximum passband is achieved at 12 GHz. The maximum isolation is seen at 10.5 GHz. The minimum return loss is found at 9 GHz.

6.2 Fulfilling the Goal of the Thesis

A novel PBG engineered microstrip transmission line has been designed and investigated theoretically. The overall performance of the proposed model is always superior to conventional PBG structured transmission line. The present work has been extended further where both the tapering of the amplitudes of the PBG elements are done on the basis of binomial and *Chebyshev* polynomial. The PBGSs with binomial and *Chebyshev* distribution have been investigated. Binomial and *Chebyshev* distribution has been used in calculating the amplitudes of the PBG elements. It is pleasant to observe that simple change in the design provides enormous rejection bandwidth. In chapter 3, conventional DGSs have been reported. Very few works on DGSs are found in the open literature. In chapter 4, some parametric studies of DGSs have been accomplished. Among them the effect of the width of the narrow connecting vertical slot of dumbbell shaped DGS is novel investigation. Non-uniform DGSs and hybrid DGSs have been investigated. The hybrid DGSs are realized by placing conventional square patterned PBGSs in between conventional DGSs. The hybrid DGSs with non-uniform distribution provides excellent performance as LPF.

6.3 Recommendation for Future Work

In the whole research work, attention has been paid to simulate all the structures by commercial EM software Zeland IE3D. The future work can be mentioned in the following manner. The PBGSs are actually complex geometries. For such geometries it is a difficult task to calculate the value of the propagation constant. The future task could be reducing the complexity of geometry. VNA can measure the s-parameter performances of the PBGS structures. Investigations need to be justified experimentally by VNA and compared with simulated results. Theoretical modeling is to be made for rectangular, circular PBGS and dumbbell shaped DGS. Other complex designs like dual T-line designs need further research work to explain the behavior theoretically as well as multiple T-lines need to be considered.

Researching proper algorithms for designing dumbbell shaped DGS is left for further work as currently there is no such direct method of calculating correct parameters or correct size of dumbbell shaped EBGs for designing a filter for a particular predefined performance i.e. for a particular type of dual band performance how a dumbbell shaped DGS can be chosen.

References

- [1] Li Yang, M.Fan, F.Chen, J.She, Z.Feng, “A Novel Compact Electromagnetic Bandgap (EBG) Structure and Its Applications for Microwave Circuits”, *IEEE Trans. Microw. Theory Techn.*, Vol. 53, No.1, pp. 183-190,Jan. 2005.
- [2] J. Liang, H. Y. D. Yang, “Microstrip Patch Antennas on Tunable Electromagnetic Band-Gap Substrates,” *IEEE Trans. on Microw. Theory Tech.*, Vol. 57, pp. 1612-1617, No.6, Jun. 2009.
- [3] P. Baccarelli, et al., “Dispersive Analysis of Wide-Bandstop Compact EBG Microstrip Lines for Filter Applications”, International Symposium on Microwave and Optical Technology, Rome, Italy, 2007.
- [4] R.S. Kshetrimayum, L. Zhu, “ EBG Design using FSS Elements in Rectangular Waveguide”, *Appl. Comp. Electrom. Society*, Vol. 21, NO. 2, Mar. 2006.
- [5] R. Verma, K. Daya, “Effect of Forbidden Bands of Electromagnetic Bandgap Engineered Ground Plane on the Response of Half Wave Length Linear Microwave Resonator”, *J. Appl. Phys* vol. 109, no. 8, pp. 084505, Apr. 2011.
- [6] E. Yablonovitch, “Inhibited spontaneous emission in solid-state physics and electronics”, *Phys. Rev. Lett.*, vol. 58, pp. 2059-2063, 1987.
- [7] S. John, “Strong Localization of Photons in Certain Disordered Dielectric Super Lattices,” *Phys. Rev. Lett.* 58, 2486, 1987.
- [8] Md. S. Alam, N. Misran, B. Yatim, and Md. T. Islam, “Development of Electromagnetic Band Gap Structures in the Perspective of Microstrip Antenna Design”, *Int. J. Antennas and Propagation*, vol. 2013, pp. 22, 2013.
- [9] P. de Maagt, R. Gonzalo, Y. C. Vardaxoglou, and J. M. Baracco, “Electromagnetic bandgap antennas and components for microwave and (sub)millimeter wave applications,” *IEEE Trans. Antennas and Propagation*, vol. 51, no. 10 , pp. 2667–2677, 2003.
- [10] M. S. Alam, et al., “Design analysis of an electromagnetic bandgap microstrip antenna,” *The American Journal of Applied Sciences*, vol. 8, no. 12, pp. 1374–1377, 2011.
- [11] D. Sievenpiper, “Review of theory, fabrication, and applications of high impedance ground planes,” in *Metamaterials: Physics and Engineering Explorations*, N. Engheta and R. Ziolkowski, Eds., chapter 11, John Wiley & Sons, New York, NY, USA, 2006.
- [12] G. H. Li, X. H. Jiang, and X. M. Zhong, “A novel defected ground structure and its application to a lowpass filter,” *Microw. Optic. Tech.Lett.*, vol. 48, no. 9, pp. 1760–1763, 2006.
- [13] C. S. Kim, et al., “Equivalent circuit modelling of spiral defected ground structure for microstrip line,” *Electro.Lett.*, vol. 38, no. 19, pp. 1109–1110, 2002.
- [14] M. Islam and M. Alam, “Design of high impedance electromagnetic surfaces for mutual coupling reduction in patch antenna array,” *Materials*, vol. 6, pp. 143–155, Jan. 2013.

- [15] M. Faruque, M. Islam, and N. Misran, "Evaluation of specific absorption rate (SAR) reduction for PIFA antenna using metamaterials," *Frequenz*, vol. 64, no. 7-8, pp. 144–149, 2010.
- [16] M. Faruque, M. Islam, and N. Misran, "Study of specific absorption rate (SAR) in the human head by metamaterial attachment," *IEICE Electronics Express*, vol. 7, no. 4, pp. 240–246, 2010.
- [17] M. Islam, M. Faruque, and N. Misran, "SAR reduction in a muscle cube with metamaterial attachment," *Applied Physics*, vol. 103, no. 2, pp. 367–372, 2011.
- [18] T. Lopetegi, M. Laso, R. Gonzalo et al., "Electromagnetic crystals in microstrip technology," *Optical and Quantum Electronics*, vol. 34, no. 1–3, pp. 279–295, 2002. .
- [19] F. Yang, K. Ma, M. Qian, and T. Itoh, "A uniplanar compact photonic-bandgap (UC-PBG) structure and its applications for microwave circuits," *IEEE Trans. Microw. Theory Tech*, vol. 47, no. 8, pp. 1509–1514, 1999.
- [20] M. Mollah, N. Karmakar and J. Fu, 'Uniform circular photonic bandgap structures (PBGs) for harmonic suppression of a bandpass filter', *AEU - International Journal of Electronics and Communications*, vol. 62, no. 10, pp. 717-724, 2008.
- [21] N. Karmakar, M. Mollah, S. Padhi and R. Lim Li Ling, "Investigations into Planar Electromagnetic Bandgap," *IEEE Trans. Microw. Theory Tech.*, vol 25, no 5, pp. 419-426, Dec. 2006.
- [22] M. Mollah, N. Karmakar and J. Fu, 'Investigation of novel tapered hybrid defected ground structure (DGS)', *Int. J RF and Microw. Comp. Aid. Eng.*, vol. 15, no. 6, pp. 544-550, 2005.
- [23] Chul-Soo Kim, Jun-Seok Park, Dal Ahn and Jae-Bong Lim, 'A novel 1-D periodic defected ground structure for planar circuits', *IEEE Microw. Guid. Wave Lett.*, vol. 10, no. 4, pp. 131-133, Apr. 2000.
- [24] T. Euler, J. Papapolymerou, "Silicon Micromachined EBG Resonator and Two-Pole Filter with Improved Performance Characteristics," *IEEE Microw. Wirel. Compon. Lett*, vol. 13 no. 9, pp. 373, 2003.
- [25] Hsiuan-ju Hsu, M. Hill, R. Ziolkowski and J. Papapolymerou, 'A Duroid-based planar EBG cavity resonator filter with improved quality factor', *Antennas Wirel. Propag. Lett.*, vol. 1, no. 1, pp. 67-70, 2002..
- [26] W. J. Chappell, M. P. Little, and L. P. B. Katehi, "High Isolation, Planar Filters Using EBG Substrates," *IEEE Microw. Wirel. Compon. Lett.*, vol. 11, No. 6, pp. 246-248, 2001.
- [27] W. Chappell and Xun Gong, "Wide bandgap composite EBG substrates", *IEEE Trans. Antennas Propagat.*, vol. 51, no. 10, pp. 2744-2750, 2003.
- [28] J. Vardaxoglou, "Tunable Metallodielectric Electromagnetic Band Gap (MEBG) Structures with defects", in *IEEE International Conference on Electromagnetics in Advanced Applications*, Torino, Italy, 2003, pp. 667-670.
- [29] M. Hill, R. Ziolkowski, and J. Papapolymerou, "A High-Reconfigurable Planar EBG Cavity Resonator," *IEEE Microw. Wirel. Comp. Lett.*, vol. 11, No. 6, pp. 255-257, 2001.

- [30] V. Radisic, Y. Qian, R. Coccioli, and T. Itoh, "Novel 2-D photonic bandgap structures for microstrip lines," *IEEE Microw. Guid. Wave Lett.*, vol. 8 no. 2, pp. 69-71, Feb. 1998.
- [31] T. Lopetegui, M. Laso, J. Hernandez, M. Bacaicoa, D. Benito, M. J. Garde, M. Sorolla, and M. Guglielmi, "New Microstrip Wiggly - Line Filters with Spurious Passband Suppression," *IEEE Trans. Microw. Theory Tech.*, vol. 49, no. 9, pp. 1593-1598, 2001.
- [32] D. Nestic, "A New Type of Slow-Wave 1-D PBG Microstrip Structure without Etching in the Ground Plane for Filter and Other Applications," *Microw. Optic. Tech. Lett.*, Vol. 33, No. 6, pp. 440-443, 2002.
- [33] D. Nestic, "A New Type of Slow-Wave 1D PBG Microstrip Band-Pass Filter," *Microw. Optic. Tech. Lett.*, Vol.37, No.3, pp.201-203,2003.
- [34] D. M. Pozar, *Microwave Engineering*. Reading, MA: Addison-Wesley, 1990.
- [35] V. Radisic, Y. Qian, and T. Itoh, "Novel architectures for high-efficiency amplifiers for wireless applications," *IEEE Trans. Microw. Theory Tech.* vol.46. no. 11, pp. 1901-1909, Nov. 1998.
- [36] M. Rahman and M. Stuchly, "Transmission line – periodic circuit representation of planar microwave photonic bandgap structures," *Microw. Optic. Tech. Lett.*, vol. 30, no. 1, pp. 15–19, 2001.
- [37] Paul J. Shields, "Bragg's Law and Diffraction," Center for High Pressure Research, State University of New York, Stony Brook, NY 11794-2100. <http://www.eserc.stonybrook.edu/ProjectJava/Bragg/>
- [38] C. Balanis, *Antenna theory*. Hoboken, NJ: Wiley Interscience, 2005.
- [39] M. Mollah, "Planar Electromagnetic Bandgap Structures and Applications", Ph.D, Nanyang Technological University, Singapore, Mar. 2005.
- [40] Y. Sung., "Tunable BandStop Filter Based Defected Ground Structure using a Metal Plate", *Microw. Optic. Tecn. Lett.*, Vol. 51, No. 9, pp. 2254-2255, 2009.
- [41] M. Laso, T. Lapetegui, M. Erro, D. Benito, M. J. Garde and M. Sorolla, "Multiple-Frequency-Tuned Photonic Bandgap Microstrip Structures", *IEEE Microw. Guid. Wave Lett.*, vol. 10, No. 6, pp. 220-222, 2000.
- [42] S. Tse, B. Sanz Izquierdo, J. Batchelor and R. Langley, "Reduced sized Cells for Electromagnetic Bandgap Structures," *Electron. Lett.*, vol. 39, No. 24, pp. 1699, 2003.
- [43] G. Goussetis, A. Feresidis and J. Vardaxoglou, "Periodically loaded 1-D metallodielectric electromagnetic bandgap structures for miniaturisation and bandwidth enhancement", *IEE Proceedings - Microwaves, Antennas and Propagation*, vol. 151, no. 6, p. 481, 2004..
- [44] A. Feresidis, G. Apostolopoulos, N. Serfas and J. Vardaxoglou, "Closely Coupled Metallodielectric Electromagnetic Band-Gap Structures Formed by Double-Layer Dipole and Tripole Arrays", *IEEE Trans. Antennas Propagat.*, vol. 52, no. 5, pp. 1149-1158, 2004.

- [45] J. Vardaxoglou, G. Goussetis and A. Feresidis, "Miniaturisation schemes for metallodielectric electromagnetic bandgap structures", *IET Microw. Antennas Propag.*, vol. 1, no. 1, p. 234, 2007.
- [46] G. Goussetis, A. Feresidis and J. Vardaxoglou, "Performance of Metallodielectric EBG Structures with Periodic Loaded Elements", in *IEE Seminar on Metamaterials, for Microwave and (Sub) Millimetre Wave Applications*, London, UK, 2003.
- [47] A. Feresidis, A. Chauraya, G. Goussetis, J. Vardaxoglou and P. deMaagt, "Multiband Artificial Magnetic Conductor Surfaces", in *IEE Seminar on Metamaterials for Microwave and (Sub) Millimetre Wave Applications*, London, UK, 2003.
- [48] S. Haykin, *Communication Systems*, Third Edition, New York, Wiley, 1994.
- [49] David M. Pozar, *Microwave Filters*, Fourth Edition, New Jersey, Wiley, 1998.
- [50] Wikipedia, 'Filter (signal processing)', 2015. [Online]. Available: [http://en.wikipedia.org/wiki/Filter_\(signal_processing\)](http://en.wikipedia.org/wiki/Filter_(signal_processing)).
- [51] J. Shumpert, T. Ellis, G. Rebeiz and L. Katehi, "Microwave and Millimeter-Wave Propagation in Photonic Band-Gap Structures," AP-S/URSI, pp. 678, Oct. 1997.
- [52] C. Soukoulis, "The History and Review of the Modelling and Fabrication of Photonic Crystals", *Nanotechnology*, vol 13, pp 420-423, 2002
- [53] D. Prather, S. Shi, A. Sharkawy, J. Murakowski and G.J. Schneider, "Photonic Crystals: Theory, Applications, and Fabrication", N. J, Wiley 2009.
- [54] F. Falcone, T. Lopeteggi, M. Sorolla, "1D and 2D Photonic BandGap Microstrip Structures," *Microw. Optic. Techn. Lett.*, Vol. 22, No. 6, 1999.
- [55] G. Cakir, L. Sevgi, "Design of A Novel Microstrip Electromagnetic BandGap (EBG) Structures," *Microw. Optic. Techn. Lett.*, Vol. 46, No. 4, pp 399-401, 2005.
- [56] J. D. Joannopoulos, R. D. Meade and J. N. Winn, "Photonic Crystals: Molding the Flow of Light", New Jersey: Princeton University Press, 1995.
- [57] M. Laso, M. Erro, D. Benito, M. Grade, T. Lapetegi, F. Faleone, and M. Sorolla, "Analysis and Design of 1D Photonic BandGap Microstrip Structure using a Fiber Grating Model", *Microw. Optic. Tech. Lett.*, vol. 22, No. 4, pp 223-226, 1999.
- [58] T. Akaline, M. A. G. Laso, T. Lopetgi, and O. Vanbesien, "PBG-type microstrip filters with one-end and two-sided patterns," *Microw. Optic. Tech. Lett.*, vol. 30, no. 1, pp 69-72, Jul. 2001.
- [59] D. Nestic and A. Nestic, "Bandstop microstrip PBG filter with sinusoidal variation of the characteristic impedance and without etching in the ground plane," *Microw. Optic. Tech. Lett.*, vol. 29, no. 6, pp. 418-420, Jun. 2001.
- [60] Q. Xue, K. M. Shum and C.H Chan, "Novel 1-D photonic bandgap microstrip transmission line," APS-International symposium, 2000, IEEE, vol. 1, page(s), 354-356.
- [61] Y. Qian, R. Coccioli, F-R. Yang and T. Itoh "Passive and active component design using PBG," Terahertz Electronics proceedings, 1998, IEEE sixth Int. Conf., pp. 42-45.

- [62] H. W. Liu, Z. F. Li, and X. W. Sun, "A novel fractal defected ground structure and its application to the low-pass filter," *Microwave ant Opt. Tech. Lett.* vol. 39, no. 6 pp. 453-456, Dec. 2003.
- [63] Y. Qian, F.R. Yang, and T. Itoh, "Characteristics of microstrip lines on a uniplanar compact PBG ground plane," *1998 Asia-Pacific Microwave Conf. Dig.*, pp.589-592, Dec. 1998.
- [64] J. Bahl and P. Bhartia, *Microwave solid state circuit design*, Wiley, New York, 1998.
- [65] G. Larkins, R. Socorregut and Y. Vlasov, 'Superconducting microstrip hairpin filter with BaTiO/sub 3/ patches', *IEEE Trans. Appl. Supercond.*, vol. 13, no. 2, pp. 724-726, Jun. 2003.
- [66] DušanNešić, "A brief Review of Microwave Photonic Bandgap (PBG) Structures", *Mikrotalasnarevija*, vol. 7, iss. 1, pp. 18-24, 2001
- [67] R. Levy, R. Snyder and G. Matthaei, "Design of microwave filters," *IEEE Transactions on Microwave Theory & Techniques*, Vol. 50, No. 3, pp. 783-793, Mar. 2002.
- [68] P. I. Richards, "Resistor-Transmission Line Circuits," *Proceedings of the IRE*, vol. 36, pp. 217–220, Feb. 1948.